UNIVERSITÀ DEGLI STUDI DI ROMA "TOR VERGATA"

FACOLTA' DI INGEGNERIA

DOTTORATO di RICERCA in
MATERIALI per l'AMBIENTE e l'ENERGIA

XX CICLO

Development and characterization of ceramic materials for direct hydrocarbon oxidation in Solid Oxide Fuel Cells operating at intermediate temperature

Massimiliano Lo Faro

Tutor: Dr. Antonino Salvatore Aricò

Coordinatore: Prof. Enrico Traversa

That from which is everything that exists (ἅπαντα τὰ ὄντα) and from which it first becomes (ἐξ οὗ γίγνεται πρῶτου) and into which it is rendered at last (εἰς ὃ φθείρεται τελευταῖον), its substance remaining under it (τῆς μὲν οὐσίας ὑπομενούσης), but transforming in qualities (τοῖς δὲ πάθεσι μεταβαλλούσης), that they say is the element (στοιχεῖον) and principle (ἀρχήν) of things that are. For it is necessary that there be some nature (φύσις), either one or more than one, from which become the other things of the object being saved

Aristotle's *Metaphysics* 983 b6 8-11

Thales of Miletos (Θαλῆς ὁ Μιλήσιος, ca. 624 BC–ca. 546 BC),

INDEX

Preface

This thesis is submitted for the 'PhD' in Materials for Environment and Energy at the University Tor Vergata in Rome.

The work was carried out at the Institute of Advanced Technology for Energy of the Italian National Research Council (CNR-ITAE "Nicola Giordano"), under the supervision of Dr. Antonino S. Aricò as tutor.

The research was financed by MIUR.

ACKNOWLEDGEMENTS

There are several people that I would like to thank. First of all I would like to thank my supervisor, Dr. Antonino S. Aricò of the CNR-ITAE; I have had the privilege of working with him in the past four years. Dr. Aricò has helped me to overcome problems, giving me substantial insights into the field of electrochemistry and skilful, reliable guidance during my PhD project. He dedicated time and effort, much more than expected, to listen my difficulties and help me in learning and succeeding. Secondly, I would like to thank Dr. Vincenzo Antonucci, who was always willing to listen and always had an open door. Their flexibility, friendliness and encouragement made completing my work at the CNR-ITAE very pleasant and rewarding. Third, I would also like to thank my coordinator, Prof. Enrico Traversa for the efforts he put into my work.

I would like to thank Mr. Giuseppe Monforte and Mr. Maurizio Minutoli for their patience in the laboratory experiments shared with me, and Ing. Giovanni Brunaccini for his availability to repair the out of order instruments. Thanks go to Dr. Isabella Nicotera for her NMR analysis and Prof. PierLuigi Antonucci for the catalytic activity measurements. I would like to thank all my friends in the office for their support and friendship, especially Francesco Sergi, Stefania Siracusano, Ruben Jacopo Ornelas and Fabio Matera. At the same time, I also want to thank the whole CNR-ITAE colleagues for the relaxing breaks and funny discussions that made the workplace enjoyable.

I would like to pay a special thank to Dr. Daniela La Rosa for the productive collaboration I had with her during my PhD. She spent an enormous amount of time helping me in every aspect of my research and professional life. Thank you Daniela, you must know that working with you was always fun. Good lucky for your career!

Gratitude goes to any person who actually reads this thesis with enthusiasm and interest.

And finally I would like to thank my family for their support throughout my time as a graduate student and for providing an environment of encouragement that was for me of great support.

1

INTRODUCTION

Significance of this Research

The current energy supply system, which is based on the combustion of fossil fuels, causes many environmental problems: air pollution, acid gas emissions, and the emission of greenhouse gases. At the same time supply of electricity and transport of goods/persons are the basis of modern life. These two sectors are strongly related to mass consumption of energy. The increasing energy demands and emerging energy crisis pose the question on how energy can be used in the earth more efficiently while keeping our living space clean. An urgent and continuing problem in the 21st century will be how to conserve energy resources and how to decrease the emission of CO_2. This problem can be translated as how to eliminate the mass consumption of energy in developed countries and how to build the most advanced/efficient energy system in the developing countries. This requirement can be summarized as "highly efficient technology in electricity generation and transportation sector."

Solid-state ionic devices, such as SOFCs are promising energy conversion and storage technologies that could solve some environmental issues, while simultaneously curbing the consumption of resources and providing employment opportunities. Solid oxide fuel cell (SOFC) is expected to play a major role in the stationary generation of energy as well as in transportation in the coming decades.

The solid oxide fuel cell is currently attracting tremendous interest because of its huge potential to enhance energy conversion efficiency, reliability and security, and reducing environmental impact. As well as, fuel flexibility is one of the significant advantages of solid oxide fuel cells (SOFCs) over other types of fuel cells The major drawback in commercializing SOFCs is concerning with high costs which result from the use of special high temperature ceramic materials. There is considerable interest in lowering the operating temperature from 950°C to 700-800°C, in particular, to reduce the cost of

interconnects, manifolding and sealing materials, as well to preclude the potential problem resulting from the sintering of electrode particles over time. Although significant advances have been achieved in the development of materials with improved ionic and electronic conductivity and of manufacturing processes to fabricate thinner electrolytes to reduce ohmic losses, the performance at low temperatures is severely limited by interfacial polarization resistance at the cathode/electrolyte interfaces. Design and fabrication of functional, porous, nanostructured electrode to maximize the area of the three-phase boundary (TPB) between ionic, electronic conductor and oxygen gas, remain at the forefront of fuel cell research and development. Nonetheless, considerable work remains to be done to study anodic catalysts with ability to work properly in the presence of a wide range of hydrocarbon fuels and with good performance under redox cycling. This work addresses mainly these aspects i.e. direct oxidation of hydrocarbons at intermediate temperatures.

Overview of the Upcoming Chapters

The thesis begins with the state - of - art chapter that introduces a general review of the SOFCs, the challenges of the current research and an outline of the work carried out to achieve the goal.

Chapter 3 gives the basics of operations and working conditions of SOFCs including their thermodynamic and kinetic aspects influencing the performances. This chapter discusses the fundamental concepts of fuel cells concentrating on the underlying chemical and electrochemical processes in the upstream condition.

Experimental work, results and discussion are described in Chapter 4. In this chapter materials, mechanism and related electrochemical and catalytic properties are investigated.

Keywords: Intermediate temperature solid oxide fuel cells (IT-SOFCs), propane electro-oxidation, LSCF, CGO

2

STATE-OF-ART (Background)

Principle of operation

A Solid Oxide Fuel Cell (SOFC) is an energy conversion device that produces electricity by electrochemically combining a fuel and an oxidant across an ionic conducting oxide electrolyte, the principles of operation are illustrated in Fig. 1. The dense electrolyte is sandwiched between two porous electrodes, the anode and the cathode (the anode/electrolyte/cathode sandwich is referred to as a single cell). Fuel is fed to the anode, undergoes an oxidation reaction, and releases electrons to the external circuit. Oxidant is fed to the cathode, accepts electrons from the external circuit, and undergoes a reduction reaction. The electron flow in the external circuit from the anode to the cathode produces electricity. The difference in oxygen activity of the two gases at the electrodes provides a driving force for motion of the oxide ions in the electrolyte. Oxide ions formed by dissociation of oxygen at the cathode under electron consumption migrate through the electrolyte to the anode where they react with the oxidation products to form water and CO_2.

The electrochemical reactions occur in the electrodes within a distance of less than 10-20 microns from the electrolyte surface [1, 2]. This zone is referred to as the functional layer. The part of the electrode exceeding this thickness is primarily a current collector structure, which must be porous to allow gas access to the functional layer. The electrolyte has to be gas impermeable to avoid direct mixing and combustion of the gases. The electrolyte is ceramic, and the electrodes are also based on ceramic materials. Under cell operating conditions, the cell produces current as long as the reactants are provided to the electrodes. An open circuit voltage of about 1 volt is attained when the

[1] M. Juhl, S. Primdahl, C. Manon and M. Mogensen, J. Power Sources 61, 173, 1996.
[2] M. Brown, S. Primdahl and M. Mogensen, 'Structure/performance relations for Ni/YSZ anodes for SOFC', J. Electrochem. Soc. 147, 2, 475-485, 2000.

cell is not loaded, as determined by the Nernst equation which will be discussed in the next chapter.

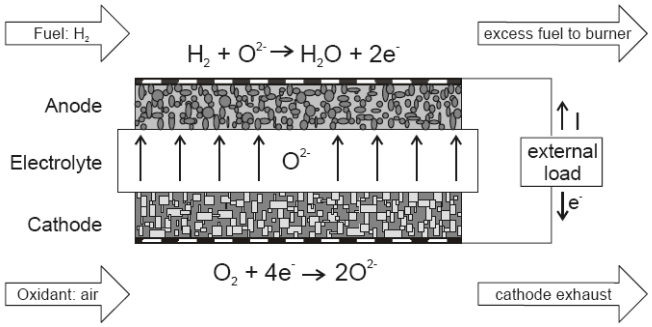

Fig. 1. A Solid Oxide Fuel Cell

SOFCs provide many advantages over traditional energy conversion systems including high efficiency (in the range 45-60%), reliability, modularity, and extremely low emissions of major local air pollutants (CO, NO_x, and unburned hydrocarbons). A SOFC converts the chemical energy of fuel directly into electrical energy. Thus the usual losses involved in the conversion of fuel to heat, to mechanical energy, and then to electrical energy of conventional combustion systems are avoided. SOFCs can potentially be operated on a range of fuels, including pipeline natural gas and bio-mass, without a significant loss of efficiency or increase in system complexity and cost. Furthermore, because of their high temperature of operation (500-1000°C), natural gas can be reformed within the cell stack eliminating the need of an expensive, external reformer. Rather tight limits on fuel sulphur contents are nevertheless still required. In adding, SOFC are characterized by high temperature exhaust gases which could be used in combined cycles. Not least, quiet, vibration free operation of solid oxide fuel cells also eliminates noise usually associated with conventional power generation systems.

Among fuel cell types, only the SOFC has the recognized potential to achieve power generation efficiencies in excess of 70% using a hybrid cycle that is both simple and dry, i.e., the SOFC/Gas Turbine.

Configurations for SOFC

SOFCs have been tested since 1930 under several configurations among which the most widespread and tested are the planar and tubular arrangements. However, a number of technological problems still need to be solved, basically related to the high operating temperature and then to thermal cycling issues. Research and development are therefore still proceeding both to test new materials and to optimize the design of single cells and complete stacks as well. The materials for cell components in these different designs are either the same or very similar in nature. Fig. 2 (a) illustrates the design of the tubular geometry cell developed by Westinghouse [3] and (b) illustrates the planar designs.

The materials for different cell components have been selected based on the following criteria.

(a) Suitable electrical conducting properties required by different cell components to perform their intended cell functions.

(b) Adequate chemical and structural stability at high temperatures during cell operation as well as during cell fabrication.

(c) Minimal reactivity and interdiffusion among different cell components.

(d) Matching thermal expansion among different cell components.

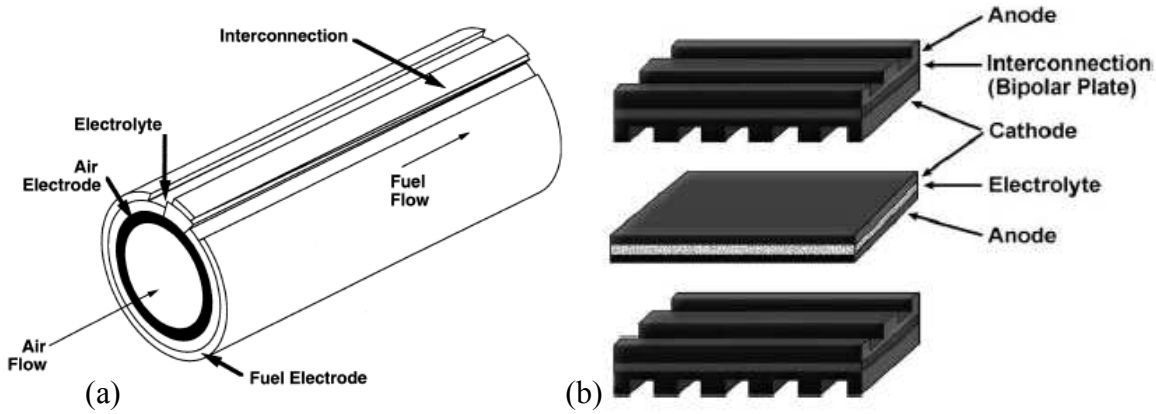

Fig. 2. Schematics of SOFC designs. (a) Tubular design developed by Westinghouse. (b) Planar design most used today

In addition to the above materials selection criteria, the fabrication processes have been chosen in such a way that every sequential component fabrication process does not affect

[3] S.C. Singhal, K. Kendall, High Temperature Solid Oxide Fuel Cells, Elsevier, New York, 2003.

those components already fabricated and to minimise the cell fabrication cost. The fabrication routes for the individual cell components of SOFC differs greatly depending on which cell component is to perform the supporting function in the cell. Whereas, in most cases the electrolyte or the anode (in case of planar configuration) and cathode (in case of tubular configuration) ensure the mechanical stability of the cells. Common planar cells are shaped rectangularly (square) or circularly. The designs discussed above differ in the current path within a stack of cells, in the gas flow configuration and gas manifolding, and in the cell-to-cell electrical connection.

Materials for SOFC

The basic components of a ceramic fuel cell stacks are the electrolyte, the anode, the cathode and the interconnect. The materials for different cell components have been selected based on the following criteria.

Cathode (*air electrode*)

The air electrode operates in an oxidising environment of air or oxygen at temperatures between 700-1000°C . It is responsible for the electrochemical reduction of oxygen in the gas phase to oxide ions consuming two electrons in the process as shown in Reaction 1.

$$\frac{1}{2}O_2(g) + 2e^- = O^{2-}(s) \qquad (1)$$

The oxygen ions formed by reduction then are incorporated into the electrolyte, through oxygen vacancies, and migrate to the anode. In order to function properly, SOFC cathode materials must be catalytically active for the oxygen reduction and have to meet the following requirements.

(a) High ionic conductivity is required to facilitate transport of oxygen anions between the electrolyte and active reaction zone.

(b) High electronic conductivity is necessary to provide pathways between the reaction sites and external circuit.

(b) Chemical and dimensional stability in environments encountered during cell operation and during fabrication of interconnection, electrolyte and fuel electrode layers are required.

(c) Thermal expansion should match with other cell components.

(d) Compatibility and minimum reactivity with the electrolyte and the interconnection is required for the electrodes.

(e) Sufficient porosity is necessary to facilitate transport of molecular oxygen from the gas phase to the air electrode / electrolyte interface.

In addition to being an electronic conductor, performance and activation overpotential can be significantly improved if the cathode is also an ionic conductor [4, 5, 6].

Since the cathode is constantly in an oxidizing atmosphere, the electrode materials are mostly oxide-based, which typically aren't known for high electronic conductivities.

To satisfy these requirements, doped perovskite oxides of generic formula $La_{1-x}A_xCo_{1-y}B_yO_{3-\delta}$ (A = Sr, Ba, Ca and B = Cr, Mn, Fe, Ni, Cu) and such as lanthanum manganite (LSM), lanthanum ferrite/cobaltite (LSFCO) and lanthanum chromite/manganite (LSCM) show reversible oxidation–reduction behaviour. The ABO_3 crystal structure type can be described as follows: The A-cations are located at the corners of a cube. O2- ions occupy the face-centred positions and one of the smaller B-cations sits in the centre of the cube. Hence, the B-site cations are surrounded octahedrally by oxide ions. In general, the cation with the larger ionic radius occupies the A-sites, the smaller cation the B-sites.

The partial substitution of cations in the ABO_3 perovskite structure by cations with a lower valence either leads to formation of oxygen vacancies or to charge compensation by electronic charge carriers.

The material can have oxygen excess or deficiency depending upon the ambient oxygen partial pressure and temperature. Large numbers of disordered oxygen vacancies at elevated temperatures may lead to the onset of high ionic conductivity. For example, in the series $La_{1-x}Sr_xCo_{1-y}Fe_yO_{3-\delta}$, the ionic conductivity in air at temperatures 700–1000 ºC can be one to two orders of magnitude larger than that of known zirconia-based solid electrolytes [7]. The presence of multivalent cations in the perovskite compositions, on the other hand, ensures a high, often predominating electronic conductivity. In addition to conductivity considerations, the stability and thermomechanical properties of the

[4] E. Koep, D. Mebane, R. Das, C. Compson and M. Liu, "Characteristic Thickness of a Dense La0.8Sr0.2MnO3 Electrode," Electrochem. and Solid State Lett., 8[11], A592-A595 (2005).

[5] E. Koep, A Quantitative Determination of Electrode Kinetics using Micropatterned Electrodes. PhD Thesis, School of Materials Science and Engineering, Georgia Institute of Technology, May 2006. Available at <http://etd.gatech.edu/theses/available/etd-04032006-224453/>.

[6] E. Koep, C. Compson, M. Zhou and M. Liu, "A Photolithographic Process for Investigation of Electrode Reaction Sites in Solid Oxide Fuel Cells," Solid State Ionics, 176, 1-8 (2005).

[7] Y. Teraoka, H.M. Zhang, K. Okamoto and N. Yamazoe, Mater. Res. Bull. 23, 51-58 (1988).

materials are dictated by the choice of cation. A balance must be necessary between the desire for high flux and considerations of long term stability.

Typical data of oxygen nonstoichiometry for some simple perovskite oxides are shown in Fig. 3. As can be seen the substitution of trivalent lanthanum by divalent strontium ions in $La_{1-x}Sr_xFeO_{3-\delta}$ is charge compensated by the formation of p-type charge carriers (Fe^{4+}) at relatively high oxygen partial pressure, whereas compensation at oxygen partial pressures corresponding to the plateau in the (3-δ) sub-stoichiometry versus $\log(pO_2)$ plot occurs predominantly by formation of oxygen vacancies. Oxygen vacancies that are generated upon further decreasing pO_2 are predominantly charge compensated by reduction of Fe^{3+} to Fe^{2+}. In contrast to $La_{1-x}Sr_xFeO_{3-\delta}$, a pO_2 region where the oxygen stoichiometry is virtually constant is lacking in $La_{1-x}Sr_xCoO_{3-\delta}$[8]

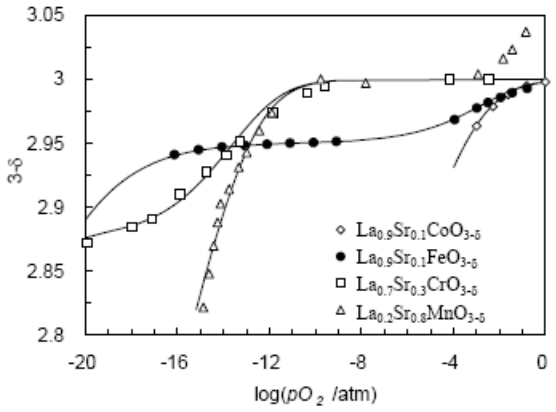

Fig. 3. Data of oxygen nonstoichiometry of some simple perovskite-type oxides at 1273K. Solid lines are results from a fit of the random point defect model to the experimental data.

Current SOFC technologies satisfy these requirements through the use of porous multi-phase composite electrodes where, in general, one phase provides ionic conductivity and another electronic. The catalytic activity is usually provided by the electronically conductive phase. The active area of such composite electrodes is inherently restricted to the interfacial regions where these phases meet. Mixed conducting materials can provide both ionic and electronic conductivity in one phase, greatly enhancing the active electrode area. The reaction sites in SOFC electrodes are commonly discussed using the concept of a triple-phase boundary (TPB). The TPB is the location at which the electron conducting, ion conducting and gas phases come into contact.

[8] Proceedings of the 26th Risø International Symposiumon Materials Science: Solid State Electrochemistry Editors: S. Linderoth, A. Smith, N. Bonanos, A. Hagen, L. Mikkelsen, K. Kammer, D. Lybye, P.V. Hendriksen, F.W. Poulsen, M. Mogensen, W.G. Wang Risø National Laboratory, Roskilde, Denmark 2005

The general macroscopic reaction pathways available for oxygen reduction processes on porous cathode/solid electrolyte structure were already discussed more than 35 years ago [9], and can be summarised in the following diagram (Fig 4)

Reaction pathway (1): The oxygen absorbs dissociatively on the surface of the perovskite phase before diffusing along the surface to the triple phase boundary (TPB) where it is incorporated into the ionic phase.

Reaction pathway (2): Gas-phase oxygen is incorporated directly into the electrolyte phase at the TPB

Reaction pathway (3): This involves incorporation of oxygen at the surface of the mixed ionic-electronic conductor (MIEC) coupled to bulk diffusion to the electrolyte/MIEC interface. Bulk pathway is enabled when the electronic phase is replaced by a mixed-conductor.

The distance from the interface, λ, where this third mechanism occurs is dictated by a balance between surface exchange rates and bulk ionic conductivity which are related to the vacancy concentration. Low ionic conductivity and fast surface incorporation rates reduces the mechanism to that of the purely electronic conductor. In contrast, high ionic conductivity and low surface rates can extend the reaction zone far from the interface region. Using the characteristic thickness criterion as for MIEC membranes the mixed conducting zone is estimated to extend up to ~10 μm from the interface [10].

At distances greater than this the net current is electronic and only equilibrium exchange occurs between gas phase oxygen and the MIEC. This MIEC zone represents an extension of the TPB region, and increase in active electrode area.

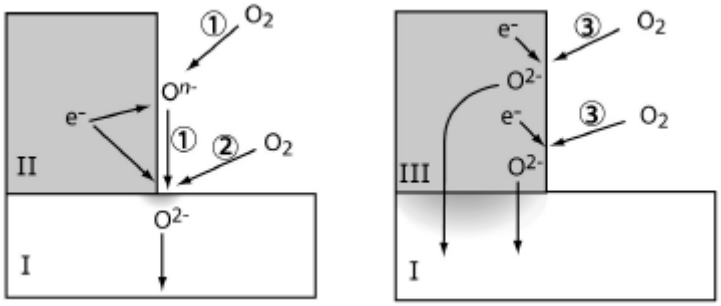

Fig. 4. Schematic showing cathode reaction pathways between ionic, I, electronic, II, and mixed-conducting III materials. (1) surface dissociation and diffusion followed by incorporation at the TPB. (2) direct incorporation at the TPB. (3) incorporation along the length of the MIEC followed by bulk diffusion.

[9] S. Pizzini, in: Fast Ion Transport in Solids, Ed. W. van Gool (North-Holland, 1973) p. 461

[10] S.B. Adler, J.A. Lane and B.C.H. Steele, J. Electrochem. Soc. 143, A3554-A3564 (1996).

Steele and Bae [11] found that the performance of LSCF-GDC cathodes could be interpreted in terms of surface exchange kinetics; that is that the surface reaction limits the performance. Increased understanding of the relative importance of bulk vs. surface kinetics in MIEC cathodes is required to provide guidelines for both cathode manufacture and the development of new cathode materials.

J.A. Lane, et al [12] have obtained information of Oxygen transport and oxygen surface reaction for $La_{0.6}Sr_{0.4}Co_{0.2}Fe_{0.8}O_{3-\delta}$ using the conductivity relaxation technique. They have given information on the variation of electrical conductivity of $La_{0.6}Sr_{0.4}Co_{0.2}Fe_{0.8}O_{3-\delta}$ with oxygen partial pressure at 800°C.

$La_{0.6}Sr_{0.4}Co_{0.8}Fe_{0.2}O_{3-\delta}$, the most thoroughly studied composition in the framework of this thesis, has a rhombohedral structure at room temperature, and shows a phase transition to cubic between 400 and 500°C in air [13]. The expansion of the perovskite lattice upon heating is associated to a major part with the formation of oxygen vacancies (in addition to the usual thermal lattice expansion), and therefore related to the defect chemistry of the material. The behaviour is typical of an acceptor doped perovskite in a mixed electronic ionic compensation regime. Fe^{3+} and Co^{3+} play a similar role, and a statistical distribution of the two types of ions on the B-sites in the perovskite lattice is usually assumed [14].

The substitution of La^{3+} ions on the A-sites of the perovskite lattice by the dopant Sr^{2+} requires a charge compensation. Electroneutrality can be maintained in two ways: either by a valence change of the B-site cation (creation of holes, electronic compensation) or by the formation of oxygen vacancies (ionic compensation).

In general, both processes occur and compete with each other, depending on composition, oxygen partial pressure and temperature.

The oxygen nonstoichiometry δ is a function of oxygen partial pressure. At high value of $p(O_2)$, the charge is compensated mainly by electron holes, while at lower partial pressures ($< 10^{-3}$ bar) oxygen vacancies become the dominating defects.

[11] B.C.H. Steele and J.-M. Bae, Solid State Ionics 106, 255-261 (1998).
[12] J.A. Lane, S.J. Benson, D. Waller, J.A. Kilner; Solid State Ionics 121 (1999) 201–208
[13] S. Wang, M. Kasatoshi, M. Dokiya, and T. Hashimoto, Solid State Ionics 159, 71-78 (2003).
[14] S. Wang, M. Kasatoshi, M. Dokiya, and T. Hashimoto, Solid State Ionics 159, 71-78 (2003).

Electrolyte

The main purpose of an electrolyte is to conduct a specific ion between two electrodes in order to complete the overall electrochemical reaction. Without conduction of that specific ion, no appreciable current would be able to flow through the fuel cell and only potential would exist.

With the advancements in fabrication technology, the overall performance of SOFCs is eventually limited by the conductivity of the electrolyte materials. Ideally, an electrolyte is an ionic conductor and an electronic insulator. SOFC electrolytes work in the most stringent environment: hydrogen or hydrocarbons on the anode side, oxygen on the cathode side, and also high temperatures.

Solid oxide fuel cells are based on the concept of an oxygen ion conducting electrolyte through which the oxide ions (O^{-2}) migrate from the air electrode (cathode) side to the fuel electrode (anode) side where they react with H_2 to form water and electricity. In the case where hydrocarbons serve as the fuel, an oxygen ion conductor offers, in principle, the prospect of direct electro-oxidation:

$$CH_4 + O^{2-} \rightarrow CO_2 + 2H_2O + 8e^- \qquad (2)$$

Generally, it is instead presumed that the high temperature of operation associated with oxygen ion conductors can be used to facilitate internal steam reforming:

$$CH_4 + H_2O \rightarrow CO + 3H_2 \qquad (3)$$

with CO and H_2 then used in the electro-oxidation reactions. Even in this more conservative scenario, oxygen-ion conducting electrolytes are preferred because CO can be electro-oxidized, rather than (particularly in the case of low temperature systems) poisoning the anode catalyst. Ceramic proton conductors may offer an interesting combination of benefits because of their ability to transport both protons and oxygen ions. It has been suggested [15] that water can diffuse across the electrolyte membrane, inducing steam reforming and even conversion of CO to CO_2 through the water-gas shift reaction:

$$CO + H_2O \rightarrow CO_2 + H_2 \qquad (4)$$

Hydrogen generated by reactions (3) and (4) is then electro-oxidised to form protons. In this case, hydrocarbons can be directly utilized and no water is produced at the anode,

[15] Coors G. J Power Sources 2003;118:150.

again avoiding dilution effects as fuel utilization increases (although CO_2 dilution still occurs).

Fundamentally, for optimum cell performance, the electrolyte must be free of porosity so as not to allow gases to permeate from one side of the electrolyte to the other, it should be uniformly thin to minimize ohmic loss, and it should have high ion conductivity with transport number for ions close to unity and a transport number for electrons as close to zero as possible. At the end, electrolytes with these desired properties must be deposited as thin as possible in order to work with low ohmic loss.

Conductivity data of a broad range of materials are summarized in Fig. 5 [16, 17,18].

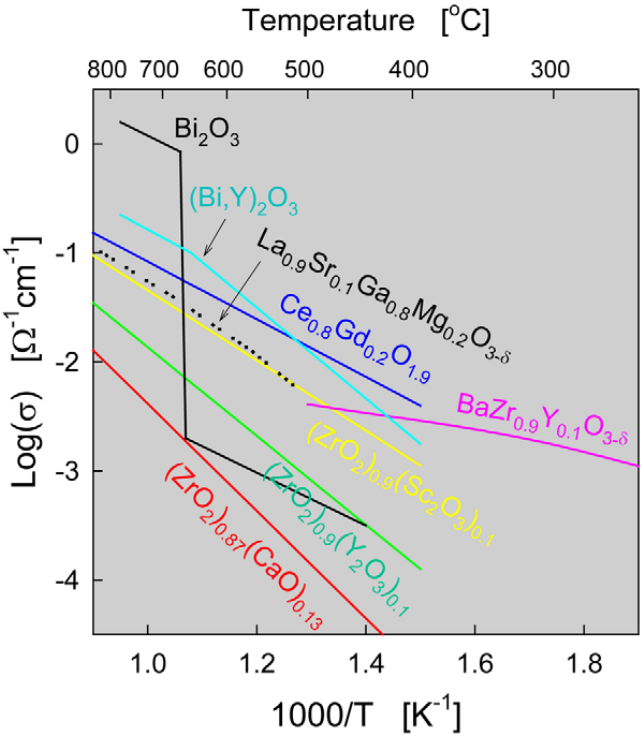

Fig. 5. Conductivities of selected electrolyte materials which are high temperature conductors

The general criteria for the quality of a solid electrolyte material to be used in an SOFC are:

(a) Ease of fabrication into a mechanically strong dense membrane of small thickness and large area to minimize bulk resistance.

(b) An oxide-ion conductivity $\sigma_0 > 10^{-2}$ S/cm at the cell operating temperature.

[16] Steele BCH, Mat Sci and Eng 1992;B13:79.
[17] Ishihara T, Matsuda H, Takita Y. J Am Chem Soc 1994;116:380
[18] Bohn HG, Schober T. J Am Cer Soc 2000;83:768.

(c) Excellent chemical and mechanical compatibility with electrodes to avoid formation of blocking interface phases and minimize interfacial resistances.
(d) A negligible electronic conductivity at cell operating temperature to retain a transport number close to 1.
(e) Compatibility of thermal-expansion coefficients between electrolyte, electrodes, interconnects, and seals from ambient temperature and cell operating temperature.
(f) Relatively low costs of material and fabrication.

Oxygen ion conductors

The classic oxygen ion conductors are based on fluorite-structured oxide materials such as yttria stabilized zirconia (YSZ) or , rare earth doped ceria (CGO, SDC, YDC), and rare earth doped bismuth oxide. Recently also perovskite oxides such as lanthanum gallate (LSGM), have been widely investigated as electrolytes for a fuel cell [19, 20]. These membranes conduct oxygen ion through oxygen vacancy [21, 22] at high temperature of around 600-1000°C. The oxygen vacancies for a typical tri-valent dopant, M, can be written in the Kröger–Vink notation:

$$M_2O_3 \xrightarrow[ZrO_2]{} 2M'_{Zr} + 3O_O^{\times} + V_O^{\bullet\bullet} \qquad (5)$$

with one oxygen vacancy created for every two M atoms incorporated. For both zirconia and ceria, conductivity increases with increasing dopant concentration up to some maximum value and then decreases sharply. Similarly, the conductivity increases then decreases across the rare earth series from Yb to La. For zirconia, Sc gives rise to the highest conductivity, but Y is typically utilized for reasons of cost. With yttrium as the dopant, the conductivity of zirconia peaks at about 8 mole % dopant concentration. The activation energy for oxygen diffusion varies from 0.6 to 1.0 eV depending on the yttria content.

---

[19] J.A. Kilner, B.C.H. Steele, in: O.T. Sorensen (Ed.), Non-stoichiometric Oxides, Academic Press, New York, 1981, p.233.
[20] R.M. Dell, A. Hooper, in: P. Hagenmuller, W. van Gool (Eds.), Solid Electrolytes, Academic Press, New York, 1978, p. 291.
[21] J.W. Stevenson, T.R. Armstrong, R.D. Carneim, L.R. Pederson and W.J. Webel, Electrochemical properties of mixed conducting perovskite La1-xMxCol-yFeyO3-δ (M=Sr, Ba, Ca), J. Electrochem. Soc., 143 (1996) 2722-2729.
[22] L. Shiguang, W. Jin, P. Huang, N. Xu, J. Shi and Y.S. Lin, Tubular lanthanum cobaltite perovskite type membrane for oxygen permeation, J. Membr. Sci., 166 (2000) 51-61.

In the case of ceria, Sm [23] and Gd [24] give the highest values of conductivity, and optimal dopant concentrations are 10–20%. The strong dependence of ionic conductivity on dopant type and concentration has been explained in terms of the lattice distortions introduced by the dopant, with those that produce the least amount of strain causing the smallest variation in the potential energy landscape [25]. Overall, the ionic conductivity of ceria is approximately an order of magnitude greater than that of stabilized zirconia for comparable doping conditions.

This is a result of the larger ionic radius of Ce^{4+} (0.87 Å in 6-fold coordination) than Zr^{4+} (0.72 Å), which produces a more open structure through which $O^{=}$ ions can easily migrate.

Despite its favourable ion transport properties, ceria had not, until quite recently, been considered a realistic candidate for fuel cell applications because of its high electronic conductivity. In particular, under reducing conditions, CeO_2 (Fig. 6) is not stable and becomes CeO_{2-x}, and n-type conductivity increases with a $P(O_2)^{-1/4}$ dependence.

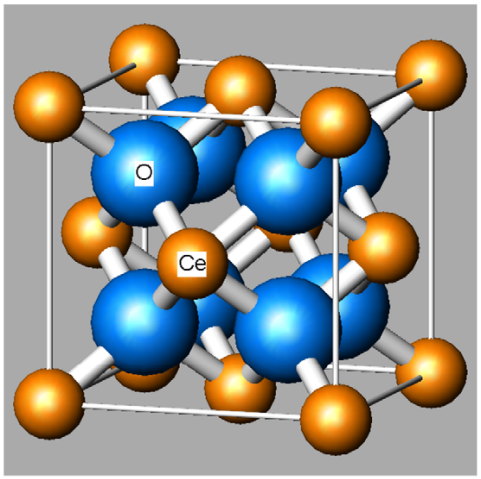

Fig. 6. Crystal structure of fluorite exhibited by ceria

Although the strategy gives a transport number $t_0 \equiv \sigma_0/\sigma \approx 1$ in air or an inert atmosphere such as argon, Ce^{3+} ions are created in a reducing atmosphere to give a measurable electronic component σ_e in the total conductivity σ.

From an analysis of relevant literature data, Steele [26] has proposed that the electrolytic domain boundary, the oxygen partial pressure at which electronic and ionic conductivities are equal, can be estimated for 10 and 20% Gd doped ceria.

[23] Eguchi K, Setoguchi T, Inoue T, Arai H. Solid State Ionics 1992;52:165.
[24] Steele BCH. Solid State Ionics 2000;129:95.
[25] Mogenson M, et al. 2003 (manuscript in preparation).
[26] Steele BCH. Solid State Ionics 2000;129:95.

In principle, one expects to be well within the electrolytic domain of ceria for fuel cells operated below 700 °C, although even at these temperatures some voltage loss is expected. Reported open circuit potentials for doped ceria are lower than what one would expect on the basis of the electronic conductivity of ceria and represented simply as the multiple of the ionic transference number (greater than ~0.9 [27] at 700 °C and 10^{-18} atm oxygen partial pressure) and the Nernst potential. For $Gd_{0.2}Ce_{0.8}O_2$ (GDC), which gives the highest oxide-ion conductivity of the rare-earth doped ceria, [28] the open circuit voltage of a hydrogen-air fuel cell was reduced to about 0.89 V at 650ºC[29].

The reasons for this discrepancy are not entirely obvious, but are likely due to electrode (in particular cathode) overpotentials, and emphasize the importance of developing electrodes compatible with ceria that enable theoretical open circuit potentials to be reached. An additional challenge lies with the chemical expansion of ceria under reducing conditions and the internal stress that result [30]. At this stage, the significance of this issue on the long-term viability of ceria-based fuel cells is unknown. It is noteworthy that planar cells experience lower stresses than tubular cells, suggesting that clever designs may alleviate possible stresses.

Equation 6 describes the ionic conductivity based upon the migration via oxygen vacancies.

$$\sigma T = \sigma_0 \exp\left(-\frac{\Delta E}{kT}\right) \qquad (6)$$

In this equation ΔE, the activation energy, involves both ΔH_m and ΔH_a, which are the enthalpy for migration of oxygen and the association enthalpy of defect complexes, respectively. Doping the ceria with certain rare earth oxides can markedly reduce the enthalpy of association. These rare earth oxide are Gd_2O_3, Sm_2O_3 and Y_2O_3. In low pO_2 the ceria becomes reduced according to the following process:

$$O_O + 2Ce_{Ce}^{\times} \rightarrow V_O^{\bullet\bullet} + 2Ce_{Ce}^{'} + \frac{1}{2}O_2(g) \qquad (7)$$

$$O_O + 2Ce_{Ce}^{\times} + H_2(g) \rightarrow V_O^{\bullet\bullet} + 2Ce_{Ce}^{'} + H_2O(g) \text{ in hydrogen gas} \qquad (8)$$

When ceria is doped with oxides of lower valences, the oxygen vacancy concentration is mainly determined by the concentration of dopant.

---

[27] Milliken C, Guruswamy S. J Am Cer Soc 2002;85:2479.

[28] K. Eguchi, T. Setoguchi, T. Inoue, and H. Arai, "Electrical-Properties Of Ceria-Based Oxides And Their Application To Solid Oxide Fuel-Cells." Solid State Ionics 52 (1992) 165-172.

[29] C. Lu, W. L. Worrell, R. J. Gorte, and J. M. Vohs, "SOFCs for direct oxidation of hydrocarbon fuels with samaria-doped ceria electrolyte." Journal Of The Electrochemical Society 150 (2003) A354-A358.

[30] Atkinson A, Ramos TMGM. Solid State Ionics 2000;129:259.

$$Gd_2O_3 \xrightarrow{CeO_2} 2Gd'_{Ce} + V_O^{\bullet\bullet} + 2O_O^{\times} \qquad (9)$$

In doped ceria equation (7) still takes place. Doping affects however the equilibrium of this reaction, by changing the oxygen vacancy concentration and the concentration of Ce'_{Ce} . For undoped ceria, the oxygen vacancy concentration is determined by the concentration of Ce'_{Ce} i.e. $Ce'_{Ce} = 2[V_O^{\bullet\bullet}]$. In doped ceria, $[V_O^{\bullet\bullet}]$ can be assumed to be constant. For undoped and doped ceria the concentration of Ce'_{Ce} is given by equation (10) and (11), respectively.

$$[Ce'_{Ce}] = \tfrac{1}{2} K_R \cdot pO_2^{-1/6} \qquad \text{for undoped ceria} \qquad (10)$$

$$[Ce'_{Ce}] = \tfrac{1}{2} K_R \cdot pO_2^{-1/4} \qquad \text{for doped ceria} \qquad (11)$$

The electronic conductivity is caused by polaron hopping. So σ_e is determined by the concentration of the electron carrier, Ce'_{Ce} (see equation (12).

$$\sigma_e = ne\mu_e \qquad (12)$$

in which e is the elementary charge of an electron and μ_e is the electron mobility.
Eventually the electronic conductivity can be described by equation (13), which has the Arrhenius form, as the electron mobility is temperature dependent.

$$\sigma_n T = \sigma_n^0 \exp\left(-\frac{\Delta H_n}{kT}\right) pO_2^{-\frac{1}{4}} \qquad (13)$$

As becomes clear from this equation, the electronic conductivity increases with increasing temperature and decreasing oxygen partial pressure. The electronic conductivity remains, however too low at high temperatures (about 0.16 S/cm at 800ºC).
Oxide-ion conducting perovskites have appeared in the literature for several years, but only recently have compositions with conductivities high enough for consideration in fuel cell applications appeared.
The ABO_3 perovskite structure, Fig. 7, is extremely amenable to tailoring via doping on both the A and B cation sites. A large variety and concentration of dopants can be accommodated in a wide range of host compounds.

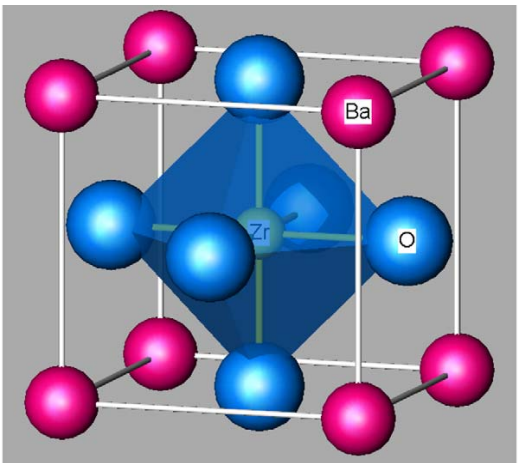

Fig. 7. Crystal structure of perovskite exhibited by oxygen ion conducting $LaGaO_3$ and by proton conducting $BaZrO_3$

Introduction of divalent dopant ions, typically Sr and Mg, onto the La and Ga sites, respectively, of lanthanum gallate produces a material with a high concentration of mobile oxygen vacancies and thereby high oxygen ion conductivity. The transport properties of the particular composition $La_{0.9}Sr_{0.1}Ga_{0.8}Mg_{0.2}O_{3-\delta}$ (LSGM) are comparable to those of scandia-doped zirconia. The conductivity is entirely ionic over an extremely wide oxygen partial pressure range at temperatures as high as 1000 °C, but is not as high as that of suitably doped ceria. Thus, the conditions under which LSGM might be preferable to doped ceria appear limited to the temperature range of 700–1000 °C. Moreover, lanthanum gallate suffers from reactivity with nickel, the typical SOFC anode electrocatalyst. To address this challenge, (non-reactive) ceria buffer layers have been incorporated between the electrolyte and the anode [31].

Nevertheless, intensive research efforts to develop SOFCs incorporating lanthanum gallate continue, and recent work suggests that the ionic conductivity can be increased by further adjustments to the stoichiometry, in particular, via the addition of small concentrations of Ni or Co [32].

Ceramic proton conductors

In analogy to the defect chemistry of lanthanum gallate, proton transport in barium zirconate, barium cerate and related materials is achieved by first doping the material with a trivalent species (such as yttrium) on the B site so as to introduce oxygen vacancies.

[31] Huang HQ, Wan JH, Goodenough JB. J Electrochem Soc 2001;148:A788.
[32] Ishihara T, Shibayama T, Nishiguchi H, Takita Y. J Mat Sci 2001;36:1125.

The dopant incorporation reaction is normally assumed to occur as per Eq. (14) (written in Kroeger-Vink notation).

$$2Ce_{Ce}^{\times} + O_O^{\times} + Gd_2O_3 \Rightarrow 2Gd_{Ce}^{'} + V_O^{\bullet\bullet} + 2CeO_2 \qquad (14)$$

Subsequent exposure of the material to humid atmospheres is presumed to lead to the incorporation of protons as per Eq. (15).

$$H_2O(g) + V_O^{\bullet\bullet} + O_O \Rightarrow 2OH_O^{\bullet} \qquad (15)$$

The protons introduced by this manner are generally not bound to any particular oxygen ion, but are instead free to migrate from one ion to the next. This easy migration results in the high proton conductivity (as high as 10^{-2} Ω^{-1} cm^{-1} at 500 °C) observed in these oxides. Much like the oxide conductors, proton conductivity peaks at intermediate dopant concentrations and with suitable matching of the dopant ionic radius to the host structure. Furthermore, proton transport dominates the overall electrical transport to temperatures of approximately 600 °C; the proton transference number of $BaCe_{0.95}Sm_{0.05}O_3$, for example, is ~0.85 at this temperature [33]. At higher temperatures, both oxide ion transport and electron transport become significant.

The defect chemistry of doped $A^{2+}B^{4+}O_3$ perovskites is complicated by the possibility that the trivalent ion may reside on both cation sites, and not only the B^{4+} site as desired [34]. The consequence of partial incorporation of the dopant onto the A^{2+} site is that fewer oxygen vacancies than anticipated will result. The effect is exacerbated by high temperature processing which can induce BaO evaporation.

A second complication arises from the highly refractive nature of the zirconate proton conductors, e.g. doped $BaZrO_3$. In comparison to the cerates ($BaCeO_3$ and $SrCeO_3$), barium zirconate offers high conductivity and excellent chemical stability against reaction with CO_2. However, fabrication of dense electrolyte membranes from this material remains a significant challenge. Indeed, the high bulk conductivity of $BaZrO_3$ had, for several years, remained obscured as a consequence of the material's refractory nature, which results in fine-grained samples with high total grain boundary resistance [35, 36]. In light of the reactivity of cerates with CO_2 and the difficultly of fabricating dense zirconate electrolytes, it is perhaps no surprise that few complete cells of proton-conducing electrolytes have been constructed and characterized.

---

[33] Iwahara H, Yajima T, Hibino T, Ushida H. J Electrochem Soc 1993;140:1687.
[34] Haile SM, Staneff G, Ryu KH. J Mat Sci 2001;36:1149.
[35] Kreuer KD. Solid State Ionics 1999;125:285.
[36] Bohn HG, Schober T. J Am Cer Soc 2000;83:768.

Thermal expansion of these electrolyte materials is also very important. Table 1 lists the average thermal expansion coefficient (CTE) for candidate SOFC electrolyte materials from 25-800ºC and 25-1000ºC. Since the CTE of the electrolyte material is harder to change without also altering its physical properties, most other SOFC components are chosen and/or designed to match the expansion of the electrolyte.

Material	$\alpha*10^{-6}$ K^{-1} (25-800°C)	$\alpha*10^{-6}$ K^{-1} (25-1000°C)	Reference
$Y_{0.15}Zr_{0.85}O_{1.93}$	10.5	10.9	37, 38
$Y_{0.18}Zr_{0.82}O_{1.91}$	10.6	11	39
$Sc_{0.15}Zr_{0.85}O_{1.93}$	10.3	10.4	40
$Sc_{0.18}Al_{0.02}Zr_{0.8}O_{1.9}$	10.5	10.9	41
$Gd_{0.2}Ce_{0.8}O_{1.9}$	12.5	12.7	42
$Sr_{0.1}Ce_{0.9}O_{1.9}$	12.8	13.1	43
$La_{0.8}Sr_{0.2}Ga_{0.9}Mg_{0.1}O_{3-x}$	10.4	10.8	44
$La_{0.8}Sr_{0.2}Ga_{0.8}Mg_{0.2}O_{3-x}$	10.5	11.3	45
$La_{0.9}Sr_{0.1}Ga_{0.75}Mg_{0.2}Co_{0.05}O_{3-x}$	10.9	11.4	46
$La_{0.9}Sr_{0.1}Ga_{0.8}Mg_{0.2}O_{3-x}$	12.3	13	47

[37] R. Maenner, E. Ivers-Tiffée, W. Wersing, W. Kleinlein, in Proceedings of the 2nd European Ceramics Society Conference, G. Zeigler and H. Hausner eds., Deutsche Keramische Gesellschaft, pp. 2085 (1991).
[38] F. Tietz, G. Stochniol and A. Naoumidis, in Proceedings of the 5th European Conference on Advanced Ceramics, Processes and Applications, L.A.J.L. Sarton and H.B. Zeedijk, Nertherlands Society for Materials Science, 2, 271, 1997.
[39] F. Tietz, G. Stochniol and A. Naoumidis, in Proceedings of the 5th European Conference on Advanced Ceramics, Processes and Applications, L.A.J.L. Sarton and H.B. Zeedijk, Nertherlands Society for Materials Science, 2, 271, 1997.
[40] Y. Mizutani, M. Tamura, M. Kawai and O. Yamamoto, "Development of High Performance Electrolyte in SOFC," Solid State Ionics, 72[2], 271-275 (1994).
[41] F. Tietz, G. Stochniol and A. Naoumidis, in Proceedings of the 5th European Conference on Advanced Ceramics, Processes and Applications, L.A.J.L. Sarton and H.B. Zeedijk, Nertherlands Society for Materials Science, 2, 271, 1997.
[42] F. Tietz, G. Stochniol and A. Naoumidis, in Proceedings of the 5th European Conference on Advanced Ceramics, Processes and Applications, L.A.J.L. Sarton and H.B. Zeedijk, Nertherlands Society for Materials Science, 2, 271, 1997.
[43] F. Tietz, G. Stochniol and A. Naoumidis, in Proceedings of the 5th European Conference on Advanced Ceramics, Processes and Applications, L.A.J.L. Sarton and H.B. Zeedijk, Nertherlands Society for Materials Science, 2, 271, 1997.
[44] F. Tietz, "Innovative Materials in Advanced Energy Technologies," in Proceedings of the 9th CIMTEC – World Ceramic Congress and Forum on New Materials, P. Vincenzini ed., Techna Publishers S.R.L., Faenza, Italy, 24, 61, 1999.
[45] I. Yasuda and M. Hishinuma, in Proceedings of the 64th Annual Electrochemical Society of Japan, Extended Abstracts, Yokohoma, Japan, The Electrochemical Society of Japan, pp. 63, 1997
[46] F. Tietz, "Innovative Materials in Advanced Energy Technologies," in Proceedings of the 9th CIMTEC – World Ceramic Congress and Forum on New Materials, P. Vincenzini ed., Techna Publishers S.R.L., Faenza, Italy, 24, 61, 1999.
[47] F. Tietz, "Thermal Expansion of SOFC Materials," Ionics, 5 129-139 (1999).

Table 1. Thermal expansion coefficients for candidate SOFC electrolyte materials.

Anode (*fuel electrode*)

In the SOFC, the fuel arriving at the anode is generally reducing in nature. Thus, the fuel electrode must be stable in the reducing environment of the fuel, catalytic activity to hydrogen and hydrocarbons oxidation and with high ionic and electronic conductivity over a wide pO_2 range. Especially in the anode supported SOFC design it must have sufficient porosity to allow the transport of the fuel to and the transport of the products of fuel oxidation away from the electrolyte / fuel electrode interface where the fuel oxidation reaction takes place, i.e.:

$$O^{2-}(s) + H_2(g) = H_2O(g) + 2e^- \qquad (16)$$

Furthermore, the anode must be characterised by chemical and physical compatibility with surrounding components.

Stability and compatibility of the anode applies to both chemical and dimensional/phase changes, which could occur due to interactions with other SOFC components, the highly reducing atmosphere, the byproduct water vapour, CO_2 and/or the 450-1000ºC operating temperatures [48, 49].

In order to perform its proper electrochemical functions, the anode must be able to transport oxygen ions to the active oxidation sites as well as product electrons away from the active sites. Since there are no adequate mixed-conducting materials available to perform both functions, ceramic-metallic or 'cermet' composites of electronic and ionic conducting materials are used.

The reducing conditions present on the fuel side of an SOFC permit the use of a metal such as nickel as the fuel electrode. Alternatively, cobalt or ruthenium and noble metals are good choices as SOFC anode since they have excellent electrical conductivities in reducing atmosphere. Among them, Ni and Cu are the most popular ones owing to excellent catalytic properties for breaking hydrogen bonds, for the low reactivity with other components and they fairly low cost [50]. However, the thermal expansion of nickel is considerably larger than that of YSZ. Nickel can also sinter at the cell operating

[48] N.Q. Minh and T .Takahashi, Science and Technology of Ceramic Fuel Cells. Elsevier Science B.V., Amsterdam, The Netherlands, 1995.
[49] N.Q. Minh, "Ceramic Fuel Cells," J. Am .Cer. Soc., 76[3], 563-588 (1993).
[50] B.C.H. Steele, 'Materials for fuel cell technology', Nature 414, 345-352, 2001.

temperature resulting in a decrease in the fuel electrode porosity. These problems are circumvented by forming a skeleton of electrolyte ceramic around the nickel particles. The ceramic electrolyte skeleton prevents sintering of the nickel particles, decreases the fuel electrode thermal expansion coefficient bringing it closer to that of the electrolyte minimising the TEC mismatch, and provides better adhesion of the fuel electrode with the electrolyte. In addition, it operate to increase the triple phase boundary (TPB).

Porosity is engineered into the structure through addition of pore forming agents to the ceramic-metallic composite as well as the increased volume associated with the reduction of NiO to Ni.

Percolation theory relates the volume fraction of each component within a composite to the connectivity of those phases. As a rough estimate, for three phases to achieve connectivity within a composite, each should be 33 volume %. The content of anode cermets is traditionally aimed at achieving percolation between the metallic, ionic and porous phases, thus each phase should account for about 33% of the anode structure.

Electrocatalysis of hydrogen on metals such as Ni is relatively facile, and anode overpotentials are a small contribution to the overall drop in fuel cell voltage. The rate limiting step is the adsorption of hydrogen onto the metal surface, as opposed to the subsequent reaction of that hydrogen to yield protons and electrons.

Nickel is also an excellent catalyst for cracking of hydrocarbons under deposition of carbon. The carbon formation can cause clogging of gas channels, physical disintegration of the nickel structure and fragmentation of the porous anode.

Therefore nickel-based anodes are not suitable for direct operation in dry natural gas without modifications of the catalytic properties.

Another drawback of nickel is its reactivity at elevated temperature under high partial pressures of water, such as in partially spent fuel gas. Volatile $Ni(OH)_2$ is formed and it exerts a partial pressure of about 10^{-6} atm at 950°C [51]. This is not itself critical but due to the rapid passage of fuel gas, the formed $Ni(OH)_2$ is swept away, diminishing the long term stability of the anode. Equations 17-22 show the reaction that occur when methane is fed to a Ni-YSZ anode

$$CH_4 + H_2O \rightarrow CO + 3H_2 \quad (17)$$

$$H_2 + O^{2-} \rightarrow H_2O + 2e^- \quad (18)$$

$$CO + O^{2-} \rightarrow CO_2 + 2e^- \quad (19)$$

[51] A. Gubner, H. Landes, J. Metzger, H. Seeg and R. Stübner, SOFC V, U. Stimmimg, S.C. Singahl, H. Tagawa and W. Lehnert Eds., PV97-40, The Electrochem. Soc., Pennington, 540, 1997.

Steam reforming is associated with the following gas shift reaction, in which carbon monoxide is converted into hydrogen and carbon dioxide:

$$CO + H_2O \rightarrow CO_2 + H_2 \quad (20)$$

If the steam content in the feed gas is insufficient for reaction 1 to occur, carbon will be deposited according to:

$$CH_4 \rightarrow C + 2H_2 \quad (21)$$

$$2CO \rightarrow C + CO_2 \quad (22)$$

Based on these drawbacks, the ultimate objectives are the investigation of new Solid Oxide Fuel Cell anodes capable of efficient operation under hydrogen and hydrocarbons and which avoid the problems that the Ni based cermet anode presents.

During the past few years a lot of work has been done to investigate alternative anode materials, especially the mixed conducting ceramics like ceria, e.g. doped with gadolinium (GDC). As CeO_2 exhibits both ionic and some electronic conduction under reduction conditions, this material can be used for anodes without forming a composite [52]. Nevertheless this material presents a drawback, which is a redox change in volume for ceria as a consequence of part of the present Ce^{4+} being reduced

to Ce^{3+} under release of oxygen from the lattice. By partially doping with 10 mol% Gd this redox change in volume for ceria is reduced but not eliminated [53].

In recent reports where SOFCs directly utilised hydrocarbon fuels, alternative anode cermet compositions were used introducing metals such as Co, Ru, Cu and alloys of these metals with each other and with Ni, namely, Ni-ceria [54, 55], Cu-ceria [56, 57, 58], Ru-CGO [59]. However, there are still considerable limitations. Ni-ceria is not well suited for use with hydrocarbon fuels because the high Ni content (~50 vol %) promotes coking. Thus Ni-ceria was successfully used only with methane and at relatively low temperatures (~500°C). Moreover, British Gas [60] have examined the steam reforming rates of CH_4 over Ni-GDC anodes and obtained activation energy of 0.52 eV while using

---

[52] O.A. Marina, C. Bagger, S. Primdahl and M. Mogensen, 'A solid oxide fuel cell with gadolinia doped ceria anode: preparation and performance', Solid Oxide Fuel Cell 123, 199-208, 1999.
[53] S. Primdahl, PhD Thesis, University of Twente, The Netherlands, 1999.
[54] E.P. Murray, T. Tsai and S.A. Barnett, Nature 400, 649, 1999.
[55] E.P. Murray and S.A. Barnett, in Solid Oxide Fuel Cells VI, S.C. Singhal and M. Dokiya Eds., PV 99-19, The Electrochem. Soc. Proc. Series, Pennington, NJ, 1001, 1999.
[56] S.D. Park, J.M. Vohs and R.J. Gorte, Nature 404, 625, 2000.
[57] R.J. Gorte, S.D. Park, J.M. Vohs and C.H. Wang, Adv. Mater., 12, 1465, 2000.
[58] S.D. Park, R.J. Gorte and J.M. Vohs, Appl. Catal. A, 200, 55, 2000.
[59] M. Lo Faro, D. La Rosa, G. Monforte, V. Antonucci, A. S. Aricò, P. Antonucci, Journal Applied Electrochemistry, 37 (2007) 203-208
[60] British Gas, Investigation of Internal Reforming on Solid Oxide Fuel Cell Anodes. ETSU Report No. F/01/00013/REP. DTI. UK (ETSU, Harwell. Oxon., UK, 1995)

natural gas containing higher alkanes resulted in much higher activation energies (1.5-3.6 eV). Copper is, like nickel, an excellent electronic conductor, but is a poor catalyst towards hydrocarbon cracking. However Cu is not as good electrocatalyst as Ni. Furthermore, Cu has a relatively low melting point, and is thus tricky and limiting the high temperature SOFC fabrication techniques. Another disadvantage of using copper in anodes is the precipitation of Cu-metal between the anode and electrolyte after prolonged SOFC operation. This precipitation decreases the performance of the anode [61].

Stability and performance in hydrocarbon fuels is the single biggest challenge facing anode development. There have been considerable efforts to understand the mechanism of anode poisoning and to improve the design of anodes, such that SOFC performance doesn't significantly degrade when carbon deposits occur.

La Rosa et al. [62, 63] have proposed Ni-Cu alloy combined with ceria for the direct utilization of hydrocarbons. The possibility to use this alloy is owing to the substitution of the Ni-Ni-Ni with Ni-Cu-Ni patterns avoiding the cracking process.

In the search for alternative anode materials that are capable to withstand sulfur contamination, volume instability upon redox cycling, and carbon deposition, perovskite oxides have drawn considerable attention. With these materials the catalytic oxidation of hydrocarbons appear to involve lattice oxygen (Mars van Krevelen mechanism), and there is also some evidence that the presence of protonic conductivity can also activate absorbed CH_4 molecules [64].

They can be easily substituted on the A and B sites with alkali earth and transition metal elements respectively. This allows interesting modifications of their electronic and catalytic properties. These perovskite materials are reported to be stable at operating temperature of SOFC (600-1000°C) and across a wide oxygen partial pressure range (1-10^{-20}atm)[65].

Accordingly Steele et al. [66] proposed the following criteria for the selection of alternative oxide anode materials:

---

[61] Gorte, R.J., Vohs, J.M., Journal of catalysis, vol. 216, 2003, p. 477 – 486, Novel SOFC anodes for the direct electrochemical oxidation of hydrocarbons

[62] A. Sin, E.Kopnin, Y. Doubitsky, A. Zaopo, A.S. Aricò, L.R. Gullo, D. La Rosa, V. Antonucci, CNR ITAE. Journal of Power Sources 164 (2007) 300-305

[63] D. La Rosa, M. Lo Faro, V. Antonucci, A. S. Aricò, G. Monforte, Sin Agusti, 10th Symposium on Solid Oxide Fuel Cells, 2007

[64] C.B. Alcock, J. Catal. 140 (1993) 557

[65] M. Guilodo, E. Djurado, P. Vernoux ,"Catalytic and Electrochemical Properties of Doped Lanthanum Chromites as New Anode Materials for SOFC", J. Am. Ceram. Soc. October 2001.

[66] B.C.H Steele, P. H. Middleton and R.A. Rudkin, Solid State Ionics 40/41 (1990) 810

1. Good electronic conductivity, preferably $>10^2$ S cm^{-1} at anode operating potentials (0.7-0.9 V). Probably n-type behaviour is preferable.
2. Predominant anion lattice disorder to enhance oxygen diffusion coefficients and possibly protonic conductivity.
3. High values for oxygen surface exchange kinetics.
4. Fabrication of adherent films with minimal processing problems.
5. Compatibility with solid electrolyte substrate (Thermal expansion and interdiffusion values).
6. Stability in anode environment including gaseous species H_2, H_2O, CO, CO_2, etc.

Interesting results have been obtained with lanthanum-doped strontium titanates [67]. It has been established that strontium titanate exhibits n-type semi-conducting behaviour when it is donor-doped (e.g. with La^{3+}, Y^{3+}) and/or exposed to a reducing atmosphere. It means that its electrical conductivity increases with increasing donor content and/or decreasing pO_2.

Lanthanum is an appropriate donor dopant because its radius (0.132 nm) is similar to that of Sr^{2+} (0.140 nm). Owing to the difference in valence between La^{3+} and the Sr^{2+}, introduction of La into the $SrTiO_3$ lattice requires that the lattice defect structure is modified to maintain electroneutrality. Under reducing conditions (low pO_2), it was concluded that the charge compensation for the La^{3+} becomes electronic in nature through the formation of electrons in the conduction band or (if the electron are localized) conversion of Ti^{4+} to Ti^{3+}[68, 69, 70].

A maximum solubility level of 40 at % for La in $La_xSr_{1-x}TiO_3$ has been previously reported[71]. Therefore, $La_{0.4}Sr_{0.6}TiO_3$ was synthesized and studied as a potential anode material for SOFC.

Recently, unusually high electrical conductivity has been observed for yttrium-doped $SrTiO_3$ (SYT) under reducing condition [72], therefore, $La_{0.3}Y_{0.1}Sr_{0.6}TiO_3$ was also considered as anode material for Solid Oxide Fuel Cell.

---

[67] O.A. Marina, N.L. Canfield, J.W. Stevenson, "Thermal, electrical, and electrocatalytical properties of lanthanum-doped strontium titanate," Solid State Ionics, 149 (2002) 21– 28.

[68] E. Ivers-Tiffe´ e, A. Weber, D. Herbstritt, "Materials and technologies for SOFC-components," J. Europ. Ceram. Soc. 21 (2001) 1805–1811.

[69] T. Suzuki, P. Jasinski, V. Petrovsky, H. U. Anderson, "The Optical Properties and Band Gap Energy of Nanocrystalline $La_{0.4}Sr_{0.6}TiO_3$ Thin Films", J. Am. Ceram. Soc., 88 [5] 1186–1189 (2005).

[70] O.A. Marina, N.L. Canfield, J.W. Stevenson, "Thermal, electrical, and electrocatalytical properties of lanthanum-doped strontium titanate," Solid State Ionics, 149 (2002) 21– 28.

[71] O.A. Marina, N.L. Canfield, J.W. Stevenson, "Thermal, electrical, and electrocatalytical properties of lanthanum-doped strontium titanate," Solid State Ionics, 149 (2002) 21– 28.

Liu et al. [73] have reported a composition consisting of a mixture of $La_{0.8}Sr_{0.2}Cr_{0.8}Mn_{0.2}O_{3-\delta}$, which is an electronic conductor, $Ce_{0.9}Gd_{0.1}O_{1.95}$ which is an ionically conducting oxide, and ~4wt% Ni. In this anode composition, the metallic component is mostly replaced by an electronically conducting ceramic that does not promote coking. With an oxide taking the role of electronic conductor, the amount of metal catalyst can be reduced low enough to eliminate coking. This composition shows performances comparable to Ni-GDC with hydrogen and methane, and can be also used with propane and butane, contrarily to Ni-GDC [74].

Interconnection

SOFC interconnect serves as electrical contact between the anode of one individual cell to the cathode of the neighbouring cell and as physical barrier for the protection of the cathode/anode material of one individual cell from the reducing/oxidizing environment of the neighbouring fuel/air channel. It must provides the conductive path for electrical current to pass between the electrodes and to the external circuit. In certain stack constructions, the interconnect also serves as a structural support material [75].
The requirements of the interconnection are the most severe of all cell components and include the following.
(a) Nearly 100% electronic conductivity but it must be ionically inert during SOFC operation.
(b) Stability in both oxidizing and reducing atmospheres at the cell operating temperature since it is exposed to air (or oxygen) on one side and fuel on the other.
(c) Low permeability for oxygen and hydrogen (gas-tightness) to minimize direct combination of oxidant and fuel during cell operation.
(d) A thermal expansion close to that of the air electrode and the electrolyte.
(e) Non-reactivity with the air electrode, electrolyte and the electric contact material (e.g. nickel).

---

[72] S. Hui, A. Petric, "Electrical Properties of Yttrium-Doped Strontium Titanate under Reducing Conditions," J. Electrochem. Soc., 149 J1-J10 2002
[73] J. Liu, B.D. Madsen, Z. Ji and S.A. Barnett, Electrochem. and Solid State Letters 5 (6) A122-A124, 2002.
[74] J. Liu, B.D. Madsen, Z. Ji and S.A. Barnett, Electrochem. and Solid State Letters 5 (6) A122-A124, 2002.
[75] T. Brylewski, M. Nanko, T. Maruyama, and K. Przybylski, "Application of Fe-16Cr ferritic alloy to interconnector for a solid oxide fuel cell." Solid State Ionics 143 (2001) 131-150.

(f) Reasonable costs

In order to meet these requirements, two classes of materials are commonly used for the interconnect, namely, ceramic and metallic materials.

Whereas ceramic interconnects played a dominant role in the early SOFC developments, metallic interconnects have been frequently used in recent developments. Both variants have benefits and disadvantages and the final choice is therefore always a compromise depending, among other aspects, on the design, the operating temperature, the required service life as well as on the material and production costs of these components.

Practically all the ceramic interconnects of present SOFC systems are based on the perovskite structure of the $LaCrO_3$ type. By modifying the stoichiometry with other elements it is possible to adapt this interconnect material with respect to thermal expansion and behaviour in the presence of reaction gases [76, 77].

However, the material costs of perovskites are rather high and their application as ceramic interconnect is only meaningful as long as the stack design requires only small amounts of the material. Furthermore, lanthanum chromites are often plasma-sprayed although this technique is expensive. In this case, however, one has to consider the frequently observed low sinterability of the interconnect material, which prevents gas-tightness and low-cost production by sintering since it requires sintering temperatures between 1450 and 1600 °C.

Whereas practically all activities are related to $LaCrO_3$ modifications for the ceramic interconnects, clearly more material systems are under development for the metallic interconnects.

In general, advantages for metallic arrangements are considered to be high electrical conductivity, good processability and the lower costs to be expected, whereas especially long-term resistance, corrosion behaviour, chromium evaporation and high expansion coefficients are disadvantageous.

The success of metallic interconnects for use in the SOFC system will decisively depend on solving of these problems.

The long-term stability of the metallic interconnect is essentially governed by its corrosion characteristics.

---

[76] T. Nishi, N. Hisatome, H. Yamamoto, N. Murakami, in: P. Vincenzini (Ed.), Proc. 9th Cimtec—World Forum on New Materials, Innovative Materials in Advanced Energy Technologies, vol. 24, Techna Publishers S.r.l, Faenza, Italy, 1999, p. 41.

[77] G. Pudmich, B.A. Boukamp, M. Gonzalez-Cuenza, W. Jungen, W. Zipprich, F. Tietz, Solid State Ionics 135 (2000) 433.

Though SOFCs operating at temperatures above 750°C are currently performing better, they also cost almost 8 times more than those operating below that temperature. Current the reason for this is the cost of ceramic interconnects that can withstand those operating temperatures. At over $200 per kW, ceramic interconnect materials alone account for 90 % of the total material costs for high temperature SOFCs. Lowering the operating temperature into a range where metallic interconnects can be used reduces the interconnect materials cost by 200 % to $10 per KW. Table 4 shows a comparison of the relative cost per KW for SOFCs using metallic or ceramic interconnect materials [78].

SOFC Component	Material cost for ceramic-based SOFC ($/KW)	Percent of Total Cost (%)	Material cost for Metallic-based SOFC ($/KW)	Percent of Total Cost (%)
Electrode Stack	22.6	9.875	22.6	69.325
Interconnects	206.25	90.125	10	30.675
Total	228.85		32.6	

Table 4. Relative cost per kW of SOFC materials in a stack with metallic-based interconnects and with ceramic-based interconnects.

The interconnect composition used for SOFC is dependent on the application and temperature range. The composition determines the physical properties of the alloy and further the temperature range at which the thermal properties mirror those of the electrolyte.

The materials used for interconnects involve nickel and often chromium forming ferritic-based alloys which ensure sufficiently high conductivity for thin oxide scales.

With respect to thermal expansion, electrical conductivity and corrosion behaviour, the Cr Fe_5 Y_2O_3 ODS alloy developed by Plansee in cooperation with Siemens shows excellent behaviour at temperatures up to 950 °C [79]. A disadvantage of the alloy produced by powder metallurgy is the currently high price which could be drastically reduced by suitable production techniques. From the aspect of costs, ferritic chromium steels are attractive candidates for metallic bipolar plates. On the one hand, they form chromium oxides, have a lower thermal expansion compared to austenitic alloys and can be mechanically easily deformed and machined.

[78] N.Q. Minh and T .Takahashi, Science and Technology of Ceramic Fuel Cells. Elsevier Science B.V., Amsterdam, The Netherlands, 1995.

[79] W. Thierfelder, H. Greiner, W. Ko¨ck, in: U. Stimming, S.C. Singhal, H. Tagawa, W. Lehnert (Eds.), Proc. 5th Int. Symp. Solid Oxide Fuel Cells (SOFC-V), The Electrochemical Society, Pennington, NJ, 1997, p. 1306.

On the other hand, they have a number of properties limiting their application such as lower high-temperature strength, insufficient corrosion protection at high temperatures and brittle phase formation.

R&D work on ferritic steels therefore concentrates on application temperatures <800 °C. The application range of interest for this material class coincides with the development goals for planar anode-supported fuel cells. For this reason, such materials are being used or developed by all companies and research institutions working on this concept (e.g. Sulzer, CFCL, Plansee, Sanyo, FZJ, Hitachi Metals, ThyssenKrupp) [80, 81, 82]. For example, some investigators turn to metallic interconnect materials such as ZMG232 and JS-3 (also called Crofer 22 APU), Haynes alloy series, stainless steels and Fe-16Cr alloy [83, 84, 85].

In general, it can be stated that the long-term corrosion behaviour of commercially available materials is not yet sufficient. For example, longevity for stationary applications has been predicted to be from 40,000-80,000 hrs and therefore degradation and aging mechanism must be reduced considerably [86]. Doping of the interconnect material with rare earth oxides has shown to increase lifetime by drastically reducing the oxidation rate, while having a negligible effect on the thermal properties [87]. In order to improve the oxidation resistance a multitude of rare-earth ions such as Y, Zr, La, Ce, Sm, Ta, Ti, W and spinel formers have been doped into the alloy compositions [88, 89, 90]. In addition,

---

[80] P.H. Hou, K. Huang, W.T. Bakkerm, in: S.C. Singhal, M. Dokiya (Eds.), Proc. 6th Int. Symp. Solid Oxide Fuel Cells (SOFC-VI), The Electrochemical Society, Pennington, NJ, 1999, p. 737.

[81] Th. Malkow, U. von der Crone, A.M. Laptev, T. Koppitz, U. Breuer, W.J. Quadakkers, in: U. Stimming, S.C. Singhal, H. Tagawa, W. Lehnert (Eds.), Proc. 5th Int. Symp. Solid Oxide Fuel Cells (SOFC-V), The Electrochemical Society, Pennington,NJ, 1997, p. 1244.

[82] Y. Miyake, Y. Akiyama, T. Yasuo, S. Taniguchi, M. Kadowaki, K. Nishio, Proc. Fuel Cell Seminar, Nov. 17– 20, Orlando, 1996, p. 36.

[83] H. Kurokawa, Y. Oyama, K. Kawamura, and T. Maruyama, "Hydrogen permeation through Fe-16Cr alloy interconnect in atmosphere simulating SOFC at 1073 K." Journal Of The Electrochemical Society 151 (2004) A1264-A1268.

[84] Z. G. Yang, M. S. Walker, P. Singh, J. W. Stevenson, and T. Norby, "Oxidation behavior of ferritic stainless steels under SOFC interconnect exposure conditions." Journal Of The Electrochemical Society 151 (2004) B669-B678.

[85] T. Brylewski, M. Nanko, T. Maruyama, and K. Przybylski, "Application of Fe-16Cr ferritic alloy to interconnector for a solid oxide fuel cell." Solid State Ionics 143 (2001) 131-150.

[86] H. Tu and U. Stimming, "Advances, Aging Mechanisms and Lifetime in Solid Oxide Fuel Cells," J. of Power Sources, 127, 284-293 (2004).

[87] B. Church, Fabrication and Characterization of Solid Oxide Fuel Cell Interconnect Alloys. PhD Thesis, School of Materials Science and Engineering, Georgia Institute of Technology, May 2006. Available at <http://etd.gatech.edu/theses>.

[88] W.Z. Zhu and S.C. Deevi, "Development of Interconnect Materials for Solid Oxide Fuel Cells," Mat. Sci and Eng. A, 348[1-2], 227-243 (2003).

[89] J.W. Fergus, "Metallic Interconnects for Solid Oxide Fuel Cells," Mat. Sci and Eng. A, 397[1-2], 271-283 (2005).

the contact resistance of an oxidized metallic interconnect is usually characterized in terms of area specific resistance (ASR) and the generally accepted value is less than 0.1 Ω cm^2 [91].

In operating high-temperature fuel cells with metallic interconnects, a time-dependent degradation is observed, which is attributable to poisoning of the active centres of the cathode by chromium evaporating from the interconnect. This familiar process, already described in the reaction 19 [92], is caused by highly volatile chromium species which form when chromium oxide is in contact with oxidizing gas atmospheres.

$$Cr_2O_3 + 1.5O_2 + H_2O \rightarrow 2CrO_2(OH)_2 \qquad (19)$$

$CrO_2(OH)_2$ and CrO_3 are particularly critical here [93] and can react with the perovskite of the cathode to more stable but less catalytically active Cr–Mn spinels [94].

At the anode side of the SOFC, the interconnect could encounter any number of different reducing gases. Therefore the interface would also be influenced by any reactions due to deposition of carbon and subsequent degradation that could potentially have drastic consequence modifying the physical properties than those of the parent metal and ruin the interface [95, 96].

Attempts are being made to reduce the damaging effect of chromium vapours on the cathode side by suitable protective layers of $LaCrO_3$ or by neutralizing the chromium atoms in the applied layers by gettering. Lanthanum chromite is a p-type conductor; its conductivity is due to a small polaron hopping from temperature to 1400°C at oxygen pressures as low as 10^{-18} atm. The conductivity is enhanced as lower valence ions (e.g. Ca, Mg, Sr, etc.) are substituted on either the La^{3+} or the Cr^{3+} sites. This development is most advanced for the Cr Fe_5 Y_2O_3 chromium-base interconnect, on which La–Sr–Cr oxides have yielded the best results [97]. Disadvantages of these materials include poor tolerance of sudden temperature changes, extreme sensitivity to oxygen partial pressure, Cr

---

[90] W.J. Quadakkers, T. Malkow, J. Piro´n-Abella´n, U. Flesch, V. Shemet, L. Singheiser, in: A.J. McEvoy (Ed.), Proc. 4th Eur. SOFC Forum, The European Fuel Cell Forum, Oberrohrdorf, Switzerland, 2000, p. 827.

[91] T. Brylewski, M. Nanko, T. Maruyama, and K. Przybylski, "Application of Fe-16Cr ferritic alloy to interconnector for a solid oxide fuel cell." Solid State Ionics 143 (2001) 131-150.

[92] Y. Matsuzaki and I. Yasuda, "Electrochemical Properties of a SOFC Cathode in Contact with a Chromium-Containing Alloy Separator," Solid State Ionics, 132, 271-278 (2000).

[93] K. Hilpert, D. Das, M. Miller, D.H. Peck, R. Weiß, J. Electrochem. Soc. 143 (1996) 3642.

[94] S.P. Jiang, J.P. Zhang, L. Apateanu, K. Fo¨ger, J. Electrochem. Soc. 147 (2000) 4013.

[95] L. Aguilar, S. Zha, S. Li, J. Winnick and M. Liu, "Sulfur-Tolerant Materials for the Hydrogen Sulfide SOFC," Electrochem. and Solid State Letts., 7[10], A324-A326 (2004).

[96] H. He, R.J. Gorte and J.M. Vohs, "Highly Sulfur Tolerant Cu-Ceria Anodes for SOFCs," Electrochem. and Solid State Letts., 8[6], A279-A280 (2005).

[97] R. Ruckda¨schel, R. Henne, G. Schiller, H. Greiner, in: U. Stimming, S.C. Singhal, H. Tagawa, W. Lehnert (Eds.), Proc. 5th Int. Symp. Solid Oxide Fuel Cells (SOFC-V), The Electrochemical Society, Pennington, NJ, 1997, p. 1273.

poisoning to electrodes, and difficulties in producing interconnectors with complex geometries.

Vacuum plasma spraying and physical vapour deposition have proved to be effective application processes [98, 99]. The best result so far has been obtained with a $La_{0.9}Sr_{0.1}CrO_3$ coating for operation temperatures of about 950 °C. At a temperature of 850 °C, the chromium vaporisation rate was only half as great [100].

Since no single alloy has thermal expansion characteristic identical to the electrolyte from room temperature to SOFC operating temperatures, an alloy has to be picked specifically for the application, as shown in Table 5[101].

Material	$\alpha*10^{-6}$ K^{-1} (25-800°C)	$\alpha*10^{-6}$ K^{-1} (25-1000°C)	Reference
Cr Fe_5 Y_2O_3	-	11.3	[102]
Cr Fe_5 Y_2O_3	11.3	12	[103]
X 10 CrAl 18 (1.4|742)	12.9	13.9	[104]
$La_{0.9}Sr_{0.1}CrO_3$	-	10.7	[105]
$La_{0.79}Sr_{0.2}CrO_3$	-	11.1	[106]
$La_{0.7}Ca_{0.3}Cr_{0.5}Ti_{0.5}O_3$	9.6	10.1	[107]
$La_{0.7}Sr_{0.3}Cr_{0.8}Ti_{0.2}O_3$	10.4	10.7	[108]

Except for the Cr-base material, the metallic interconnects are manufactured using the casting-rolling-(forging) route with mechanical machining of the semi-finished products.

[98] N. Oishi, Y. Yamazaki, in: S.C. Singhal, M. Dokiya (Eds.), Proc. 6th Int. Symp. Solid Oxide Fuel Cells (SOFC-VI), The Electrochemical Society, Pennington, NJ, 1999, p. 759.

[99] E. Batawi, A. Plas, W. Straub, K. Honegger, R. Diethelm, in: S.C. Singhal, M. Dokiya (Eds.), Proc. 6th Int. Symp. Solid Oxide Fuel Cells (SOFC-VI), The Electrochemical Society, Pennington, NJ, 1999, p. 767.

[100] C. Gindorf, K. Hilpert, H. Nabielek, L. Singheiser, R. Ruckdäschel, G. Schiller, in: A.J. McEvoy (Ed.), Proc. 4th Eur. SOFC Forum, vol. 2, The European Fuel Cell Forum, Oberrohrdorf, Switzerland, 2000, p. 845.

[101] K. Choy, W. Bai, S. Charojrochkul and B.C.H. Steele, "The Development of Intermediate Temperature Solid Oxide Fuel Cells for the Next Millennium," J. of Power Sources, 71 361-369 (1998).

[102] E. Koep, C. Compson, M. Zhou and M. Liu, "A Photolithographic Process for Investigation of Electrode Reaction Sites in Solid Oxide Fuel Cells," Solid State Ionics, 176, 1-8 (2005).

[103] F. Tietz, "Innovative Materials in Advanced Energy Technologies," in Proceedings of the 9th CIMTEC – World Ceramic Congress and Forum on New Materials, P. Vincenzini ed., Techna Publishers S.R.L., Faenza, Italy, 24, 61, 1999.

[104] F. Tietz, "Innovative Materials in Advanced Energy Technologies," in Proceedings of the 9th CIMTEC – World Ceramic Congress and Forum on New Materials, P. Vincenzini ed., Techna Publishers S.R.L., Faenza, Italy, 24, 61, 1999.

[105] N.Q. Minh, "Ceramic Fuel Cells," J. Am .Cer. Soc., 76[3], 563-588 (1993).

[106] H. U. Anderson, "Review of P-Type Doped Perovskite Materials for SOFC and other Applications," Solid State Ionics, 52, 33 (1992).

[107] F. Tietz, "Thermal Expansion of SOFC Materials," Ionics, 5 129-139 (1999).

[108] F. Tietz, "Thermal Expansion of SOFC Materials," Ionics, 5 129-139 (1999).

The solutions have not yet reached the cost goal. Intensive work is being performed to find cheaper solutions by simplifying and adapting the design and using other modern manufacturing techniques (e.g. punching, laser cutting, brazing, etc.).

Sealant

One of the major challenges for implementation of solid oxide fuel cells (SOFCs) is the development in design and in suitable sealant materials to separate each individual cell and the air and fuel. The harsh SOFC operation conditions of elevated temperatures (700-1000°C), oxidising, reducing, and moist environment, electrical loading, and thermal stresses from transient or steady-state operations have put great constraints in seal development. Useful power output requires series of single cells to be connected through gas tight seals, which illustrates the importance of developing reliable joining methods for such systems.

Candidate sealant or sealants must satisfy these requirements:

(a) Mechanical

- Hermetic/marginal leak rate
- TEC matching, or mitigation of TCE mismatch stresses (i.e. 9-13 10^{-6}/°C)
- Acceptable bond strength or compressive loading requirement (i.e. load frame design)
- Resistant to degradation due to thermal cycling/thermal shock
- Robustness under external static and dynamic forces

(b) Chemical

- Long-term chemical stability under simultaneous oxidizing/wet fuel environments
- Long-term chemical compatibility with adjacent sealing surfaces
- Resistance to hydrogen embitterment

(c) Electrical

- Non-conductive (non-shorting configuration, i.e. lower than 10^{-4} S cm^{-1})

(d) Design/fabrication

- Low cost
- Facile application/processing
- High reliability with respect to a achieving initial hermeticity (i.e. seal conforms to non-flat substrate surfaces).

- Acceptable sealing environment/temperature (i.e. has little effect on the subsequent performance of the stack)
- Design flexibility – for example, allows use of Ni-based alloys in the interconnect

To date, there are two approaches for SOFC seal development: glass/glass-ceramic seals and metallic brazing (no applied load during operation), mica-based compressive seals and metallic brazes (load applied to seal during operation). Inherent advantages and limitations are found with each method.

For example, a suitable glass system for sealing SOFCs stacks has sufficient viscosity, flow and adhesion to ensure the formation of a reliable interface during the sealing cycle but it also must be viscous enough to avoid creep during service while avoiding deleterious interfacial reactions. Moreover it is relatively simple method of bonding ceramic to metal. Nevertheless, the final glass and ceramic seals have been found unreliable due to the lack of their long-term stability at elevated temperatures and brittle fracture behaviour below their glass transition temperatures (T_g)[109, 110]. Degradation can be due to ionic diffusion leading to secondary phase formation as the glass reacts with the SOFC materials or can be due to reactions with the oxidizing and reducing atmospheres causing leaks[111, 112, 113, 114]. Glass seals also have difficulty relaxing to the thermal stresses of cycling and often crack the materials in which they are in contact.

Rather than using traditional glass-based materials, which provide a rigid seal, many groups are working with soft or compressive sealant materials such as various mica compositions or metallic gaskets, and ceramic fibre seals such as vermiculite and thermiculite, to construct a more flexible system. These solution is more forgiving seal in terms of thermal expansion mismatch because it is made of parallel layer that de-bond from each other under high temperatures. As a result, if a certain fuel cell component

[109] K. Eichler, G. Solow, P. Otschik and W. Schaffrath (1999) BAS (BaO·Al2O3·SiO2)-glasses for high temperature applications, J. European Ceramic Soc. 19(6/7) 1101–1104.

[110] Z.G. Yang, K.S. Weil, D.M. Paxton, K.D. Meinhardt and J. W. Stevenson (2003) Considerations of glass sealing solid oxide fuel cell stacks, in: J.E. Indacochea, J.N. DuPont, T.J. Lienert, W. Tillmann, N. Sobczak, W.F. Gale and M. Singh (Eds), Joining of Advanced and Specialty Materials V (ASM International, Materials Park, OH, USA), 40–48.

[111] Z. Yang, J.W. Stevenson, K.D. Meinhardt, "Chemical Interactions of Barium- Calcium Aluminosilicate-based Sealing Glasses with Oxidation Resistant Alloys," Solid State Ionics, 160, 213-225 (2003).

[112] S.-B. Sohn, S.-Y. Choi, G.-H. Kim, H.-S. Song and G.-D. Kim "Stable Sealing Glass for Solid Oxide Fuel Cells," J. of Non-Crystalline Solids, 297, 103-112 (2002).

[113] R. Zheng, S.R. Wang, H.W. Nie and T.-L. Wen "SiO2-CaO-B2O3-Al2O3 Ceramic Glaze as Sealant for Planar ITSOFC," J. of Power Sources, 128, 165-172 (2004).

[114] Y.-S. Chou and J.W. Stevenson, "Thermal Cycling and Degradation Mechanisms of Compressive Mica-Based Seals for Solid Oxide Fuel Cells," J. of Power Sources, 112, 376-383 (2002).

expands significantly more than an adjacent component, the gasket can mechanically de-couple the two components, preventing the build-up of destructive stresses.

Unfortunately, this technology remains incomplete, because of the lack of a reliable high-temperature sealing material that would form the basis of the compressive seal. Furthermore, these materials leak more than the rigid glass materials, but show better thermal cycling characteristics. In fact soft seals are not actually seals, but rather permeation resistors aimed to reduce leakage rates rather than eliminate them. An additional difficulty is in designing the load frame, as it must be capable of delivering moderate-to-high loads in a high temperature oxidizing environment over the entire period of stack operation.

Most research in this area involves a metallic gasket formed within or welded to the metallic interconnect. This metallic gasket consists of one or more thin deformable contours that will under pressure mate hermetically to the ceramic plate. The advantage to these seals is that since they do not bond the layers, they are free to expand differentially without building up stress during thermal cycling. Another advantage to these soft sealing systems is their ability to be readily disassembled.

Another type of soft seal based on ceramic materials is the application of mica as a gasket material [115]. Mica, a mineral composed of layers of thin plates, is suitable for high temperatures and has the ability to deform and compress due to the natural gaps between the plates. In both the case of mica and with the metallic compression seals, many problems have been encountered. In each case, the quality of the seal is a reflection on the flatness and smoothness of the surfaces to be mated. Minor defects in the ceramic fuel cell or the interconnect can eliminate the possibility of ever attaining a complete seal. Vermiculite and thermiculite represent an advancement of this concept, since they are free from components that would poison or inhibit the catalysts, are electrically insulating and have thermal resistance to above 1000°C and above of all they are not injurious. In addition, gaskets of complex shapes can be cut easily and are robust during stack assembly

[115] S. P. Simner and J.W. Stevenson, "Compressive Mica Seals for SOFC Applications," J. Power Sources, 102, 310-316 (2001).

World wide factories overview

Being essentially modular, SOFC systems will be highly attractive for the distributed power market where units can be sized and configured to meet a particular local power generation demand.

In an SOFC stack, single cells are connected in electrical series via a component called the interconnect.

One of the keys to commercialisation of SOFC-based power generation systems is a major reduction in costs of the SOFC stack. It is now widely accepted that planar cell and stack configurations offer the best prospect for commercially viable SOFC systems. Furthermore, the planar designs can be divided into stack systems with metallic or ceramic interconnect material as well as into cells with thick (electrolyte-supported) or thin (electrode-supported) membranes with thicknesses usually of 100–250 and 5–20 μm, respectively.

Such geometries offer high power densities and the potential for low-cost production of the cell and stack components.

Different processes are used for the low-cost fabrication of electrodes and electrolyte for the solid oxide fuel cell. The components produced must display specific properties to ensure cyclable and long-term stable operation in the fuel cell stack. In the case of electrolyte-supported cells (Table 2), the fabrication of the electrolyte and of the electrodes is dominated by tape casting and screen printing, respectively. Both fabrication processes are well-established methods in the electroceramics industry and a scale-up is easily feasible. The thickness of the components varies only little: the membrane foils have a thickness between 100 and 200 μm, and both the cathode and the anode are screen printed onto the electrolyte sheets with thicknesses of 40–60 μm. The tape cast electrolyte foils usually have a size of up to 10X10 cm, because larger tapes are difficult to handle after sintering.

Company	Country	Component	Material	Production process	Thickness	References
Sulzer Hexis	CH	Electrolyte	YSZ	Tape casting	Ns	[116]
		Cathode	(La, Sr)MnO_3	Screen printing	Ns	
		Anode	Ni/YSZ	Screen printing	Ns	
ECN/InDec	NL	Electrolyte	YSZ	Tape casting	Ns	[117, 118]

[116] R. Diethelm, E. Batawi, in: A.J. McEvoy (Ed.), Proc. 4th Eur. SOFC Forum, The European Fuel Cell Forum, Oberrohrdorf, Switzerland, 2000, p. 183.

[117] G.M. Christie, J.P.P. Huijsmans, in: U. Stimming, S.C. Singhal, H. Tagawa, W. Lehnert (Eds.), Proc. 5th Int. Symp. Solid Oxide Fuel Cells (SOFC-V), The Electrochemical Society, Pennington, NJ, 1997, p. 718.

		Cathode	(La, Sr)MnO_3	Screen printing	50µm (two layers)	[119, 120]
		Anode	Ni/YSZ	Screen printing	graded composite	[121]
Fraunhofer Ges., IKTS	D	Electrolyte	YSZ	Tape casting	150µm	[122]
		Cathode	(La, Sr)MnO_3	Screen printing	ns, two layers	[123]
		Anode	Ni/YSZ	Screen printing	Ns	
CFCL	AUS	Electrolyte	3YSZ, 8YSZ	Tape casting	100µm	[124, 125]
		Cathode	(La, Sr)MnO_3	Screen printing	50-60µm	[126, 127]
		Anode	Ni/YSZ	Screen printing	50µm	[128, 129]
SOFCo	USA	Electrolyte	YSZ, (Ce, Sm)O_2	Pressing and sintering	180µm, 300µm	[130, 131]
		Cathode	(La, Sr)CoO_3	Screen printing	ns	[132]
		Anode	Ni/YSZ	Screen printing	ns	[133]
Tokyo Gas	JP	Electrolyte	3YSZ	Tape casting	50-100µm	[134]
		Cathode	(La, Sr)MnO_3	Screen printing	150µm	[135]
		Anode	Ni/(Ce, Y)SZ	Screen printing	30µm	[136]

[118] G.M. Christie, J.P. Ouweltjes, R.C. Huiberts, E.J. Siewers, F.P.F. van Berkel, J.P.P. Huijsmans, Proc. 3rd Int. Fuel Cell Conf., Nagoya, Japan, 1999, p. 361.
[119] G.M. Christie, J.P.P. Huijsmans, in: U. Stimming, S.C. Singhal, H. Tagawa, W. Lehnert (Eds.), Proc. 5th Int. Symp. Solid Oxide Fuel Cells (SOFC-V), The Electrochemical Society, Pennington, NJ, 1997, p. 718.
[120] G.M. Christie, J.P. Ouweltjes, R.C. Huiberts, E.J. Siewers, F.P.F. van Berkel, J.P.P. Huijsmans, Proc. 3rd Int. Fuel Cell Conf., Nagoya, Japan, 1999, p. 361.
[121] G.M. Christie, J.P.P. Huijsmans, in: U. Stimming, S.C. Singhal, H. Tagawa, W. Lehnert (Eds.), Proc. 5th Int. Symp. Solid Oxide Fuel Cells (SOFC-V), The Electrochemical Society, Pennington, NJ, 1997, p. 718.
[122] M. Kuznecov, H. Greiner, M. Wohlfahrt, K. Eichler, P. Otschik, in: A.J. McEvoy (Ed.), Proc. 4th Eur. SOFC Forum, The European Fuel Cell Forum, Oberrohrdorf, Switzerland, 2000, p. 261.
[123] M. Kuznecov, H. Greiner, M. Wohlfahrt, K. Eichler, P. Otschik, in: A.J. McEvoy (Ed.), Proc. 4th Eur. SOFC Forum, The European Fuel Cell Forum, Oberrohrdorf, Switzerland, 2000, p. 261.
[124] K. Föger, B. Godfrey, in: A.J. McEvoy (Ed.), Proc. 4th Eur. SOFC Forum, The European Fuel Cell Forum, Oberrohrdorf, Switzerland, 2000, p. 167.
[125] R. Bolden, K. Föger, T. Pham, in: S.C. Singhal, M. Dokiya (Eds.), Proc. 6th Int. Symp. Solid Oxide Fuel Cells (SOFCVI), The Electrochemical Society, Pennington, NJ, 1999, p. 80.
[126] K. Föger, B. Godfrey, in: A.J. McEvoy (Ed.), Proc. 4th Eur. SOFC Forum, The European Fuel Cell Forum, Oberrohrdorf, Switzerland, 2000, p. 167.
[127] R. Bolden, K. Föger, T. Pham, in: S.C. Singhal, M. Dokiya (Eds.), Proc. 6th Int. Symp. Solid Oxide Fuel Cells (SOFCVI), The Electrochemical Society, Pennington, NJ, 1999, p. 80.
[128] K. Föger, B. Godfrey, in: A.J. McEvoy (Ed.), Proc. 4th Eur. SOFC Forum, The European Fuel Cell Forum, Oberrohrdorf, Switzerland, 2000, p. 167.
[129] R. Bolden, K. Föger, T. Pham, in: S.C. Singhal, M. Dokiya (Eds.), Proc. 6th Int. Symp. Solid Oxide Fuel Cells (SOFCVI), The Electrochemical Society, Pennington, NJ, 1999, p. 80.
[130] A. Khandkar, S. Elangovan, J. Hartvigsen, D. Rowley, R. Privette, M. Tharp, in: S.C. Singhal, M. Dokiya (Eds.), Proc. 6th Int. Symp. Solid Oxide Fuel Cells (SOFC-VI), The
[131] W. Bakker, C. Milliken, J. Hartvigsen, S. Elangovan, A. Khandkar, in: U. Stimming, S.C. Singhal, H. Tagawa, W. Lehnert (Eds.), Proc. 5th Int. Symp. Solid Oxide Fuel Cells (SOFC-V), The Electrochemical Society, Pennington, NJ, 1997, p. 254.
[132] W. Bakker, C. Milliken, J. Hartvigsen, S. Elangovan, A. Khandkar, in: U. Stimming, S.C. Singhal, H. Tagawa, W. Lehnert (Eds.), Proc. 5th Int. Symp. Solid Oxide Fuel Cells (SOFC-V), The Electrochemical Society, Pennington, NJ, 1997, p. 254.
[133] W. Bakker, C. Milliken, J. Hartvigsen, S. Elangovan, A. Khandkar, in: U. Stimming, S.C. Singhal, H. Tagawa, W. Lehnert (Eds.), Proc. 5th Int. Symp. Solid Oxide Fuel Cells (SOFC-V), The Electrochemical Society, Pennington, NJ, 1997, p. 254.
[134] K. Ogasawara, I. Yasuda, Y. Matsuzaki, T. Ogiwara, M. Hishinuma, in: U. Stimming, S.C. Singhal, H. Tagawa, W. Lehnert (Eds.), Proc. 5th Int. Symp. Solid Oxide Fuel Cells (SOFC-V), The Electrochemical Society, Pennington, NJ, 1997, p. 143.
[135] K. Ogasawara, I. Yasuda, Y. Matsuzaki, T. Ogiwara, M. Hishinuma, in: U. Stimming, S.C. Singhal, H. Tagawa, W. Lehnert (Eds.), Proc. 5th Int. Symp. Solid Oxide Fuel Cells (SOFC-V), The Electrochemical Society, Pennington, NJ, 1997, p. 143.

Mitsui Eng. & Shipbuilding	JP	Electrolyte	8YSZ	Tape casting	300µm	[137, 138]
		Cathode	(La, Sr)(Mn, Cr) O_3	Painting	150µm	[139, 140]
		Anode	Ni/YSZ	Painting	150µm	[141, 142]

ns=not specified

Table 2. Developers of SOFC in electrolyte-supported planar cell design and corresponding fabrication and design details

Other developers aiming at the kW range during the next few years prefer planar anode-supported SOFCs owing to their potential of lowering the operating temperature. Several companies and research organizations in Australia, America and Europe have concentrated on cells with a thick, porous anode substrate and a 5–20 µm thin electrolyte membrane. Besides the frequently used ceramic processing techniques, i.e. tape casting and screen printing, also alternative methods like warm pressing, tape calendaring and wet powder spraying are under investigation.

The main selection criteria for the future fabrication route are the cost aspects, the potential for automation, reproducibility and precision of the different techniques.

In the anode substrate concept the anode is the supporting component of the cell and must therefore display sufficient mechanical stability. The substrates are predominantly produced by tape casting. Pressing processes and extrusion moulding are very rarely applied.

The reason is presumably that the substrates in such processing routes can hardly be fabricated thinner than 1 or 1.5 mm and most of the developers aim at substrates with thicknesses of around 0.5 mm.

Usually an anode functional layer of a few micrometers in thickness is then deposited onto the substrate to enhance the electrochemical performance [143]. A widely used

---

136 K. Ogasawara, I. Yasuda, Y. Matsuzaki, T. Ogiwara, M. Hishinuma, in: U. Stimming, S.C. Singhal, H. Tagawa, W. Lehnert (Eds.), Proc. 5th Int. Symp. Solid Oxide Fuel Cells (SOFC-V), The Electrochemical Society, Pennington, NJ, 1997, p. 143.

137 M. Izumi, T. Makino, N. Nishimura, K. Murata, M. Shimotsu, Proc. 3rd Int. Fuel Cell Conf., Nagoya, Japan, 1999, p. 379.

138 M. Shimotsu, M. Izumi, K. Murata, in: S.C. Singhal, H. Iwahara (Eds.), Proc. 3rd Int. Symp. Solid Oxide Fuel Cells (SOFC-III), The Electrochemical Society, Pennington, NJ, 1993, p. 732.

139 M. Izumi, T. Makino, N. Nishimura, K. Murata, M. Shimotsu, Proc. 3rd Int. Fuel Cell Conf., Nagoya, Japan, 1999, p. 379.

140 M. Shimotsu, M. Izumi, K. Murata, in: S.C. Singhal, H. Iwahara (Eds.), Proc. 3rd Int. Symp. Solid Oxide Fuel Cells (SOFC-III), The Electrochemical Society, Pennington, NJ, 1993, p. 732.

141 M. Izumi, T. Makino, N. Nishimura, K. Murata, M. Shimotsu, Proc. 3rd Int. Fuel Cell Conf., Nagoya, Japan, 1999, p. 379.

142 M. Shimotsu, M. Izumi, K. Murata, in: S.C. Singhal, H. Iwahara (Eds.), Proc. 3rd Int. Symp. Solid Oxide Fuel Cells (SOFC-III), The Electrochemical Society, Pennington, NJ, 1993, p. 732.

deposition technique for the thin anode, electrolyte and cathode layers is screen printing (Table 3).

In few cases slip casting and wet powder spraying is applied, whereas magnetron sputtering is a curiosity for achieving very thin layers rather than a realistic approach for cost-effective products with high throughput. Also rather seldom is plasma spraying either as vacuum plasma spraying (VPS) for anodes and electrolytes [144] or as atmospheric (APS) or flame spraying (FS) for electrolytes and cathodes [145]. However, the cost targets of commercial SOFC are difficult to achieve with plasma spraying techniques.

Apart from tape casting, calendering, screen printing, slip casting, plasma spraying, wet powder spraying, electrochemical vapour deposition for the manufacturing of electrolytes or the coating of substrates with electrolyte layers, other methods have been applied and tested such as laser ablation, multiple spin coating, colloidal deposition, reactive magnetron sputtering, chemical vapour deposition, spray pyrolysis and electrophoresis.

All these alternative methods are of scientific interest rather than having the potential to be commercially relevant. A brief overview is also provided by Minh [146].

Company	Country	Component	Material	Production process	Thickness	References
Sulzer Hexis	CH	Anode	Ni/YSZ	Tape casting	250-500µm	[147]
		Electrolyte	YSZ/(Ce, Y)O_2	Reactive magnetron sputtering	5/1µm	[148]
		Cathode	$La_{0.6}Sr_{0.4}Co_{0.2}Fe_{0.8}O_3$	Screen printing	ns	[149]
ECN/InDec	NL	Anode substrate	Ni/YSZ	Tape casting	500-800µm	[150, 151, 152]

[143] H.P. Buchkremer, U. Diekmann, L.G.J. de Haart, H. Kabs, U. Stimming, D. Stöver, in: U. Stimming, S.C. Singhal, H. Tagawa, W. Lehnert (Eds.), Proc. 5th Int. Symp. Solid Oxide Fuel Cells (SOFC-V), The Electrochemical Society, Pennington, NJ, 1997, p. 160.

[144] M. Lang, R. Henne, G. Schiller, N. Wagner, in: U. Stimming, S.C. Singhal, H. Tagawa, W. Lehnert (Eds.), Proc. 5th Int. Symp. Solid Oxide Fuel Cells (SOFC-V),

[145] T. Iwata, N. Kadokawa, S. Takenoiri, in: M. Dokyia, O. Yamamoto, H. Tagawa, S.C. Singhal (Eds.), Proc. 4th Int. Symp. Solid Oxide Fuel Cells (SOFC-IV), The Electrochemical Society, Pennington, NJ, 1997, p. 110.

[146] N.Q. Minh, in: S.C. Singhal, M. Dokiya (Eds.), Proc. 6th Int. Symp. Solid Oxide Fuel Cells (SOFC-VI), The Electrochemical Society, Pennington, NJ, 1999, p. 127.

[147] K. Honegger, E. Batawi, Ch. Sprecher, R. Diethelm, in: U. Stimming, S.C. Singhal, H. Tagawa, W. Lehnert (Eds.), Proc. 5th Int. Symp. Solid Oxide Fuel Cells (SOFC-V), The Electrochemical Society, Pennington, NJ, 1997, p. 321.

[148] K. Honegger, J. Krumeich, R. Diethelm, in: A.J. McEvoy (Ed.), Proc. 4th Eur. SOFC Forum, The European Fuel Cell Forum, Oberrohrdorf, Switzerland, 2000, p. 29.

[149] K. Honegger, J. Krumeich, R. Diethelm, in: A.J. McEvoy (Ed.), Proc. 4th Eur. SOFC Forum, The European Fuel Cell Forum, Oberrohrdorf, Switzerland, 2000, p. 29.

[150] G.M. Christie, J.P.P. Huijsmans, in: U. Stimming, S.C. Singhal, H. Tagawa, W. Lehnert (Eds.), Proc. 5th Int. Symp. Solid Oxide Fuel Cells (SOFC-V), The Electrochemical Society, Pennington, NJ, 1997, p. 718.

[151] G.M. Christie, J.P. Ouweltjes, R.C. Huiberts, E.J. Siewers, F.P.F. van Berkel, J.P.P. Huijsmans, Proc. 3rd Int. Fuel Cell Conf., Nagoya, Japan, 1999, p. 361.

		Anode	Ni/YSZ	Screen printing	3-7µm	[153]
		Electrolyte	YSZ	Screen printing	7-10µm	[154]
		Cathode	(La, Sr)MnO_3+YSZ	Screen printing	ns	[155]
FZJ	D	Anode substrate	Ni/YSZ	Tape casting	200-500µm	[156]
		Anode substrate	Ni/YSZ	Warm pressing	1500µm	[157, 158]
		Anode	Ni/YSZ	Vacuum slip casting	5-15µm	[159, 160]
		Electrolyte	YSZ	Vacuum slip casting	5-30µm	[161]
		Electrolyte	YSZ	Reactive magnetron sputtering	2-10µm	[162]
		Cathode	(La, Sr)MnO_3+YSZ	Wet powder spraying	50µm	[163, 164]
Risø	DK	Anode substrate	Ni/YSZ	Tape casting	200-300µm	[165]
		Electrolyte	YSZ	Wet powder spraying	10-25µm	[166]
		Cathode	(La, Sr)MnO_3+YSZ	Screen printing	50µm	[167]

[152] J.P. Ouweltjes, F.P.F. van Berkel, P. Nammensma, G.M. Christie, in: S.C. Singhal, M. Dokiya (Eds.), Proc. 6th Int. Symp.Solid Oxide Fuel Cells (SOFC-VI), The Electrochemical Society, Pennington, NJ, 1999, p. 803.

[153] J.P. Ouweltjes, F.P.F. van Berkel, P. Nammensma, G.M. Christie, in: S.C. Singhal, M. Dokiya (Eds.), Proc. 6th Int. Symp.Solid Oxide Fuel Cells (SOFC-VI), The Electrochemical Society, Pennington, NJ, 1999, p. 803.

[154] G.M. Christie, P. Nammensma, J.P.P. Huijsmans, in: A.J. McEvoy (Ed.), Proc. 4th Eur. SOFC Forum, The European Fuel Cell Forum, Oberrohrdorf, Switzerland, 2000, p. 3.

[155] J.P. Ouweltjes, F.P.F. van Berkel, P. Nammensma, G.M. Christie, in: S.C. Singhal, M. Dokiya (Eds.), Proc. 6th Int. Symp.Solid Oxide Fuel Cells (SOFC-VI), The Electrochemical Society, Pennington, NJ, 1999, p. 803.

[156] D. Simwonis, H. Thu¨len, F.J. Dias, A. Naoumidis, D. Stöver, J. Mater. Process. Technol. 92–93 (1999) 107.

[157] H.P. Buchkremer, U. Diekmann, L.G.J. de Haart, H. Kabs, U. Stimming, D. Stöver, in: U. Stimming, S.C. Singhal, H. Tagawa, W. Lehnert (Eds.), Proc. 5th Int. Symp. Solid Oxide Fuel Cells (SOFC-V), The Electrochemical Society, Pennington, NJ, 1997, p. 160.

[158] D. Sto¨ver, U. Diekmann, U. Flesch, H. Kabs, W.J. Quadakkers, F. Tietz, I.C. Vinke, in: S.C. Singhal, M. Dokiya (Eds.), Proc. 6th Int. Symp. Solid Oxide Fuel Cells (SOFC-VI), The Electrochemical Society, Pennington, NJ, 1999, p. 813.

[159] H.P. Buchkremer, U. Diekmann, L.G.J. de Haart, H. Kabs, U. Stimming, D. Stöver, in: U. Stimming, S.C. Singhal, H. Tagawa, W. Lehnert (Eds.), Proc. 5th Int. Symp. Solid Oxide Fuel Cells (SOFC-V), The Electrochemical Society, Pennington, NJ, 1997, p. 160.

[160] D. Sto¨ver, U. Diekmann, U. Flesch, H. Kabs, W.J. Quadakkers, F. Tietz, I.C. Vinke, in: S.C. Singhal, M. Dokiya (Eds.), Proc. 6th Int. Symp. Solid Oxide Fuel Cells (SOFC-VI), The Electrochemical Society, Pennington, NJ, 1999, p. 813.

[161] H.P. Buchkremer, U. Diekmann, L.G.J. de Haart, H. Kabs, U. Stimming, D. Stöver, in: U. Stimming, S.C. Singhal, H. Tagawa, W. Lehnert (Eds.), Proc. 5th Int. Symp. Solid Oxide Fuel Cells (SOFC-V), The Electrochemical Society, Pennington, NJ, 1997, p. 160.

[162] B. Hobein, F. Tietz, D. Sto¨ver, M. C ˇ ekada, P. Panjan, J. Eur. Ceram. Soc. 21 (2001) 1843.

[163] H.P. Buchkremer, U. Diekmann, L.G.J. de Haart, H. Kabs, U. Stimming, D. Stöver, in: U. Stimming, S.C. Singhal, H. Tagawa, W. Lehnert (Eds.), Proc. 5th Int. Symp. Solid Oxide Fuel Cells (SOFC-V), The Electrochemical Society, Pennington, NJ, 1997, p. 160.

[164] R. Wilkenho¨ner, W. Malle´ner, H.P. Buchkremer, T. Hauber, U. Stimming, in: B. Thorstensen (Ed.), Proc. 2nd Eur. SOFC Forum, vol. 1, The European Fuel Cell Forum, Oberrohrdorf, Switzerland, 1996, p. 279.

[165] S. Primdahl, M.J. Jørgensen, C. Bagger, B. Kindl, in: S.C. Singhal, M. Dokiya (Eds.), Proc. 6th Int. Symp. Solid Oxide Fuel Cells (SOFC-VI), The Electrochemical Society, Pennington, NJ, 1999, p. 793.

[166] M.J. Jørgensen, P.H. Larsen, S. Primdahl, C. Bagger, in: A.J. McEvoy (Ed.), Proc. 4th Eur. SOFC Forum, The European Fuel Cell Forum, Oberrohrdorf, Switzerland, 2000, p. 203.

[167] M.J. Jørgensen, P.H. Larsen, S. Primdahl, C. Bagger, in: A.J. McEvoy (Ed.), Proc. 4th Eur. SOFC Forum, The European Fuel Cell Forum, Oberrohrdorf, Switzerland, 2000, p. 203.

Global Thermoelectric	CAN	Anode substrate	Ni/YSZ	Tape casting	1000µm	[168]
		Electrolyte	YSZ	Vacuum slip casting	10µm	[169]
		Electrolyte	YSZ	Screen printing	ns	[170]
		Cathode	(La, Sr)MnO_3	Screen printing	40µm	[171]
Allied Signal	USA	Anode	Ni/YSZ	Tape casting and calendaring	100µm	[172, 173]
		Electrolyte	YSZ	Tape calendaring	5-10µm	[174, 175]
		Cathode	Doped $LaMnO_3$	Tape calendaring	ns	[176]
CFCL	AUS	Anode substrate	Ni/YSZ	Tape casting	500-700µm	[177, 178, 179]
		Electrolyte	YSZ	Lamination and sintering	10-30µm	[180, 181]
		Electrolyte	YSZ	Reactive magnetron sputtering	<16µm	[182]
		Cathode	(La, Sr)MnO_3	Screen printing	Ns	[183, 184]
Mitsui Eng. & Shipbuilding	JP	Anode substrate	Ni/YSZ	Ns	1000µm	[185]

[168] D. Gosh, G. Wang, R. Brule, E. Tang, P. Huang, in: S.C. Singhal, M. Dokiya (Eds.), Proc. 6th Int. Symp. Solid Oxide Fuel Cells (SOFC-VI), The Electrochemical Society, Pennington, NJ, 1999, p. 822.
[169] D. Gosh, G. Wang, R. Brule, E. Tang, P. Huang, in: S.C. Singhal, M. Dokiya (Eds.), Proc. 6th Int. Symp. Solid Oxide Fuel Cells (SOFC-VI), The Electrochemical Society, Pennington, NJ, 1999, p. 822.
[170] M. Pastula, R. Boersma, D. Prediger, M. Perry, A. Horvath, J. Devitt, D. Gosh, in: A.J. McEvoy (Ed.), Proc. 4th Eur. SOFC Forum, The European Fuel Cell Forum, Oberrohrdorf, Switzerland, 2000, p. 123.
[171] D. Gosh, G. Wang, R. Brule, E. Tang, P. Huang, in: S.C. Singhal, M. Dokiya (Eds.), Proc. 6th Int. Symp. Solid Oxide Fuel Cells (SOFC-VI), The Electrochemical Society, Pennington, NJ, 1999, p. 822.
[172] N.Q. Minh, K. Montgomery, in: U. Stimming, S.C. Singhal, H. Tagawa, W. Lehnert (Eds.), Proc. 5th Int. Symp. Solid Oxide Fuel Cells (SOFC-V), The Electrochemical Society, Pennington, NJ, 1997, p. 153.
[173] N.Q. Minh, T.R. Amstrong, J.R. Esopa, J.V. Guiheen, C.R. Horne, J. Van Ackeren, in: S.C. Singhal, H. Iwahara (Eds.), Proc. 3rd Int. Symp. Solid Oxide Fuel Cells (SOFC-III), The Electrochemical Society, Pennington, NJ, 1993, p. 801.
[174] N.Q. Minh, K. Montgomery, in: U. Stimming, S.C. Singhal, H. Tagawa, W. Lehnert (Eds.), Proc. 5th Int. Symp. Solid Oxide Fuel Cells (SOFC-V), The Electrochemical Society, Pennington, NJ, 1997, p. 153.
[175] N.Q. Minh, in: M. Dokiya, O. Yamamoto, H. Tagawa, S.C. Singhal (Eds.), Proc. 4th Int. Symp. Solid Oxide Fuel Cells (SOFC-IV), The Electrochemical Society, Pennington, NJ, 1995, p. 138.
[176] N.Q. Minh, in: M. Dokiya, O. Yamamoto, H. Tagawa, S.C. Singhal (Eds.), Proc. 4th Int. Symp. Solid Oxide Fuel Cells (SOFC-IV), The Electrochemical Society, Pennington, NJ, 1995, p. 138.
[177] K. Föger, B. Godfrey, in: A.J. McEvoy (Ed.), Proc. 4th Eur. SOFC Forum, The European Fuel Cell Forum, Oberrohrdorf, Switzerland, 2000, p. 167.
[178] R. Bolden, K. Fo¨ger, T. Pham, in: S.C. Singhal, M. Dokiya (Eds.), Proc. 6th Int. Symp. Solid Oxide Fuel Cells (SOFCVI), The Electrochemical Society, Pennington, NJ, 1999, p. 80.
[179] K. Föger, R. Donelson, R. Ratnaraj, in: S.C. Singhal, M. Dokiya (Eds.), Proc. 6th Int. Symp. Solid Oxide Fuel Cells (SOFC-VI), The Electrochemical Society, Pennington, NJ, 1999, p. 95.
[180] R. Bolden, K. Fo¨ger, T. Pham, in: S.C. Singhal, M. Dokiya (Eds.), Proc. 6th Int. Symp. Solid Oxide Fuel Cells (SOFCVI), The Electrochemical Society, Pennington, NJ, 1999, p. 80.
[181] K. Föger, R. Donelson, R. Ratnaraj, in: S.C. Singhal, M. Dokiya (Eds.), Proc. 6th Int. Symp. Solid Oxide Fuel Cells (SOFC-VI), The Electrochemical Society, Pennington, NJ, 1999, p. 95.
[182] P.K. Srivastava, T. Quach, Y.Y. Duan, R. Donelson, S.P. Jiang, F.T. Ciacchi, S.P.S. Badwal, Solid State Ionics 99 (1997) 311.
[183] R. Bolden, K. Fo¨ger, T. Pham, in: S.C. Singhal, M. Dokiya (Eds.), Proc. 6th Int. Symp. Solid Oxide Fuel Cells (SOFCVI), The Electrochemical Society, Pennington, NJ, 1999, p. 80.
[184] K. Föger, R. Donelson, R. Ratnaraj, in: S.C. Singhal, M. Dokiya (Eds.), Proc. 6th Int. Symp. Solid Oxide Fuel Cells (SOFC-VI), The Electrochemical Society, Pennington, NJ, 1999, p. 95.
[185] M. Izumi, T. Makino, N. Nishimura, K. Murata, M. Shimotsu, Proc. 3rd Int. Fuel Cell Conf., Nagoya, Japan, 1999, p. 379.

		Electrolyte	8YSZ	Ns	30µm	[186]
		Cathode	(La, Sr)(Mn, Cr) O_3	Ns	150µm	[187]
Eurocoating	IT	Anode substrate	Ni/YSZ	Tape casting and coopressing	1000µm	[188]
		Anode	Ni/YSZ	Tape casting and coopressing	15µm	[189]
		Electrolyte	YSZ	Tape casting and coopressing	10µm	[190]
		Porous electrolyte	YSZ	Tape casting and coopressing	15µm	[191]
		Cathode	(La, Sr)MnO_3	Vacuum gel permeation and screen printing	50µm	[192]

ns=not specified

Table 3 Developers of SOFC in anode-supported planar cell design and corresponding fabrication and design details

[186] M. Izumi, T. Makino, N. Nishimura, K. Murata, M. Shimotsu, Proc. 3rd Int. Fuel Cell Conf., Nagoya, Japan, 1999, p. 379.
[187] M. Izumi, T. Makino, N. Nishimura, K. Murata, M. Shimotsu, Proc. 3rd Int. Fuel Cell Conf., Nagoya, Japan, 1999, p. 379.
[188] D. Montinaro, V.M. Sglavo, M. Bertoldi, T. Zandonella, A. Aricò, M. Lo Faro, V. Antonucci, Solid State Ionics 177 (2006) 2093–2097
[189] D. Montinaro, V.M. Sglavo, M. Bertoldi, T. Zandonella, A. Aricò, M. Lo Faro, V. Antonucci, Solid State Ionics 177 (2006) 2093–2097
[190] D. Montinaro, V.M. Sglavo, M. Bertoldi, T. Zandonella, A. Aricò, M. Lo Faro, V. Antonucci, Solid State Ionics 177 (2006) 2093–2097
[191] D. Montinaro, V.M. Sglavo, M. Bertoldi, T. Zandonella, A. Aricò, M. Lo Faro, V. Antonucci, Solid State Ionics 177 (2006) 2093–2097
[192] D. Montinaro, V.M. Sglavo, M. Bertoldi, T. Zandonella, A. Aricò, M. Lo Faro, V. Antonucci, Solid State Ionics 177 (2006) 2093–2097

3

THERMODINAMICS and KINETICS of SOFCs

Connected to an external load, the potential difference across the electrodes of a fuel cell drives the electrons through the external circuit. However, the detailed processes in the electrochemical system are quite complex in nature.

Even though many studies have been devoted to the charge transfer at the interfaces formed by the electrodes and solid electrolyte, it still remains one of the least understood aspects of electrochemistry.

The operation of the cell is associated with various irreversibilities and leads to various potential losses. In the case of electrodes, the total resistance comprises of the internal resistance, contact resistance, activation polarization resistance, and concentration polarization resistance. Internal resistance refers to the resistance for electron transport in the electrode and ionic transport in the electrolyte which are determined by the electronic and ionic conductivity respectively and the thickness of the electrode and electrolyte. Contact resistance refers to the poor contact between the electrode and the electrolyte structure. All resistive losses are functions of the local current density. The overpotential losses can be minimized by an appropriate choice of electrode material and the control of the micro-structural properties during the manufacturing process.

SOFC characteristics

The maximum electrical work (W_{el}) obtainable in a fuel cell operating at constant temperature and pressure is given by the change in Gibbs free energy (ΔG) of the electrochemical reaction:

$$W_{el} = \Delta G = -nFE \quad (1)$$

Where n is the number of electrons participating in the reaction, F is Faraday's constant (96487 coulombs/g-mole electron), and E is the ideal potential of the cell.

The Gibbs free energy change is also given by the following state function:

$$\Delta G = \Delta H - T\Delta S \quad (2)$$

where ΔH is the enthalpy change and ΔS is the entropy change. The total thermal energy available is ΔH. It represents the heat absorbed or released by a generic chemical reaction, with a negative value (-ΔH) indicating an exothermal reaction. The available free energy is equal to the enthalpy change less the quantity TΔS which represents the unavailable energy resulting from the entropy change within the system. The entropy of a generic chemical reaction, therefore, describes the amount of its disorder or rather it's a property that monitors the proper or spontaneous direction of change for a given system and its surroundings [193]. An easy way to think about this is to consider phase changes. A gas is always more disordered than a liquid and a liquid is more disordered than a solid. Therefore the gas has the highest entropy and the solid has the lowest entropy. By convention, the entropy of a system that spontaneously moves from products to reactants always has a positive value (+ΔS) and is associated with a consumption of the available capacity for spontaneous change when a process occurs [194].

In general, thermodynamics only tells us whether a given reaction under a given set of conditions can happen, not whether it will happen; that is governed by kinetics. To determine if a reaction can happen, we must calculate the change in Gibbs Energy of the reaction. The Gibbs Energy is defined as the energy available to do work, neglecting any work done by changes in pressure or volume [195, 196]. By convention, a given reaction can proceed spontaneously if the change in Gibbs Energy is negative *(-ΔG)*, which indicates that the products of the reaction have a lower energy state or rather are more stable state than the reactants. A given reaction is favoured to occur (negative Gibbs

[193] R.T. DeHoff, Thermodynamics in Materials Science. McGraw-Hill Inc., New York, NY, 1993.
[194] R.T. DeHoff, Thermodynamics in Materials Science. McGraw-Hill Inc., New York, NY, 1993.
[195] J. Laramie and A. Dicks, Fuel Cell Systems Explained. John Wiley & Sons Ltd., Chichester, England, 2000.
[196] C.H.P. Lupis, Chemical Thermodynamics of Materials. Prentice Hall Publishing, New York, NY, 1993.

Energy) when heat is released (negative enthalpy) and disorder is increased (positive entropy).

For the general cell reaction,

$$\alpha A + \beta B \rightarrow cC + \delta D \quad (3)$$

the standard state Gibbs free energy change of reaction is given by:

$$\Delta G^0 = cG_C^0 + \delta G_D^0 - \alpha G_A^0 - \beta G_B^0 \quad (4)$$

where G_i^0 is the partial molar Gibbs free energy for species i at temperature T.

The Gibbs free energy change of reaction can be expressed by the equation:

$$\Delta G = \Delta G^0 + RT \ln \frac{f_C^c f_D^\delta}{f_A^\alpha f_B^\beta} \quad (5)$$

where ΔG^0 is the Gibbs free energy change of reaction at the standard state pressure (1atm) and at temperature T, and f_i is the fugacity of species i. Substituting Eq. 1 in Eq. 5 gives the relation:

$$E = E^0 - \frac{RT}{nF} \ln \frac{f_C^c f_D^\delta}{f_A^\alpha f_B^\beta} \quad (6)$$

Which is the general form of the Nernst equation. The reversible potential of a fuel cell at temperature T, E^0, is calculate from ΔG^0 for the cell reaction at that temperature.

Fuel cells generally operate at pressures low enough; thus, instead of fugacity the partial pressure can be used.

In an SOFC the common reactions occurring are the oxidation of H_2 to form H_2O (Eq. 7), the oxidation of CO to form CO_2 (Eq. 8) and the oxidation of CH_4 to form water and CO_2 (Eq. 9).

Under open circuit conditions (OCV), with electrochemical potential of oxide ions equilibrated across the oxide-ion conducting electrolyte, the Nernst potential (E) for the reactions can be calculated as described in table 1

Reaction	Nernst equation

$H_2 + O^= \rightarrow H_2O + 2e^-$ $\frac{1}{2}O_2 + 2e^- \rightarrow O^=$ $H_2 + \frac{1}{2}O_2 \rightarrow H_2O$	(anode) (cathode) (overall) (Eq. 7)	$E = E^0 + \frac{RT}{2F}\ln\frac{p_{H_2}\,p_{O_2}^{1/2}}{p_{H_2O}}$
$CO + O^= \rightarrow CO_2 + 2e^-$ $\frac{1}{2}O_2 + 2e^- \rightarrow O^=$ $CO + \frac{1}{2}O_2 \rightarrow CO_2$	(anode) (cathode) (overall) (Eq. 8)	$E = E^0 + \frac{RT}{2F}\ln\frac{p_{CO}\,p_{O_2}^{1/2}}{p_{CO_2}}$
$CH_4 + 4O^= \rightarrow 2H_2O + CO_2 + 8e^-$ $2O_2 + 8e^- \rightarrow 4O^=$ $CH_4 + 2O_2 \rightarrow 2H_2O + CO_2$	(anode) (cathode) (overall) (Eq. 9)	$E = E^0 + \frac{RT}{8F}\ln\frac{p_{CH_4}\,p_{O_2}^2}{p_{H_2O}^2\,p_{CO_2}}$

The Nernst potential, E, gives the ideal open circuit cell potential. This potential sets the upper limit or maximum voltage achievable by a fuel cell.

It provides a relationship between the ideal standard potential (E°) for the cell reaction and the ideal equilibrium potential (E) at other partial pressures of reactants and products.

For the overall cell reaction, the cell potential increases with an increase in the partial pressure (concentration) of reactants and a decrease in the partial pressure of products.

The ideal standard potential (E^0) at 298K for a fuel cell in which H_2 and O_2 react is 1.229 volts with liquid water product, or 1.18 volts with gaseous water product. The difference between 1.229 volts and 1.18 volts represents the Gibbs free energy change of vaporisation of water at standard conditions. Is possible, therefore, deduce that an increase of temperature gives a reduction of voltage. The electrochemical reaction of H_2 and O_2 in a SOFC working at 800°C will reach a maximum theoretical value of 0.98 volts. For the oxidation of CO will be 0.98 volts while the value expected for the oxidative reaction of CH_4 will be 1.04 volts.

The open circuit voltage of a fuel cell is also strongly influenced by the reactant concentrations.

The maximum ideal potential occurs when the reactants at the anode and cathode are pure. In an air-fed system or if the feed to the anode is other than pure dry hydrogen, the cell potential will be reduced. Similarly, the concentration of reactants at the exit of the cell will be lower than at the entrance. This reduction in partial pressure leads to a Nernst correction that reduces the open circuit voltage locally.

Solid oxide fuel cells, performs non-ideally due to irreversibilities. The performance measure of a SOFC is the voltage output as a function of electrical current density drawn, it represents a deviation from Nernst potential and is called polarization curve. Fig. 1 shows such an I-V curve along with a power density curve.

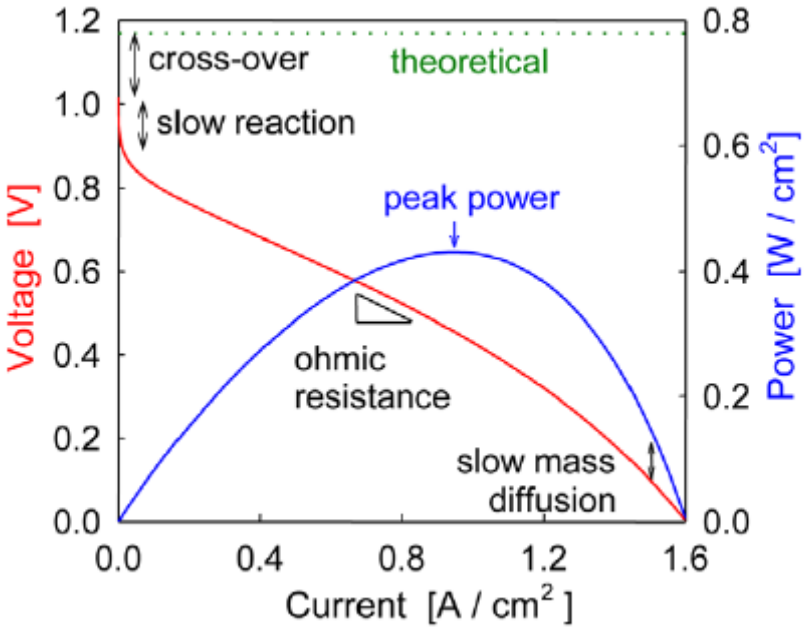

Fig. 1. Schematic fuel cell polarization (voltage vs. current density) and power density curves.

As shown in Fig. 1, there are three types of polarizations and regions of operation wherein a particular loss mechanism is dominant relative to the other polarizations. At and near open circuit voltage (low current densities), activation polarization is the dominant loss term; it is cause of slow reaction. Activation polarization is attributed energy required to sustain the electrochemical reactions. At intermediate current densities, ohmic voltage decrease is the dominant loss mechanism. Ohmic losses obey Ohm's Law in terms of proportionally increasing as current increases. Ohmic losses are associated with the resistance (i.e. area-specific- resistance or ASR) mainly caused by the

electrolyte and interfacial surfaces. At higher current demands, concentration polarization is the dominant overpotential.

Concentration losses are attributed to mass transport effects that cause a reactants partial pressure drop in both electrodes thereby decreasing cell potential.

The measured voltage, E, can be written as

$$E = E_{eq} - E_L - \eta_{act} - \eta_{ohm} - \eta_{diff} \qquad (10)$$

where E_{eq} is the equilibrium (expected or Nernstian voltage), E_L is the loss in voltage due to leaks across the electrolyte, η_{act} is the activation overpotential due to slow electrode reactions; η_{iR} is the overpotential due to ohmic resistances in the cell; and η_{diff} is the overpotential due to mass diffusion limitations.

The impact of all the terms of Eq. (6) are highlighted in Fig. 2.

The equilibrium potential, E_{eq}, can be calculated from a knowledge of the thermodynamics of the reaction in question and refers to the Eq. 10.

Under open circuit conditions (that is, no current is drawn) the measured voltage should, in principle, be exactly the Nernstian voltage. In Solid Oxide Fuel cells, in which reaction kinetics at the electrodes are fast, deviations from this voltage are attributed to gas leaks across the membrane due to poor sealing or cracks in the electrolyte, or to partial electronic conductivity. These two factors define E_L.

Activation polarizations are attributed to the energy barrier that the electrochemical reactions must overcome in order for electricity to be produced. At open circuit voltage (OCV), each electrode is in dynamic equilibrium thereby developing a potential difference. The dynamic equilibrium of each electrode at OCV is maintained by the balanced electrochemical free energies. More specifically, The electrochemical free energies associate to the hydrogen electro-oxidation are the combination of the chemical and the electric work potential associated with the de-ionization and ionization of hydrogen and oxygen.

Therefore, the electrochemical "half cell" reactions produce continual gross flows of electrons to and from the electrolyte-electrode interfaces [197]. As a result, a gross current is developed which is known as the exchange current density. When the electrode kinetics are "sluggish" the exchange current density is low; therefore, the Tafel equation is used to relate exchange current density to the activation polarization as shown below.

[197] Larminie, J., and Dicks, A. (2003). Fuel cell Systems Explained, A. Dicks, translator, J. Wiley, Chichester, West Sussex.

$$\eta_{act} = a + b \ln i \tag{11}$$

a and b are defined in the following equations:

$$a \cong -\frac{R_u T}{4\alpha F} \ln i_0 \tag{12}$$

$$b \cong -\frac{R_u T}{4\alpha F} \tag{13}$$

The term b is called the Tafel slope, and is obtained from the slope of a plot of η_{act} as a function of $\ln i$. There exists a strong incentive to develop electro-catalysts that yield a lower Tafel slop for electrochemical reactions so that increases in current density result only in nominal increases in activation polarization.

In Equations (11) and (12), i is the current density and α is the charge transfer coefficient. i_0 represents exchange current density if the current flowing equally in the forward and reverse directions at equilibrium (zero overpotential). The charge transfer coefficient is an experimentally determined constant (i.e. function of material with a value between 0 and 1) and is the proportion of the electrical energy applied that is consumed in changing the rate of the electrochemical reaction. It should be noted that activation polarization is a function of temperature and therefore is minimized in SOFCs because of the high operating temperature.

Substituting equation (12) and (13) in equation (11), it can be written as:

$$\eta_{act} \cong \frac{RT}{\alpha nF} \ln\left(\frac{i_0}{i}\right) \tag{14}$$

As written, Eq. (14) accounts only for forward reactions (i.e. reduction in the case of the cathode and oxidation in the case of the anode), and is a simplified form of the more general Bulter-Volmer equation:

$$i = i_0 \left\{ \exp\left[\frac{\alpha nF\eta}{RT}\right] - \exp\left[\frac{(1-\alpha)nF\eta}{RT}\right] \right\} \tag{15}$$

which accounts for reaction rates in both directions.

In any case, for all hydrogen/oxygen SOFCs, regardless of electrolyte type, it is the cathode which is rate limiting (hydrogen electro-oxidation is extremely rapid on a wide range of catalysts) and the activation overpotential is almost entirely due to the cathode. Differently occurs in the case fuel are impure hydrogen or hydrocarbon fuels. In these cases cathode activation overpotentials could be slight rather than anode kinetics may become rate-limiting.

The fourth term in Eq. (10), the ohmic overpotential of a cell, is simply given by *IR*, where *R* is the area specific resistance, and includes terms not only from the flow of ions across electrolyte, but also the electrons across electrodes, current collectors and lead wires in the system.

Since these losses obey ohm's law, the experimentally determined parameter, ASR, is used to account for this loss. Therefore, ohmic losses are modelled in the following equation.

$$\eta_{ohm} = iR \qquad (16)$$

Where i is the current flowing through the cell, and R is the total cell resistance, which includes electronic, ionic, and contact resistances:

$$R = R_{electronic} + R_{ionic} + R_{contact} \qquad (17)$$

Any of these components can dominate the ohmic resistance, depending on the cell type. For example, in planar electrolyte-supported SOFC the ionic resistance owing to the electrolyte usually dominates; in tubular SOFC the electronic bulk resistance usually dominates, and in planar thin-electrolyte SOFC contact resistances often dominate.

The ohmic resistance normalized by the active cell area is the Area Specific Resistance (ASR) mentioned above. It has the units Ω cm^2 and is a function of the effective resistivity and path length of the material (cell design and material choice), and is dependent upon operating temperature.

The ASR is a key performance parameter of SOFCs where the ohmic losses often dominate the overall polarization of the cell.

Experimentally, there are several ways to determine the ohmic cell resistance. If the polarization curve has a substantial linear portion (in the centre), the slope of this curve usually closely approximates the ASR of the cell. Sometimes, a more accurate way to determine the ohmic resistance is from impedance spectroscopy. In an impedance spectrum (Nyquist plot) of a fuel cell, the ohmic resistance is the intercept at high frequency, called also series resistance R_s.

The final term, η_{diff}, the mass diffusion polarization, is given to losses associated with concentration variation of critical species due to mass transport processes in the cell. Three sources of loss due to mass transport can be identified: (1) Diffusion between bulk flows and cell surfaces; (2) diffusion of oxygen ions through the electrolyte (one could also include electron transport); (3) transport of reactants and products through electrodes. Typically, is opinion of experts that only the latest can be considered to constitutes the concentration polarisation.

Both anode and cathode can contribute to this term. As greater and greater current is drawn, the reactant depletion zone or the by-product build-up become greater and greater, and thus mass diffusion overpotentials become severe at high current densities. Experimentally the effect is marked and appears as a sharp drop in cell voltage

As a reactant is consumed at the electrode by electrochemical reaction, it is often diluted by the products, when finite mass transport rates limit the supply of fresh reactant and evacuation of products. As a consequence, a concentration gradient is formed which drives the mass transport process. In SOFCs fed with hydrogen, the evacuation of product is often more limiting than the supply of fuel, given the difference between the diffusivities of hydrogen and water (vapour). While at low current densities and high bulk reactant concentrations mass-transport losses are not significant, under practical conditions (high current densities, low fuel and air concentrations), they often contribute significantly to loss of cell potential.

For gas-phase fuel cells, the rate of mass transport to an porous electrode surface in many cases can be described applying the principle of conservation of species. Fick's first law is the simplest diffusion model and used in dilute or binary system:

$$\vec{J}_l = -CD_{l,k}\nabla X_l \qquad (18)$$

Where $\vec{J}_l$ is the molar flux of species l, X_l is the concentration of species l, C is the total molar concentration, $D_{l,k}$ is the diffusion coefficient of the reacting species in binary system. ∇X_l represents the 3-D gradient from the double layer.

The distance that the diffusion process is the dominant transport mechanism depends on the convection in the bulk electrolyte. Generally, for a planar electrode, the thickness δ of the diffusion layer is approximated by:

$$\delta = \sqrt{\pi D t} \qquad (19)$$

where t expressed in seconds is the time. Experimental studies have shown that the diffusion layer and bulk convection mechanisms reach an equilibrium at approximately 0.5mm [198].

This can be represented in the same way as the Nernst losses due to the gas partial pressures, in terms of the concentration change.

The corresponding rate of electron transport (current density, i) will be controlled consequently by the diffusion of the species:

[198] P.W. Atkins, Physical Chemistry, sixth edition. Oxford UK, Oxford University Press, 1998.

$$i = \frac{nFD(C_B - C_S)}{\delta} \tag{20}$$

where C_B is the original bulk electrolyte ion concentration and C_S represents its surface concentration. The limiting current (i_L) is a measure of the maximum rate at which a reactant can be supplied to an electrode, and it occurs when C_S=0, i.e.,

$$i_L = \frac{nFDC_B}{\delta} \tag{21}$$

By appropriate manipulation of Equations (20) and (21),

$$\frac{C_S}{C_B} = 1 - \frac{i}{i_L} \tag{22}$$

The Nerst equation at equilibrium conditions is

$$E_{i=0} = E^0 + \frac{RT}{nF}\ln C_B \tag{23}$$

When current is flowing, the surface concentration becomes less than the bulk concentration, and the Nernst equation becomes

$$E = E^0 + \frac{RT}{nF}\ln C_S \tag{24}$$

The potential difference (ΔE) produced by concentration change at the electrode represents the concentration polarization:

$$\Delta E = \eta_{diff} = \frac{RT}{nF}\ln\frac{C_S}{C_B} = \frac{RT}{nF}\ln\left(1 - \frac{i}{i_L}\right) \tag{25}$$

As can be seen from equation (21), the limiting current density, i_L, can be expressed in terms of the diffusion constant. The effective diffusion constant in turn depends on porosity, V_V, and tortuosity, τ:

$$D \propto \frac{V_V}{\tau} \tag{26}$$

In effect, an open porous microstructure of the anode results in a decrease of the polarisation due to fuel gas diffusion. Virkar et al. showed that when both the concentration and activation polarisation contribute to the overall polarisation, the polarisation in an anode supported cell working for the electro-oxidation of hydrogen, could be described by the following equation:

$$\eta = iR + \frac{RT}{2F}\ln\frac{i}{i_0} + \frac{RT}{2F}\ln\left(1 + \frac{p^0_{H_2} i}{p^0_{H_2O} i_{as}}\right) - \frac{RT}{2F}\ln\left(1 - \frac{i}{i_{as}}\right) \tag{27}$$

In this equation, i_{as} is the limiting anode current density (the maximum current density), occurring when the hydrogen partial pressure at the electrolyte/anode interface is nearly zero. Fig. 2 shows the partial pressure gradient of water and hydrogen in an anode-supported cell [199]. A gradient for hydrogen that drops very quickly at the outer surface of the anode indicates poor gas transport.

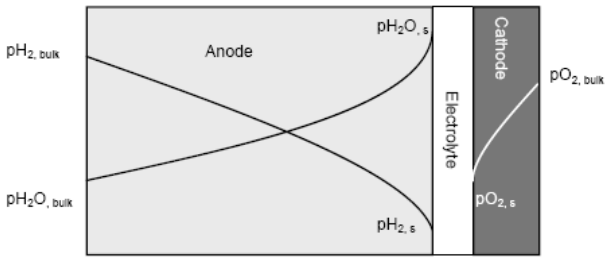

Fig. 2. Concentration profile in the electrodes of an anode-supported cell

The power density is simply multiple of the voltage and the current density, and, as also shown in the figure 2, reaches some peak value at intermediate voltages (or current density). In contrast, efficiency, which decreases with increasing overpotential, is greatest at low current densities.

The efficiency of a SOFC is dependent on the amount of power drawn from it. Drawing more power means drawing more current, which increases the losses in the fuel cell. Most losses manifest themselves as a voltage drop in the cell, so the efficiency of a cell is almost proportional to its voltage.

Efficiency

The efficiency of fuel cells is much higher than those of combustion engines because they are not governed by the Carnot Cycle [200, 201, 202] because the energy conversion pathway does not proceed via thermal energy but directly from chemical into electrical energy. Thus, the chemical reaction is controlled in such a way that the electron

[199] Virkar, A.V., et al, Solid state ionics, vol. 131, 2000, p. 189 – 198, The role of electrode microstructure on activation and concentration polarizations in solid oxide fuel cells

[200] N.Q. Minh and T .Takahashi, Science and Technology of Ceramic Fuel Cells. Elsevier Science B.V., Amsterdam, The Netherlands, 1995.

[201] R.T. DeHoff, Thermodynamics in Materials Science. McGraw-Hill Inc., New York, NY, 1993.

[202] C.H.P. Lupis, Chemical Thermodynamics of Materials. Prentice Hall Publishing, New York, NY, 1993.

exchange does not take place locally but via an external circuit.. the fuel cell is therefore a part of the electrical circuit.

SOFC efficiency can be split into three terms: Thermodynamic Efficiency (intrinsic fuel properties), Voltage Efficiency (ability to realise ideal voltage) and Current Efficiency (ability to utilise supplied fuel).

$$\varepsilon_{SOFC} = \varepsilon_T \times \varepsilon_V \times \varepsilon_I \tag{28}$$

The maximum thermodynamic efficiency, ε_T, is determined by the intrinsic fuel properties. It demonstrates the desirability of electrochemically oxidising a fuel and that some fuels can be more advantageously electrochemically oxidised than others. Thermodynamic efficiency is defined:

$$\varepsilon = \frac{\Delta G}{\Delta H} = 1 - \frac{T\Delta S}{\Delta H} \tag{29}$$

For common fuels such as hydrogen, carbon monoxide and other hydrocarbons (negative ΔH and negative ΔS), the thermodynamic efficiency is ε<1. Fuel with positive entropy values however could theoretically resulting efficiencies ≥1, as in the case of oxidation of carbon.

The voltage efficiency, ε_V, is related to the fact that the operating voltage of a cell is always less than the theoretical maximum hence a voltage efficiency can be defined:

$$\varepsilon_V = \frac{E}{E_r} \tag{30}$$

where, E is the operating cell voltage and E_r the reversible voltage. Note that E_r is generally greater than the open circuit voltage as the measured open circuit (equilibrium), voltage is that obtained after losses caused by gas leakage, side reactions, etc.

On the other hand, Current efficiency, ε_I, is reduced if not all reactants are converted to reaction products, or if some electrons are involved in alternative reactions as in the case of corrosion or parasite current into the electrolyte. For 100% conversion the cell current density, I_F, is given by Faraday's Law:

$$I_F = zF\frac{df}{dt} \tag{31}$$

Where f represents the amount of fuel supplied (mol), z is the number of electrons transferred per molecule of fuel. For incomplete conversion the current density produced is given by:

$$I = zF\left(\frac{df}{dt}\right)_{consumed} \tag{32}$$

Hence the current efficiency is given by

$$\varepsilon_I = \frac{I}{I_F} \tag{33}$$

Since high fuel utilization in general results in very high Since high fuel utilisation in general and in SOFC's in particular results in

very high concentration polarisation, fuel cells are deliberately operated at less than 100% fuel utilisation. Further current efficiency terms arise from gas leakage and electronic conductivity of the electrolyte.

The heat generated by irreversibility at the electrodes structure is given to the fuel and air flow, and partially lost by the stack external canister. A significant fraction of the heat can be used by the endothermic reforming reaction, thus, reducing the requested cooling air flow and enhancing the heating value.

SOFC systems are presently rated at a cell voltage of 0.7 V/cell. While this is a reasonable approach for performance comparisons and exhibits a high electric power output (>50% of the maximum), there are also some disadvantages. As can be seen in Fig. 3, the cell efficiency is restricted to 56% by the electricity/heat ratio of 1.3. The cell generates approximately 0.75W heat/W electricity. Removal of the heat needs large amounts of air which affect stack, heat exchanger and blower design.

A rise of the cell voltage for example to 0.8 V/cell implies an 80% increase in cell area and therefore stack size for the same electric output. However, the electricity/heat ratio increases from 1.3 at 0.7V to 1.75 at 0.8V. The cell efficiency is then raised to 64%. The resulting lower heat load reduces the size of peripherals like tubing, heat exchanger and blower, and also the power consumption of active cooling systems like blowers and pumps.

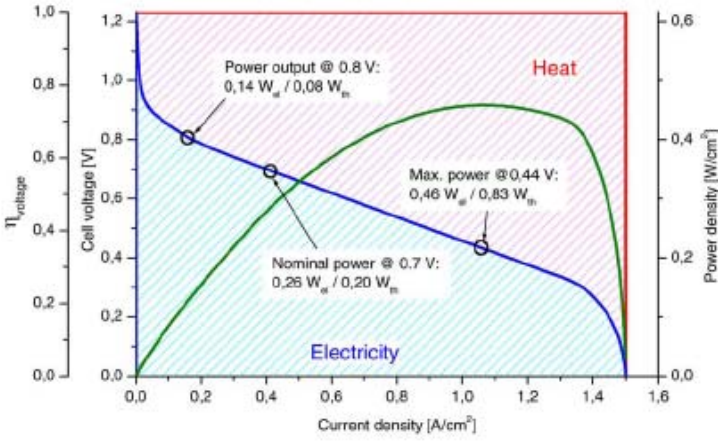

Fig. 3. Comparison of specific electricity and heat generation in an SOFC

Internal reforming and direct oxidation

Hydrogen is a vital commodity in many chemical and petroleum processing operations and is also a clean energy source. Most of the hydrogen is produced by catalytic processes, involving many steps with various catalysts and in the petrochemical industry, steam reforming, partial oxidation and autothermal reforming processes have been developed. Although fuel cells work efficiently with hydrogen as a fuel there are still some major problems related to hydrogen availability and acceptability. In particular, it is still extremely difficult to obtain clean/renewable hydrogen. In the short to medium term future, the only realistic fuels for fuel cells are hydrocarbon based, especially natural gas. In general, higher hydrocarbons such as LPG and gasoline offer better hydrogen yields than methane but are less popular, due to the possibility of coke formation during hydrogen production. However, because they are more easily transportable and readily available, they deserve more serious consideration especially for non-stationary applications.

In the short to medium term, therefore it is appropriate to look at hydrocarbon fuels, with the environmental benefit arising from the much-improved efficiency of fuel utilisation. Natural gas, e.g. North Sea gas (CH4(95%), C2H6(4%), C4H10(0.2%), S(4ppm)) is clearly the most abundant and best distributed fuel. The development of SOFC anodes capable of operating in natural gas, without suffering from carbon build up due to catalytic cracking is still far from being achieved.

In order to utilise natural gas as fuel, the fuel needs to be externally or internally reformed.

The reforming reaction (34) is generally associated with a following water gas shift equilibrium reaction (35), additionally methane may be reformed with CO2 (36).

$$CH_4 + H_2O \Leftrightarrow CO + 3H_2 \qquad \Delta H=206 kJmol^{-1} \qquad (34)$$

$$CO + H_2O \Leftrightarrow CO_2 + H_2 \qquad \Delta H=-41 kJmol^{-1} \qquad (35)$$

$$CH_4 + CO_2 \Leftrightarrow 2CO + 2H_2O \qquad \Delta H=247 kJmol^{-1} \qquad (36)$$

Steam reforming of methane is highly endothermic, requires an external heat supply and typically occurs at temperatures above 500°C in the presence of a suitable catalyst. The heat can be supplied by combusting part of the fuel into carbon dioxide and steam. Two approaches have been developed, external and internal reforming. In the first case, the reaction occurs in a separate reactor, which consists of heated tubes filled with nickel or

noble metal [203]. To obtain high methane conversion and to avoid carbon deposition by methane cracking (37) or by the Boudouard reaction (38), steam is introduced in excess. Typical conversion efficiencies for external reforming systems are c.a. 60%. The cracking reaction is even more problematic with the higher hydrocarbons, which also are present in natural gas. An alternative process, partial oxidation (POX) is occasionally used to drive reforming, (39), especially when higher hydrocarbons are used as fuel.

$$CH_4 \Leftrightarrow C + 2H_2 \qquad \Delta H=75 kJmol^{-1} \qquad (37)$$

$$2CO \Leftrightarrow C + CO_2 \qquad \Delta H=86 kJmol^{-1} \qquad (38)$$

$$CH_4 + O_2 \Leftrightarrow CO_2 + 2H_2 \qquad \Delta H=-320 kJmol^{-1} \qquad (39)$$

Internal reforming is a particularly promising concept, where steam reforming of methane takes place directly in the anode compartment,. This process not only has no requirement for additional components in the system, but also allows a better heat exchange between the endothermic reforming reaction and the exothermic electrochemical reaction within the stack. However, two major problems occur: the risk of carbon deposition and the creation of a thermal gradient that induces stress in the cell. Third possibility is the auto thermal reforming. This involves the reaction of oxygen, steam and fuels to produce H_2 and CO which can be considered as a combination of steam reforming and partial oxidation. No external heating source is required since the exothermic oxidation provides the heat for the endothermic steam reformation.

One of the most exciting possibilities is direct hydrocarbon oxidation. The direct oxidation of hydrocarbons tries to overcome some of the problems typical of the internal reforming SOFCs. Mainly operating in dry condition at the anode the management of water is absent and also the control of the temperature is simplified. Direct oxidation of methane, reaction (40) has the thermodynamic possibility of 99.2% conversion efficiency. If this reaction is to be achieved, it is necessary to avoid or inhibit methane cracking. There is also considerable controversy as to whether the reaction is actually a single step, i.e. deep oxidation, or if it involves a series of intermediate reactions with the net result shown in reaction (41).

$$CH_4 + 2O_2 \Leftrightarrow CO_2 + 2H_2O \qquad \Delta H=-802 kJmol^{-1} \qquad (40)$$

$$CH_4 + 4O^{2-} \Leftrightarrow CO_2 + 2H_2O + 8e^- \qquad \text{Electrochemical} \qquad (41)$$

---

[203] K. Ledjeff, T. Rohrbach and G. Schaumberg, Proceedings of the 2nd International Symposium of SOFCs , F. Grosz, P.
Zegers, S. C. Singhal and O. Yamamoto Eds, Athena, 1991, pp. 323.

Two major issues are known to hamper the direct oxidation of methane at SOFC anodes: carbon deposition due to low reactivity and pyrolysis to form carbon. Some experiments on competitive oxidation of hydrocarbons have revealed that the activity pattern followed $C_3H_8 > C_2H_4 > C_3H_6 > C_2H_2 >$ i-C_4H_8. Nevertheless, The rates required in a fuel cell are not extremely high. For a current density of 1 Amp/cm^2, a porous anode with only 1 cm^2 of catalytic active surface area per cm^2 of planar fuel cell (very low for a porous catalyst) would require a turnover frequency of less than 10, a reasonable value for oxidation catalysts.

For the carbon deposition issues is well known that all hydrocarbons tend to pyrolysis to give carbon deposition at high temperatures. Carbon deposition, which can cause plugging of the reaction sites and cracking of the cells, is thus detrimental to fuel cell anodes. Thermodynamic calculations to determine the stable species in typical fuel cell environment indicated that coking of methane occurs at all temperatures of interest (400 to 800°C) if no oxygen containing species (such as water or oxygen) are present. While the thermodynamic may favour methane coking, it is still possible to alter the kinetics of the reaction to avoid carbon deposition. In that direction, we found that the anode microstructure and materials can have significant effect on the amount of carbon deposited.

Highly porous structures resulted in less carbon deposition. The use of mixed ionic electronic conducting materials such as doped-ceria as ceramic matrix of the anode also yielded much lower carbon deposition than the conventional zirconia matrix.

These are the reason essentially all SOFC designs require that hydrocarbons first be converted to hydrogen through steam reforming.

High catalytic activity for oxidation of hydrocarbons in a SOFC anode is not useful if one cannot provide oxygen to the catalyst surface.

Triple Phase Boundary - TPB

In the context of the polarization curve, it is evident that high power densities (and high efficiencies) result when gas diffusion and electron transport through the electrolytes are slow, electrocatalysis at the electrodes is rapid, the conductivity of each of the components, in particular, the electrolyte, is high, and mass diffusion through the porous electrodes is facile. Thus, the ideal fuel cell electrolyte is not only highly ionically

conducting, but also impermeable to gases, electronically resistive and chemically stable under a wide range of conditions. Moreover, the electrolyte must exhibit sufficient mechanical and chemical integrity so as not to develop cracks or pores either during manufacture or in the course of long-term operation.

The demands on fuel cell electrodes are perhaps even more extreme than those on the electrolyte.

The ideal electrode must transport gaseous (or liquid) species, ions, and electrons; and, at the points where all three meet, the so-called triple phase boundaries (TPB), the electrocatalysts must rapidly catalyze electro-oxidation (anode) or electroreduction (cathode). Thus, the electrodes must be porous, electronically and ionically conducting, electrochemically active, and have high surface areas. It is rare for a single material to fulfil all of these functions, and consequently the increasing of the amount of TPB length per unit area is accomplished by using composite electrodes, with interpenetrating networks of electrolyte, electrode, and pore phases (see Fig. 4). These microstructures can be further optimised for composition and grain/pore size.

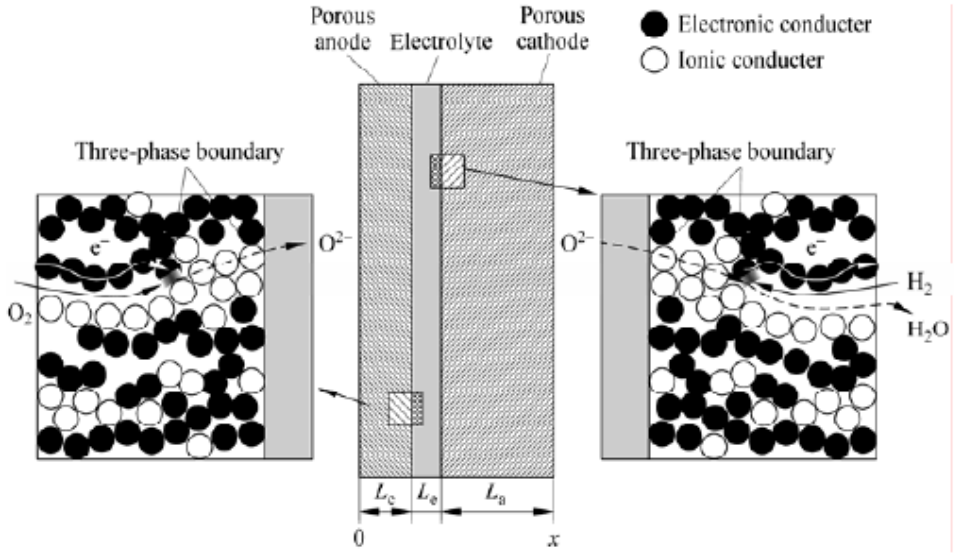

Fig. 4. Illustration of SOFC cathode, electrolyte, and anode

As the common intersection of three volumes, the TPB is ostensibly a one-dimensional region. It nevertheless has some volume, due to the non-zero electron conductivity of the electrolyte, ionic conductivity of the electrode, and/or gas permeability of either solid phase. Any of these will broaden, to some extent, the region over which reactions can occur, giving some width and depth to TPB. This idea can be carried further by intentionally using a material that is highly conductive to both ions and electrons. The

remainder of the electrode structure can be regarded as a distribution system for the current and gases. Only if the electrodes show considerable mixed conductivity, the reaction zone can be extended into the electrode. For high-temperature solid oxide fuel cells, single component electrodes are, in principle, possible because mixed conducting (O^{2-} and e^-) ceramics are known, and it is precisely such materials which facilitate electrocatalysis. Standard cathode material ($Sr_xLa_{1-x}MnO_3$) is known to have a negligible oxygen conductivity, although extreme conditions such as low oxygen potential or high cathodic polarisation conditions may increase the reaction surface due to a mixed conductor behaviour of part of the cathode structure.

The limitation of the electrode reaction to the three-phase areas implies that only part of the electrolyte/electrode interface is active in contributing to the ion flux in the electrolyte.

The current lines are constricted at the three-phase boundaries, which locally gives rise to higher current densities. As a consequence a higher electrolyte resistance is observed than what may be expected in a situation where the complete electrolyte area contributes to the ion flux. In the latter case, the electrolyte resistance will correspond with the intrinsic value for the electrolyte. A schematic representation of the two situations is given in Fig. 5.

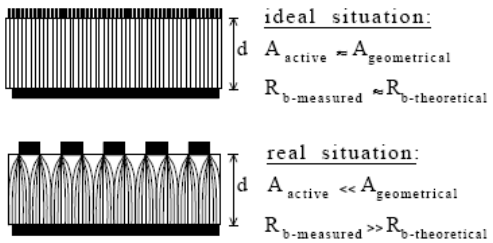

Fig. 5. Schematic representation of a "continuous" and a "discontinuous" electrode model.

In the ideal situation, the upper electrode consists of infinitesimally small particles, so the electrolyte bulk resistance may be calculated using the geometrical area of the electrode. In the second situation, a more realistic electrode is sketched with coarse particles. As a consequence the current lines will be constricted and a too high electrolyte resistance will be found. R_b = bulk electrolyte resistance, A = area and d= electrolyte thickness. The ion flux in the electrolyte is represented by thin lines.

Commonly, the active three-phase boundary (TPB) surface is expressed as a function of electrode microstructure parameters (porosity, coordination number, contact angle, etc.). All of these parameters have been taken in count from the simplified three-phase

boundary length per unit area of the electrode which is defined as the total circumference C of N particles divided by the electrode geometrical area, and is given by:

$$TPB_l = \frac{C}{A_{geo}} = \frac{4D_c A_{geo}}{\pi d_c^2} \frac{\pi d_c}{A_{geo}} = \frac{4D_c}{d_c} \tag{42}$$

Where d_c is the contact diameter, D_c is the total contact surface area and is a fraction of the total electrode area A_{geo}.

This TPB is characterised by a line, extending along the electrolyte surface, and has the dimensions of cm/cm^2 or cm^{-1}. this suggests that the electrode kinetics must depend upon the TPB length, in addition to fundamental physical parameters, such as electrocatalytic activity of the electrocatalyst, and the partial pressure of the reactant.

Better understanding of the electrode kinetics can need in order to be able to decrease TPB length. This analysis is generally carried out on the basis of the percolation theory.

4

EXPERIMENTAL PART

Preface

As above pointed out, Solid oxide fuel cells (SOFCs) have many advantages against the other kind of fuel cells; particularly, higher energy-conversion efficiency can be achieved without using expensive precious metals. Traditional high-temperature SOFCs, which usually employ a yttria-stabilized zirconia (YSZ) electrolyte, a LSM cathode and a nickel-YSZ cermet anode, operate at the temperature range of 800°C−1000°C. They are the most studied materials due to their well proven long term stability and to the good matching of thermal expansion with the low-cost ferritic stainless steel used as interconnects in SOFC stacks for intermediate temperature applications. Ni/YSZ cermets are the most commonly used anode materials for zirconia-based SOFCs and they display excellent catalytic properties for fuel oxidation and good current collection but do exhibit disadvantages, such as low tolerance to carbon deposition[204] when using hydrocarbon fuels and poor redox cycling causing volume instability. The nickel metal in the cermet tends to agglomerate after prolonged operation, leading to reduced three-phase boundary (TPB) and increasing resistance[205]. Furthermore, thermal expansion of nickel is considerably larger than that of YSZ. Last but not the least, there is a strong and important tendency to decrease the operating temperature to 600-800 ºC (Intermediate Temperature SOFC – IT-SOFC). In this range of temperature the internal resistance of the cell with Ni/YSZ cermet anode is too large i.e. the efficiency or power density is not satisfying [206].

Recent reports have described SOFC operation directly on methane and natural gas.

These results have challenged traditional views that large amounts of steam are required to prevent carbon deposition on Ni-containing anodes. Heavier hydrocarbons such as

---

[204] B. C. H. Steele, I. Kelly, H. Middleton, R. Rudkin, Solid State Ionics, 8-30, 1547 (1988).

[205] S. Tao, J.T.S. Irvine, "Synthesis and Characterization of $(La_{0.75}Sr_{0.25})Cr_{0.5}Mn_{0.5}O_{3-\delta}$ a Redox – Stable, Efficient Perovskite Anode for SOFCs," J. Electrochem. Soc., 151 (2), 2004, s.A252-A259

[206] E. Ivers-Tiffe´ e, A. Weber, D. Herbstritt, "Materials and technologies for SOFC-components," J. Europ. Ceram. Soc. 21 (2001) 1805–1811.

propane, have been used directly in SOFCs although it was necessary in this case to utilize alternative anode compositions: replacing the Ni with precious metals, conducting ceramic or a perovskite-type oxide. Ceramics based on CeO_2 exhibit mixed ionic and electronic conductivity in a reducing atmosphere due to reduction of Ce^{4+} to Ce^{3+}. In addition, it is believed that the excellent catalytic activity of CeO^2 based materials stemmed from the oxygen-vacancy formation and migration associated with reversible CeO_2–Ce_2O_3 transition [207, 208]. It has been reported that ceria-based ion conductors [209] have a high resistance to carbon deposition, which permits the direct supply of dry hydrocarbon fuels to the anode. The more effective method, however, is the addition of Ni, Co and some nobel metals, such as Pt, Rh, Pd and Ru, which are beneficial to the reforming reactions of hydrocarbon, due to their functions of breaking the C–H bond more easily, especially for the case of Ru [210, 211]. Recently, several new compounds with perovskite structure have been offered as alternative anode materials in SOFCs. With oxides the catalytic oxidation of hydrocarbons appear to involve lattice oxygen, and there is also some evidence that the presence of protonic conductivity can also activate adsorbed CH_4 molecules [212].

In this chapter three approaches have been pursued for the development of hydrocarbon fuelled SOFC. The first approach concerns the electrochemical characterization of state of art SOFC cells produced by a European Trade (Eurocoating/SOFC Power) in comparison with standard InDEC cells. This analysis is aimed to provide useful information on the perspectives of the standard processes for intermediate temperature operation. This kind of cells was based on Ni/YSZ anode materials in anode-supported cells. The use of the Ni/YSZ anode supported cell serves as an investigation of the effect of microstructure on anode performance. Microstructural optimisation of the new anode materials is relevant for improving SOFC performance especially in the presence of internal reforming process.

The second approach concerns with direct oxidation of propane at Ru-ceria based anode electro-catalysts. In the third approach the Ru noble metal was replaced by a Ni-phase

---

[207] C.W. Sun, J. Sun, G.L. Xiao, H.R. Zhang, X.P. Qiu, H. Li, L.Q. Chen, J. Phys. Chem. B 110 (2006) 13445–13452.

[208] N.V. Skorodumova, S.I. Simak, B.I. Lundqvist, I.A. Abrikosov, B. Johansson, Phys. Rev. Lett. 89 (2002) 166601.

[209] O.A. Marina, M. Mogensen, Appl. Catal. A 189 (1999) 117–126.

[210] M. Suzuki, H. Sasaki, S. Otoshi, in: F. Grosz, P. Zegers, S.C. Singhal, O. Yamamoto (Eds.), Proceedings of the Second International Symposium
of SOFC's, Athens, 1991, p. 323.

[211] M.J. Saeki, H. Uchida, M. Watanabe, Catal. Lett. 26 (1994) 149–157.

[212] C. B. Alcock, J. Catal 140 (1993) 557

highly dispersed onto a mixed ionic-electronic conductor perovskite material. Stabilisation of the perovskite and operation in combination with ceria is analysed.

This anode catalyst is characterised by mixed ionic and electronic conduction. Such property appears a suitable property for direct oxidation of hydrocarbon fuels.

CHARACTERIZATION OF SOLID OXIDE FUEL CELL MANIFACTURED BY A EUROPEAN TRADE

Introduction

The objective of this study is to investigate the correlation between microstructures, and electrochemical properties of porous electrodes prepared using tape casting fabrication and co-sintering of anode/electrolyte solid oxide "half cells". The cathode is subsequently deposited.

These relationships are vital for intelligent design of electrode structures and the corresponding properties. The SOFC cells were manufactured by a European Trade (EUROCOATING) and my principal duties were the characterization by electrochemical testing and physico-chemical analysis of the cell pre and post mortem.

The utilization of the Solid Oxide Fuel Cell as power generator and/or heat co-generator is attracting many attentions from small-medium enterprises in order to diversify their production following the necessity of the modern society. Often, these firms are not equipped with research laboratories dedicated to the electrochemical diagnosis. Accordingly, collaboration with research Institute may represent an opportunity to advance in this field.

Experimental

SOFC Architecture

Cells produced in large area (5cm x 5cm) by this trade are planar and anode supported. The scheme of the cell can be summarized as Ni/YSZ//YSZ//LSM/YSZ.

Water-base ceramic slurries containing dispersant (Darvan 821A, R.T. Vanderbilt Inc., USA) and ceramic powders (NiO/8YSZ and 8YSZ, NexTech Materials, USA) were milled 12 h by zirconia's balls (Inframat Advanced Materials), filtered to 40 μm and de-gassed by vacuum application. Then binders (B-1000 and B-1014, Duramax, Rohm and Haas, France) were added and the mixtures were mixed for 2 h by mechanical stirrer. Slurries were casted by a laboratory scale tape casting equipment. Graphite (Alfa Aesar,

7-10 micron flakes) was added to the anodic mixture in order to increase porosity. Anodic tapes without graphite was also prepared to provide a large distribution of three phase boundaries (TPBs) at the anode/electrolyte interface [213, 214, 215], to aid electrolyte sintering and to enhance mechanical strength. Anode and electrolyte layers were stacked together, laminated under 12 MPa pressure (Material Test System 810) at 80°C for 30 min. Green laminates were co-fired 6 h at 1400°C and the as sintered half cells were "warm flattened" (1400°C) by the application of a dead-load which develops a pressure of about 6 MPa. A 15 μm-thick layer (cathode functional layer) with a composition of 50wt% 8YSZ and 50% LSM35 μm and a 50-thick LSM35v layer (current collector) were then screen printed and sintered for 2 h at 1150°C. The screen printing ink was produced by dispersing 60-65% oxide powders (NexTech Materials Ltd.,USA) in a mixture of therpineol and ethylcellulose.

The complete architecture and the procedure are summarized in the Figure 1.

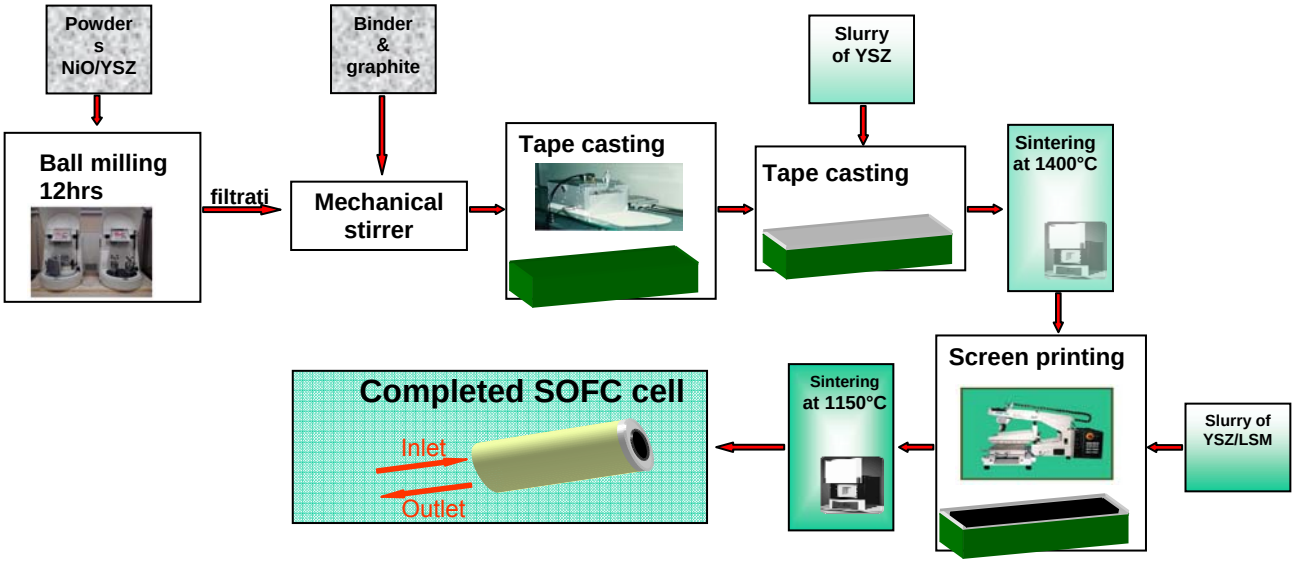

Figure 1. Cell preparation procedure

[213] Toshio Matsushima*, Himeko Ohrui, Toshiro Hirai, Solid State Ionics 111 (1998) 315–321

[214] B. de Boer, M. Gonzalez, H.J.M. Bouwmeester*, H. Verweij, Solid State Ionics 127 (2000) 269–276

[215] Mizusaki, J., Tagawa, H., Saito, T., Kamitani, K., Yamamura, T., Hirano, K., Ehara, S., Takagi, T., Hikita, T., Ippommatsu, M., Nakagawa, S. and Hashimoto, K., Preparation of nickel pattern electrodes on YSZ and their electrochemical properties in H2–H2O atmospheres. J. Electrochem. Soc., 1994, 141, 2129.

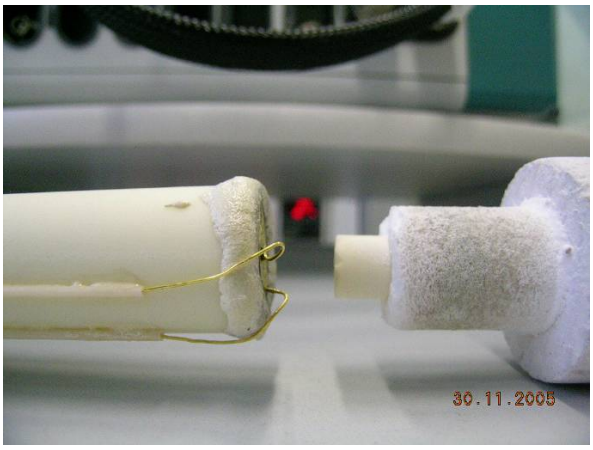

Figure 2a and 2b. Scheme of heating plant with a detailed of the Cell mounted

Finally, the cell was cut by laser in button cell and was mounted on an alumina tube and sealed with quartz adhesive (AREMCO) and heated between 750 and 850°C in presence of inert gas.

The heating system is a Lenton furnace (Figure 2a) controlled by a standard temperature controller Eurotherm 2416. The cathodic gas was supplied by an alumina tube positioned closed to the cell (Figure 2b).

Electrochemical polarizations and ac-impedance measurements were performed on anodic supported single cells in the range 750°C-850°C by using an AUTOLAB PGSTAT30 Metrohm potentiostatical frequency-response analyzer equipped with 20A booster. Gold wires were used as current collectors for the cell. A thermocouple was positioned on the cathodic surface. Impedance spectra were obtained in the frequency range from 10 mHz to 1 MHz with applied ac-voltage amplitude of 10 mV rms. The impedance measurements were taken under open-circuit conditions and 0.7V.

Results and discussion

Physic-chemical analysis on the fresh cell

SEM analysis (Figure 3a) on the unpolished cross-section fracture of complete cell shows two different morphologies for the anode: distinct porosity observed in region to contact

to the electrolyte and in the external part. These are due to a different loaded of pore former in the green cell. The microstructure obtained is very promising, since, this porosity is optimal to the gas permeability [216, 217]. Figure 3b shows the micrograph of the interfaces anode/electrolyte/cathode where the electrolyte appears to be very dense with gentle internal imperfections due to some pinholes which had not any continuity along the section in conformity to the high OCV values observed during the working.

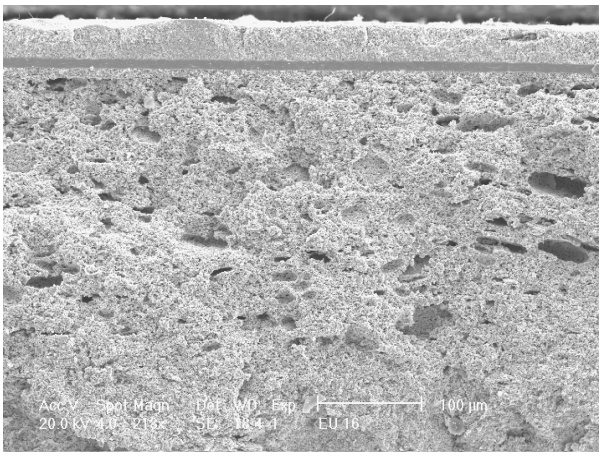

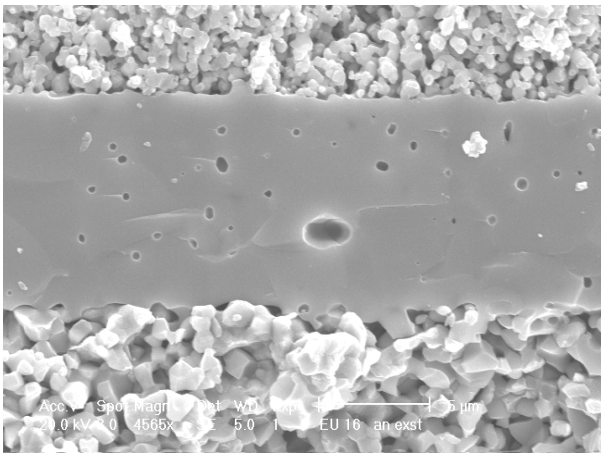

Figure 3a and 3b. SEM analysis on the complete cell

Electrochemical investigations

The cells were conditioned under He atmosphere until to reach 800°C. At this temperature started the reduction time established in 10h. These conditions were chosen in order to evaluate the real differences to InDEC cells. The measurements were done in presence of He dry and wet and of different cathodic atmospheres (Air static, Air fluxed, and Pure O_2). Moreover, experiments with syngas humidified at 50°C have been carried out in order to investigate the real perspectives of these cells in the presence of an external reformer.

Figure 4a shows the comparison of the electrochemical AC-Impedance observed for the tested cell in presence of dry H_2 under open-circuit conditions. All the tests have shown a good series resistance (Rs: ~0.1ohm·cm^2) attributed to electrolyte conductivity[218] and a polarization resistance appearing strongly affected of the cathodic flux. The

[216] Kyoung R. Han, Younji Jeong, Haiwon Lee, Chang-Sam Kim, Materials Letters 61 (2007) 1242–1245
[217] Bieberle, A. and Gauckler, L. J., Reaction mechanism of Ni pattern anodes for solid oxide fuel cells. Solid State Ionics, 2000, 135, 337.
[218] Alexandre Closset, Stefan Diethelm, Kemal Nisancioglu, Jan van Herle and A. J. McEvoy, Journal of the European Ceramic Society 19 (1999) 843±846

polarization curves (Figure 4b) shows the best performances achieved in presence of pure O_2 was about 800mW·cm^{-2}.

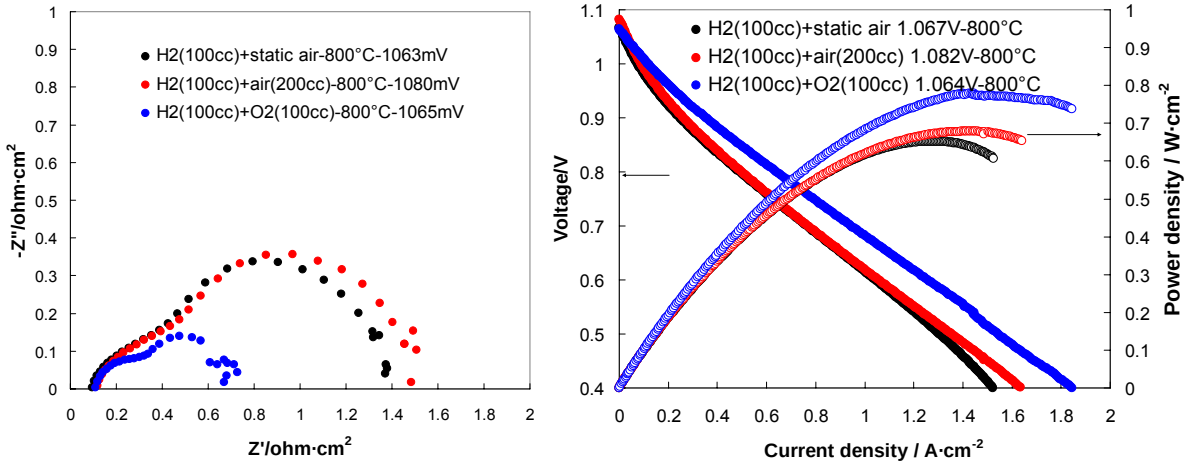

Figure 4a and 4b. AC-Impedance and Polarization measurement for the cell feed by pure H_2

The manufacturer was interested to evaluate the possibility to use them cells humidifying H_2 at room temperature, in order to slow down the degradation processes in the anode [219]. Figure 5a and 5b shown an increasing of the first semicircle appearing at high frequencies and a reduction of the performances estimated from 4% in the case of pure O_2, increasing to 11% in the case of static Air especially due to the decreased OCV. This appears especially due to the dilution of H_2 partial pressure in accordance with Nerst's equation.

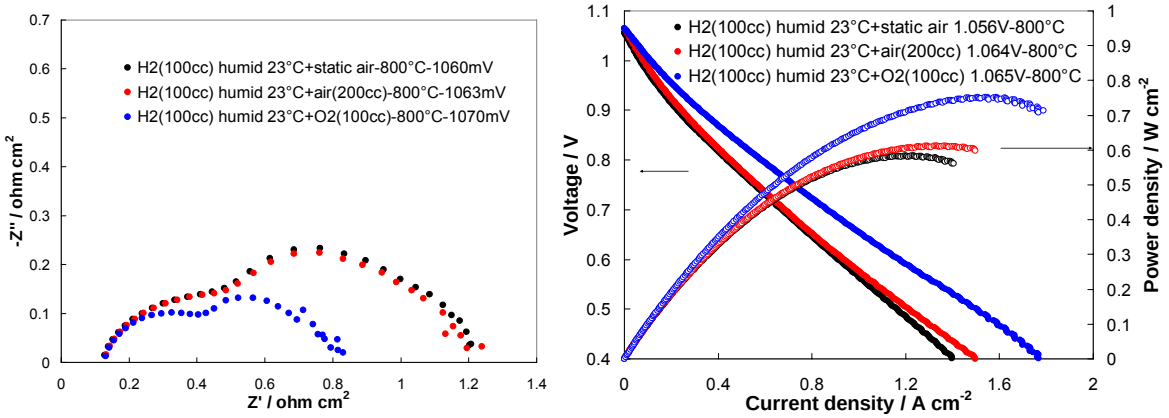

Figure 5a and 5b. AC-Impedance and Polarization measurement for the cell feed by H_2 humidified at room temperature

[219] G. Rietveld, P. Nammensma, J.P. Ouweltjes, in: H. Yokokawa, S.C. Singhal (Eds.), Proceedings of the Seventh International Symposium on Solid Oxide Fuel Cells (SOFCVII), The Electrochemical Society Proceedings Series, Pennington, NJ, 2001, p. 125, PV 2001-16.

The results obtained by feeding wet syngas at the anode with cathode fed by pure O_2 and air flux. In these conditions, an OCV larger than 1V and a maximum power densities of about 280mW·cm^{-2} and 350mW·cm^{-2} in air flux and pure O_2 , respectively, have been achieved. This performance is considerably smaller than that achieved with pure hydrogen.

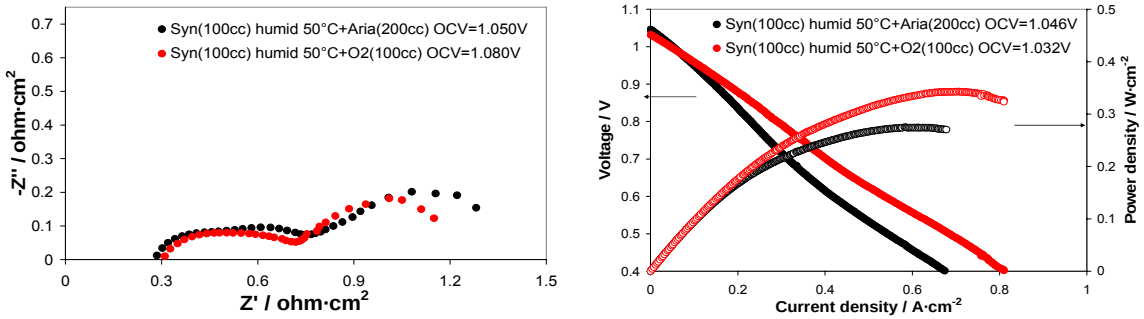

Figure 6a and 6b. AC-Impedance and Polarization measurement for the cell fed with syngas humidified at 50°C

At the same operational and fed conditions was tested an InDEC ASC1 (YSZ electrolyte, Ni/YSZ anode cermet and LSM/YSZ cathode). AC-Impedances under open-circuit conditions and polarization curves carried out in pure H_2 (Figure 7a and 7b) show that there were high differences depending from the cathode atmosphere. In particular was observed a fall in Air static at 0.9V about due to slight O_2 diffusion at the cathode. For these reasons, the maximum power density (890mW·cm^{-2}) was obtained in presence of pure O_2 flux.

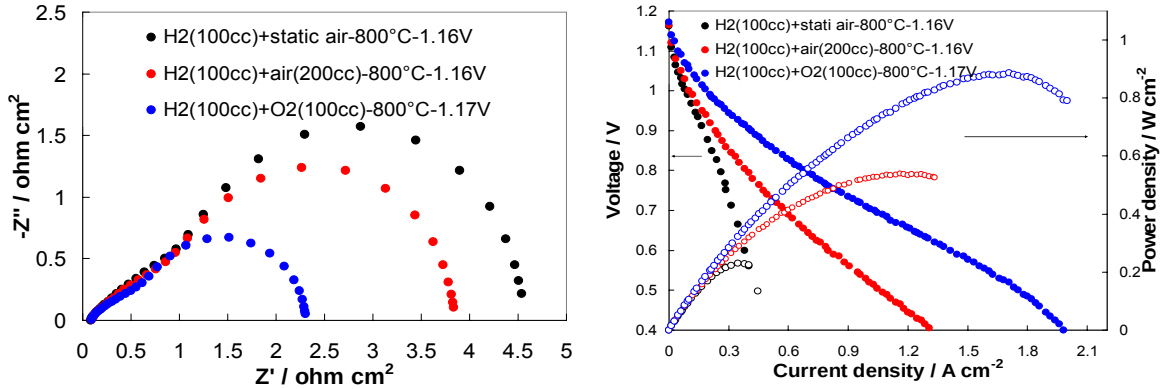

Figure 7a and 7b. AC-Impedance and Polarization measurement for InDEC cell in pure H_2.

At the same way, the performances obtained for the InDEC cell feeding humidified H_2 at room temperature were lower rather than pure H_2 of about 7% in pure O_2 and Air flux while in Air static was not represented due to the slight power density (Figure 8a and 8b).

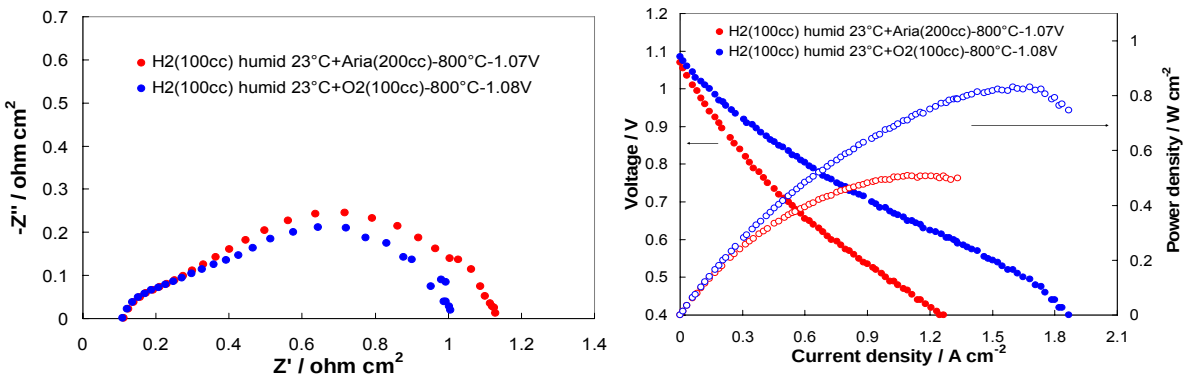

Figure 8a and 8b. AC-Impedance and Polarization measurement for the cell feed by H_2 humidified at room temperature

Table 1 summarizes the results obtained for the European trade and InDEC cells. Can be observed that the European trade cell was more efficient in every anodic and cathodic conditioning except to O_2 pure flux where the InDEC cell was 12% about more efficient. It appears especially due to the higher OCV rather that European Trade cell (about 100mV).

800°C	Anode	Cathode	OCV (V)	I@0.7V ($A \cdot cm^{-2}$)	ASR@0.7V ($ohm \cdot cm^2$)	Max Power density ($W \cdot cm^{-2}$)	OCV Resistance ($ohm \cdot cm^2$)
European trade cell	H_2(100cc/min) dry	Static Air	1.07	0.73	0.65	0.65@0.51V	0.09/1.37/1.28
		Air (200cc/min)	1.08	0.73	0.66	0.67@0.47V	0.12/1.48/1.36
		O_2(100cc/min)	1.06	0.91	0.48	0.78@0.54V	0.11/0.67/0.56
	H_2(100cc/min) humidified at 25°C	Static Air	1.06	0.67	0.56	0.58@0.47V	0.13/1.20/1.07
		Air (200cc/min)	1.06	0.68	0.58	0.61@0.46V	0.13/1.20/1.07
		O_2(100cc/min)	1.06	0.87	0.57	0.75@0.47V	0.13/0.81/0.68
	Syngas(100cc/min) humidified at 50°C	Air (200cc/min)	1.05	0.31	1.78	0.27@0.47V	0.29/
		O_2(100cc/min)	1.03	0.40	1.35	0.34@0.48	0.31/
InDEC cell	H_2(100cc/min) dry	Static Air	1.16	0.32	2.29	0.23@0.66V	0.09/4.54/4.45
		Air (200cc/min	1.16	0.58	0.80	0.54@0.42V	0.10/3.84/3.74
		O_2(100cc/min)	1.17	1.03	0.46	0.89@0.52V	0.09/2.30/2.21
	H_2(100cc/min) humidified at 25°C	Air (200cc/min)	1.07	0.52	0.88	0.51@0.46V	0.11/1.13/1.02
		O_2(100cc/min)	1.08	0.92	0.51	0.83@0.52V	0.11/1.01/0.90

Table 1. Values of the principal data of the European Trade and InDEC cells

In order to evaluate the stability of the European Trade cell, the life time test was carried out at 800°C in presence of H_2 dry and wet in galvanostatic condition (267mA cm^{-2}). It was observed (Figure 8) that a slight slope to decrease of the performance. During the

test, at regular gaps, were performed AC-Impedance and Polarization tests through to evaluate the ageing reason of the cell.

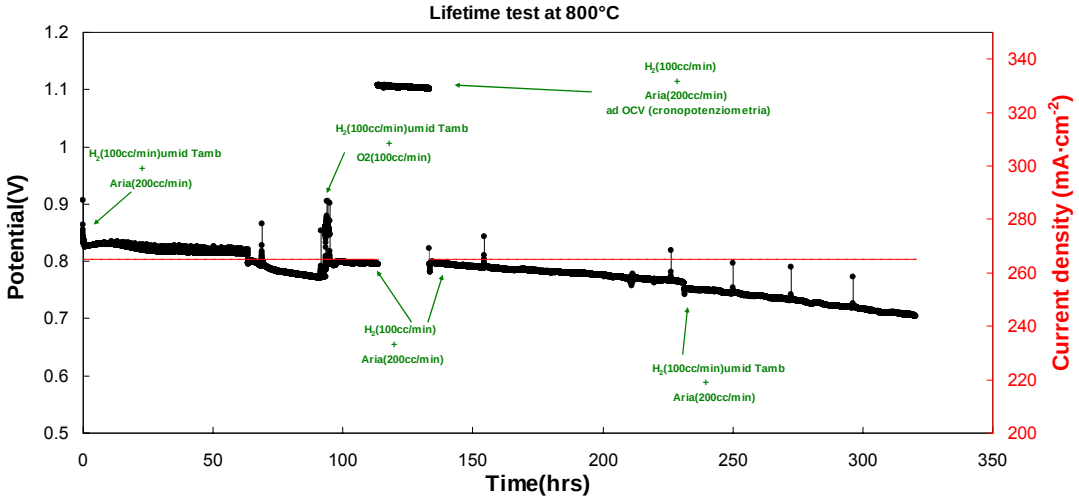

Figure 8. Lifetime test of the European Trade cell in H_2 (dry and humidified) fed.

Figure 9a shows the impedance spectra comparison for the cell during the time. It shows that during the time any significant variation of series resistance (R_s) appeared, confirming that any degradation accurse for the electrolyte as confirmed from the OCV which remained the same during all the time. In the other hand, was observed an important increasing of the polarization resistance (R_p) which was ascribe to a decrease of the catalytic activity [220, 221 , 222]. Remain to understand to which electrode attribute this ageing. Figure 9b, in accordance with the AC-Impedance investigation discussed before, shows the polarization and performance curves collected during the time, confirming that degradation occurred especially due to an increase of the ohmic loss.

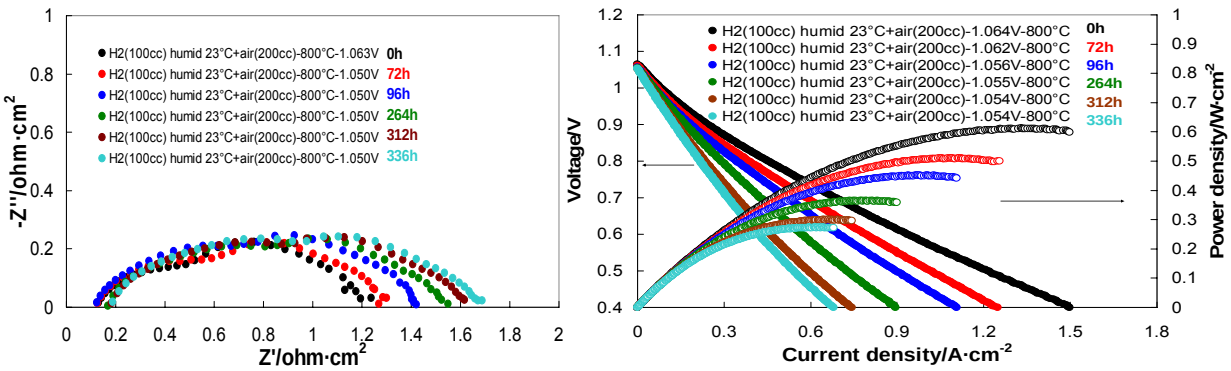

Figure 9a and 9b. AC-Impedance and Polarization investigations of the ageing for the European Trade cell feed by H_2 humidified at room temperature and Air flux.

[220] D. Waldbillig, A. Woodb, D.G. Ivey, Journal of Power Sources 145 (2005) 206–215
[221] H. Kim, C. Lu, W.L. Worrell, J.M. Vohs, R.J. Gorte, J. Electrochem. Soc. 149 (3) (2002) A247–A250.
[222] Hengyong Tu, Ulrich Stimming, Journal of Power Sources 127 (2004) 284–293

Physico-chemical analysis on post-mortem cell

SEM observation of the European Trade cell post-mortem shows (Figure 10a) the presence of strange agglomerates in the anodic side at the electrode-electrolyte interface. In order to evaluate the composition of these agglomerates was performed an EDAX analysis. Figure 10b reveals that the composition was to rich in Ni. These are in contrast with the optimal anode and anode-electrolyte interface. In fact, agglomerate non permit the supply of the reactant on the interface. In the after hand, an anode too rich in Ni cannot have an extensive Triple Phase Boundary (TPB) [223]. Both reduce the kinetic of the reaction due to a decreased surface area and at the same time should appear an increase of the ohmic loss due to the discontinuity of the composition.

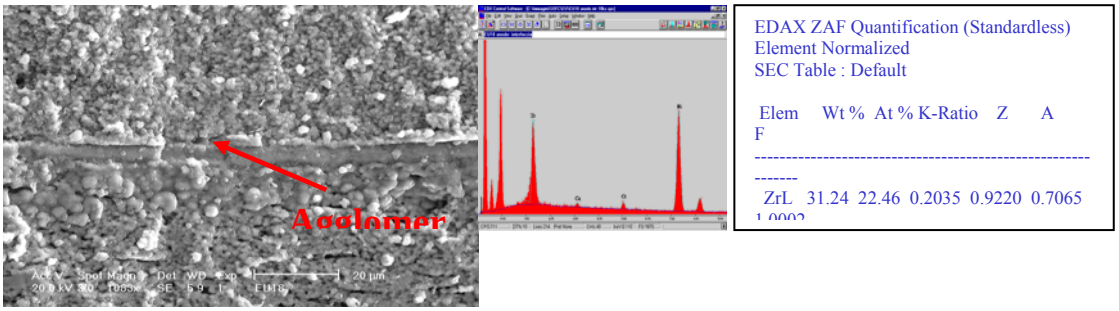

Fig. 10a and 10b. SEM and EDAX investigation on the European Trade cell post-mortem.

Conclusions

European Trade should work to improve the stability of them cells in particular in presence of humidifying. The reason of this phenomenon, at moment, is not clarified but the evidence is that during the time was observed a growth of the particles of the anodic reaction zone in the interface anode-electrolyte. Moreover, this effect is matched to an evident diffusion of the Ni particles in the electrode-electrolyte which can grow more easily rather than YSZ particles.

[223] Mizusaki, J., Tagawa, H., Saito, T., Kamitani, K., Yamamura, T., Hirano, K., Ehara, S., Takagi, T., Hikita, T., Ippommatsu, M., Nakagawa, S. and Hashimoto, K., Preparation of nickel pattern electrodes on YSZ and their electrochemical properties in H_2–H_2O atmospheres. J. Electrochem. Soc., 1994, 141, 2129.

Following our instruction, the European trade is working to prepare the cells differencing the cermet composition and the particle size, in the anode bulk and in the anode-electrolyte interface.

Nevertheless, there is to say that the European Trade Cell shows better performance in all tests, compared to the commercial InDEC cell, excluding the test in pure O2 flux. We suppose that the European Trade cell has got a better porosity which help the gas diffusion but with worse conductivity rather than InDEC cells.

Parts of these electrochemical measurements have been added as part of the work titled "Tape casting fabrication and co-sintering of solid oxide "half cells" with a cathode–electrolyte porous interface" published by Solid State Ionics 177 (2006) 2093–2097 DOI 10.1016/j.ssi.2006.01.016

PROPANE CONVERSION OVER A RU/CGO CATALYST AND ITS APPLICATION IN INTERMEDIATE TEMPERATURE SOLID OXIDE FUEL CELLS

Introduction

The direct oxidation of hydrocarbons in intermediate temperature solid oxide fuel cells (IT-SOFCs) has been intensively investigated in the last years due to the high intrinsic efficiency of the direct electrochemical oxidation process. A significant attention has been focused on methane electro-oxidation by using electrocatalysts such as Cu/CeO_2, Ni-Cu and various perovskites [224, 225, 226, 227, 228, 229]. Encouraging results have been achieved at temperatures below 800 °C especially in the presence of ceria as electrolyte.

Some attempts have been addressed to the direct oxidation of larger molecular weight hydrocarbons [230, 231]. It has been observed that the kinetics of direct electrochemical oxidation of propane is lower than methane and, moreover, it is more affected by the cracking process producing carbon fibres poisoning of the anode surface especially in the case of Ni-based catalysts. The formation of carbon deposits also occurs under steam reforming conditions at intermediate temperatures. Accordingly, it appears necessary to investigate alternative catalysts for both direct electro-oxidation and steam reforming of propane in IT-SOFCs.

Recently, several investigations have been addressed to the use of Ru as promoter of anodic processes in SOFCs [232, 233, 234, 235]. We have focused our efforts on the

[224] R. J. Gorte, S. Park, J. M. Vohs, C. Wang, Advanced Materials 2000, 12, No.19,October 2.
[225] H. Kim, C. Lu, W.L. Worrell, J,M. Vohs, R.J. Gorte, J. Electrochem. Soc. 149 (3) A247-A250 (2002).
[226] S. Tao and J. T. S. Irvine. Nature Materials 2, 320-323 (2003).
[227] S. Park, J.M. Vohs, R.J. Gorte, Nature 404 (2000) 265–267.
[228] S. Mcintosh, J.M. Vohs, R.J. Gorte, Electrochim. Acta 47 (2002) 3815–3821.
[229] H. Kim, C. Lu,W.L.Worrell, J.M. Vohs, R.J. Gorte, J. Electrochem. Soc. 149 (2002) A247–A250.
[230] R. J. Gorte, S. Park, J. M. Vohs, C. Wang, Advanced Materials 2000, 12, No.19,October 2.
[231] S. McIntosh, J.M. Vohs, R.J. Gorte, J. Electrochem. Soc. 150 (2003) A470–A476.
[232] T. Hibino, A. Hashimoto, M. Yano, M. Suzuki, M. Sano, Electrochimica Acta 48 (2003) 2531-2537
[233] M. Lo Faro, R. Bonfiglio, D. La Rosa, L. R. Gullo, V. Antonucci, A. S. Aricò, in Proceedings of the Sixth European Solid Oxide Fuel Cell Forum, M. Mogensen Editor, pp. 105-113, European Fuel Cell Forum, Lucerne, Switzerland (2004).
[234] M. Suzuki, H. Sasaki, S. Otoshi, in: F. Grosz, P. Zegers, S.C. Singhal, O.Yamamoto (Eds.), Proceedings of the Second International Symposium of SOFC's, Athens, 1991, p. 323.
[235] M.J. Saeki, H. Uchida, M. Watanabe, Catal. Lett. 26 (1994) 149–157.

investigation of the effect of Ru in combination with ceria as oxidation catalyst for propane in intermediate temperature SOFCs i.e. $Ru/Ce_{0.8}Gd_{0.2}O_{1.9}$ (CGO). In order to evaluate the characteristics of this catalytic system, out-of-cell experiments have been carried out for the propane steam reforming and both direct electro-oxidation and internal reforming have been evaluated in a ceria-electrolyte supported single cell. In this latter case, a suitable current collector, i.e. Cu, was added to the composite anodic layer to achieve proper electronic percolation within the layer.

Experimental

Ru/CGO catalyst

Beginning was prepared the Ru/CGO catalyst by the incipient wetness method [236]. The CGO powder (Praxair) was impregnated with a solution of $RuCl_3$ in ethanol at 50°C. The powder was first dried at room temperature and then calcined in oven at 500°C for 5 hours (heating rate, 1°C/min; cooling rate, 2°C/min). Reduction was carried out in 5:95 H_2/Ar flow at 400°. The powders was caracterized by X-ray fluorescence analysis (XRF Explorer, Bruker) that shows a Ru content about 18% (wt/wt). Furthermore, on the powder was carried out a XRD analysis by a X'PERT Philips diffractometer equipped with Cu Kα source. Both Bragg-Brentano and thin film (grazing angle mode) set-up were used.

Fresh and used catalysts was investigated by transmission electron microscopy (TEM) using a Philips CM12 instrument to better evaluate the morphology. Specimens were prepared by ultrasonic dispersion of the catalysts in isopropyl alcohol depositing a drop of suspension on a carbon-coated grid. A Carlo Erba CHNS-O elemental analyzer was used to determine the amount of deposited carbon on the catalysts after steam reforming catalytic experiments and electrochemical operation.

---

[236] M. Lo Faro, R. Bonfiglio, D. La Rosa, L. R. Gullo, V. Antonucci, A. S. Aricò, in Proceedings of the Sixth European Solid Oxide Fuel Cell Forum, M. Mogensen Editor, pp. 105-113, European Fuel Cell Forum, Lucerne, Switzerland (2004).

Catalytic activity

Catalytic activity measurements for propane steam reforming were carried out at atmospheric pressure in a quartz microreactor (internal diameter = 4 mm) placed in a ceramic tube furnace, at a space velocity of 60,000 h^{-1}, in the temperature range 600-800°C. The catalyst, placed between quartz wool in the middle of the reactor, was diluted with SiC (SiC/catalyst = 2). The temperature of the catalyst bed was monitored with a thermocouple sheathed in a quartz thermowell inserted into the reactor bed. An isocratic pump was used to feed water in the stream to an evaporator heated at 200°C and to control the steam to carbon ratio (S/C) in the reaction gas mixture entering the microreactor. The gas lines were maintained at approximately 70°C to prevent condensation. Before passing into the gas-chromatograph, water was eliminated from the reactor outlet gases by a condenser kept at 25°C. Gases were fed with properly calibrated mass flow controllers (Brooks 5850S) after purification by Deoxo Gas Clean Filters (Chrompack) and molecular sieve trap.

The steam to carbon (S/C) inlet flow was adjusted to 2.5. The total inlet flow was fixed at 150 cc/min, using nitrogen as balance. Reaction product gases were analyzed using a Varian micro GC. The catalytic activity results were generally taken 90 min after the setting of the reaction conditions, when reproducible data were obtained for 60 min at least.

Propane steam reforming (S/C=2.5) was investigated between 600 and 800°C at 1 atm, and at a GHSV of 60,000 h^{-1}.

SOFC characterization

In order to evaluate the behaviour of the Ru/CGO catalyst in a SOFC fed with propane, it was necessary to combine this catalyst with a suitable current collector that does not interfere with the catalytic activity and it also avoids promoting the cracking process.

Copper was selected as suitable current collector. It is known that no carbon formation occurs on Cu upon exposure to dry hydrocarbons but there is also no catalytic effect by copper on the electrochemical oxidation [237]. To facilitate the electronic percolation through the catalytic layer, the ratio between the CuO precursor (current collector) and

[237] H. Kim, C. Lu, W.L. Worrell, J,M. Vohs, R.J. Gorte, J. Electrochem. Soc. 149 (3) A247-A250 (2002).

catalyst (Ru-CGO) was maintained as 70:30 wt%. Thus the total Ru content in the anode layer was about 6%wt.

The SOFC device used in this study consisted of button cell (1cm^2 active area)containing three layers:

- anode: composite of Ru-CGO catalyst (30%wt) and CuO (70%wt) (thickness: 15 μm)
- electrolyte membrane: CGO (thickness: 250 μm)
- cathode: Composite of LSFCO ($La_{0.6}Sr_{0.4}Fe_{0.8}Co_{0.2}O_3$) and CGO (thickness: 15 μm)

The synthesis of the CGO powder was made by a co-precipitation method described elsewhere in ref. [238]. The CGO powder was compacted by uniaxial pressing (300MPa). The green pellet was treated at 1450°C for 6 hrs in air to obtain a supporting electrolyte membrane (ρ_{rel} > 95%).

The LSFCO cathode was deposited by spraying painting using isopropanol as dispersant. The raw powder was purchased from Praxair. The cathode layer deposit was fired at 1100°C for 2 hrs in air to ensure a good adhesion to the membrane. The anode containing a mixture of reduced Ru/CGO 30%wt and 70%Cu (as CuO) was also deposited by spraying using the same organic vehicle as for the cathode and thermal treated at 1100°C for 2 hrs in inert (Ar) environment. It was preferred to utilize for the anode a raw powder containing Ru in the metallic form since significantly lower losses of Ru from the layer were observed after firing than in the case of a RuO_2 containing powder. In a previous paper [239], it was reported that some loss of RuO_2 occurs upon firing a thick supporting anode at 1200°C in air. In the present work, we have observed a complete loss of RuO_2 from a thin anode layer, in several experiments carried out in the same conditions. Thus, the use of metallic Ru (Ru sublimation temperature is about 2300°C) and inert environment were necessary during the firing process. Finally, the cell was mounted on an alumina tube and sealed with quartz adhesive (AREMCO) and heated between 500 and 750°C in diluted H_2 stream. At the 750°C the gas was switched to dry propane or propane-water mixture to investigate the direct oxidation or reforming process. The C_3H_8 flow rate was 28cc/min per cm^2.

During internal reforming operation, an HPLC pump was used to feed precise amounts of liquid water that was vaporized in the propane stream.

---

[238] R. Burch, M.J. Hayes, Journal of Molecular Catalysis A: Chemical 100 (1995) 13-33

[239] T. Hibino, A. Hashimoto, M. Yano, M. Suzuki, M. Sano, Electrochimica Acta 48 (2003) 2531-2537

Electrochemical polarizations and ac-impedance measurements were performed on electrolyte supported single cells at 750°C by using an AUTOLAB PGSTAT30 Metrohm potentiostatical frequency-response analyzer equipped with 20A booster. Gold wires were used as current collectors for the cell. A thermocouple was positioned close to the cell. Impedance spectra were obtained in the frequency range from 10 mHz to 1 MHz with applied ac-voltage amplitude of 10 mV rms. All impedance measurements were taken under open-circuit conditions.

Results and discussion

Physico-chemical analysis of the Ru/CGO catalyst

TEM observation of the Ru/CGO catalyst (Fig.1) shows a distribution of fine spherical Ru particles of about 20 nm on large irregular shape CGO particle support.

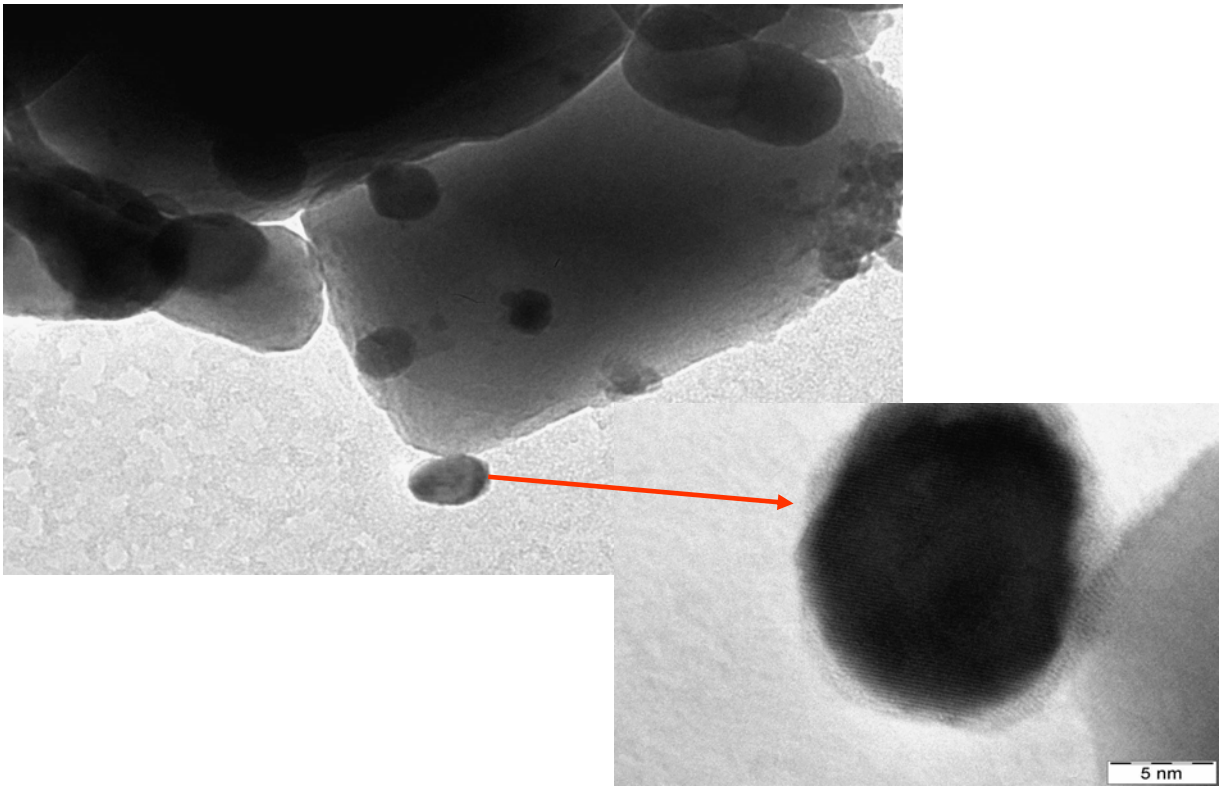

Figure 1: TEM images of 20% Ru/CGO catalyst. The small particles are composed of metallic Ru.

The XRD patterns of the fresh catalyst and after the steam reforming operation at 800°C are shown in Fig.2. The reflections due to RuO_2 are clearly visible in the diffraction

pattern of the calcined sample (a). After reduction, Ru peaks become evident (b). The pattern of the catalyst after the steam reforming process (out-of-cell test) does not show any significant formation of graphitic carbon deposits.

The X-ray scattering at about 22° is due to the catalyst dilution with SiC used for the out-of-cell steam reforming experiment. No evidence of carbon deposits was observed from TEM and CHNS-O analyses after the steam reforming test.

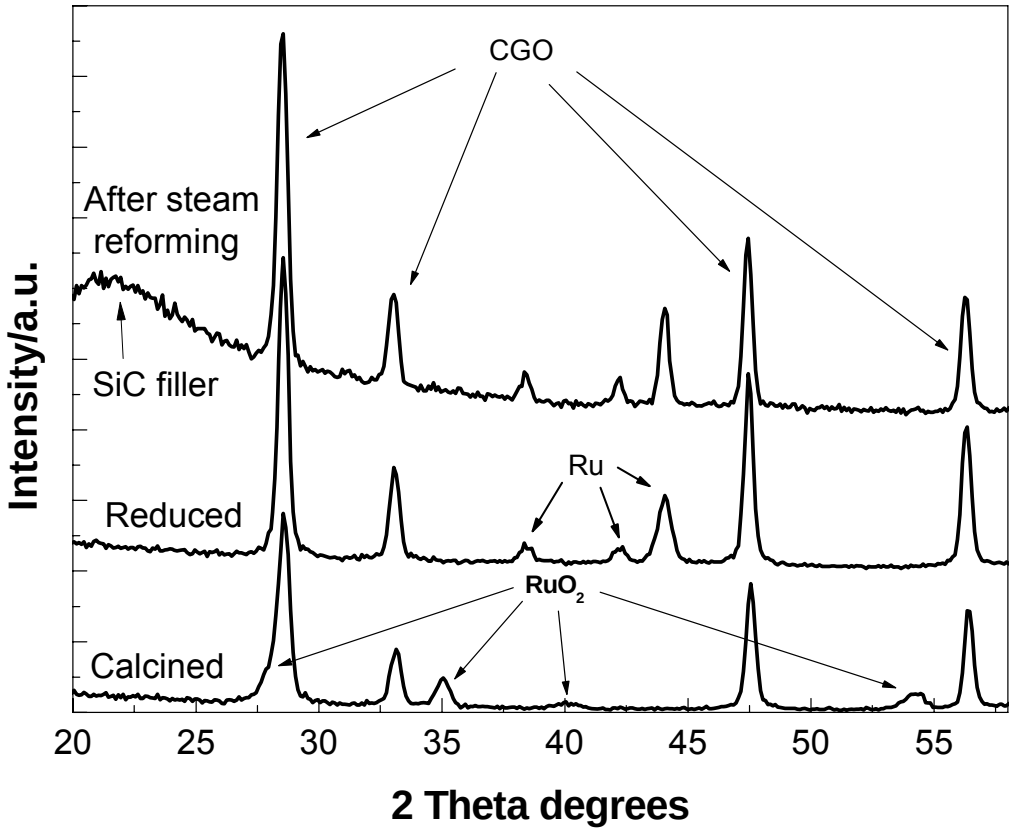

Figure 2: XRD patterns of the Ru/CGO catalyst calcined, reduced, and after the steam-reforming test.

Steam reforming process

The effect of temperature on the steam reforming catalytic activity of 20 wt% Ru/CGO catalyst was investigated. Conversions and products distribution are presented in Table 1.

		%products			
T (°C)	**H_2**	**CO**	**CO_2**	**CH_4**	**C**
600	64.96	7.59	13.68	13.56	0.21
700	68.80	14.10	9.20	7.48	0.50
800	71.08	18.11	6.27	1.17	3.38

Table 1: Distribution of products in the out-of-cell steam reforming tests

It shows the variation of conversion and selectivity towards syngas as a function of temperature. An almost complete propane conversion was observed in the temperature range investigated. The syngas concentration in the reactor outlet increases with temperature, passing from 75% at 600°C to 88% at 800°C. On the contrary, both CO_2 and CH_4 in the outlet stream decreased with temperature.

A life-time catalytic test (steam reforming process) was carried out at 800°C. Table 2 and Fig. 3 shows the distribution of reaction products as a function of time. It is observed that conversion and selectivity remain almost constant during the life-time. No decay of catalytic activity is observed with time and the concentration of syngas in the outlet stream was about 90% during the experiment.

Time(min)	**conv.**	**C_3H_8**	**CH_4**	**H_2**	**CO_2**	**CO**	**C_2H_4**
1200	98,90	0,12	2,15	74,54	6,06	17,09	0,05
2400	99,40	0,06	2,64	74,03	6,45	16,78	0,05
3600	99,24	0,07	1,69	74,79	6,59	16,80	0,05
4800	98,39	0,15	2,21	73,88	6,70	17,00	0,05
6000	97,26	0,25	2,07	73,88	5,88	17,76	0,16
7200	98,55	0,13	2,76	72,74	5,62	18,63	0,12

Table 2: Distribution of products during life-time test at 800°C in umidified propane (S/C=2.5).

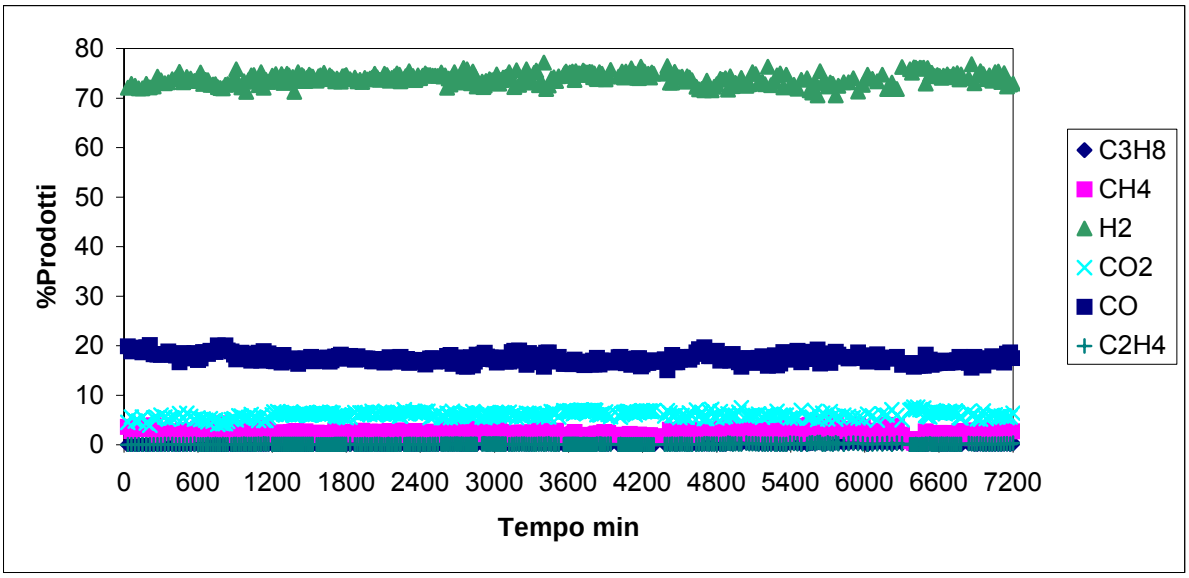

Figure 3: Life-time catalytic test of Ru/CGO at 800°C in umidified propane (S/C=2.5).

As above observed, no carbon deposits were detected after catalyst operation in propane during the steam reforming experiments. This indicates that the catalyst does not promote any cracking process under such conditions.

Electrochemical investigations

Fig. 4 shows the XRD pattern of the anode layer obtained in the grazing angle mode (1° incidence angle), reveals the presence of the typical reflections of Ru, Cu and CGO. A slight enrichment in Ru is observed in the outer layer (grazing angle mode).

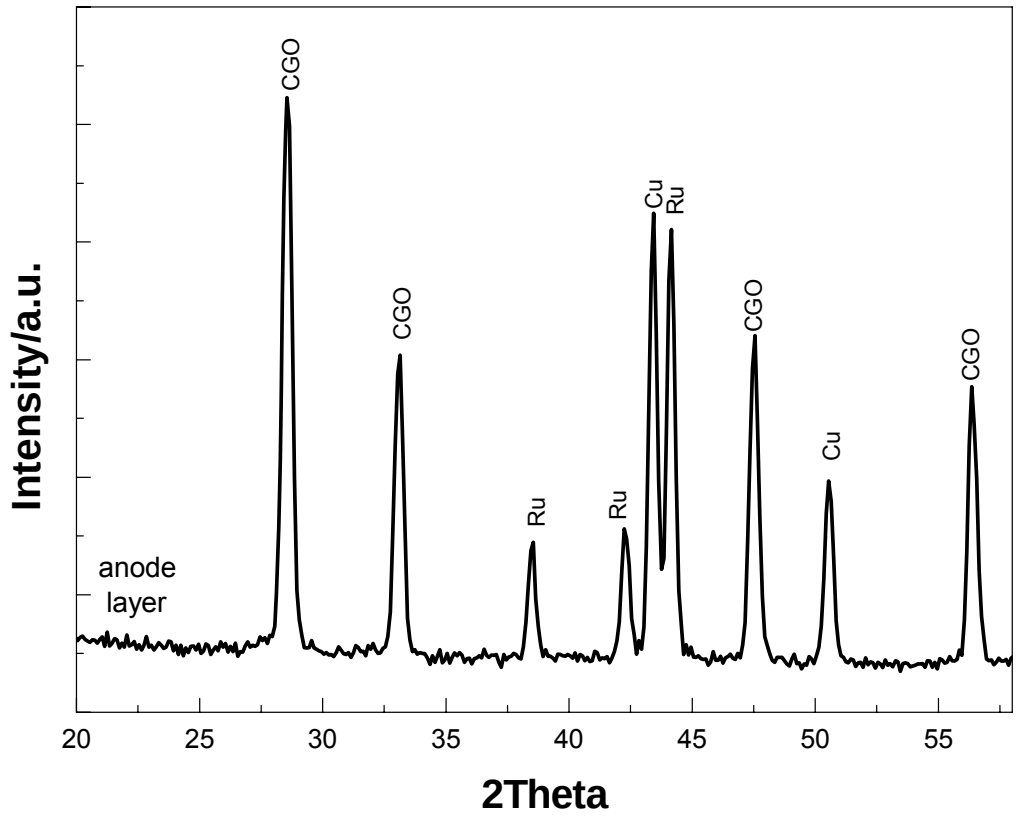

Figure 4: X-ray diffraction patterns of the anode layer.

However, no significant modification in the nominal composition was observed in the XRF analysis of the anode layer after scraping it from the fired cell. This indicates that the sublimation of RuO_2 [240] as reported in the literature does not occur with our experimental procedure. In the present process, the firing temperature is sufficiently high to promote adhesion of the anode layer to the membrane.

AC impedance analysis of the SOFC cell operating in presence of H_2 at 750°C (Fig. 5) under open-circuit conditions, shows significant ohmic resistance, 0.615 $\Omega \cdot cm^2$ (high frequency intercept), it decreases to 0.445 $\Omega \cdot cm^2$ at 800°C (Fig. 5).

[240] M. Lo Faro, R. Bonfiglio, D. La Rosa, L. R. Gullo, V. Antonucci, A. S. Aricò, in Proceedings of the Sixth European Solid Oxide Fuel Cell Forum, M. Mogensen Editor, pp. 105-113, European Fuel Cell Forum, Lucerne, Switzerland (2004).

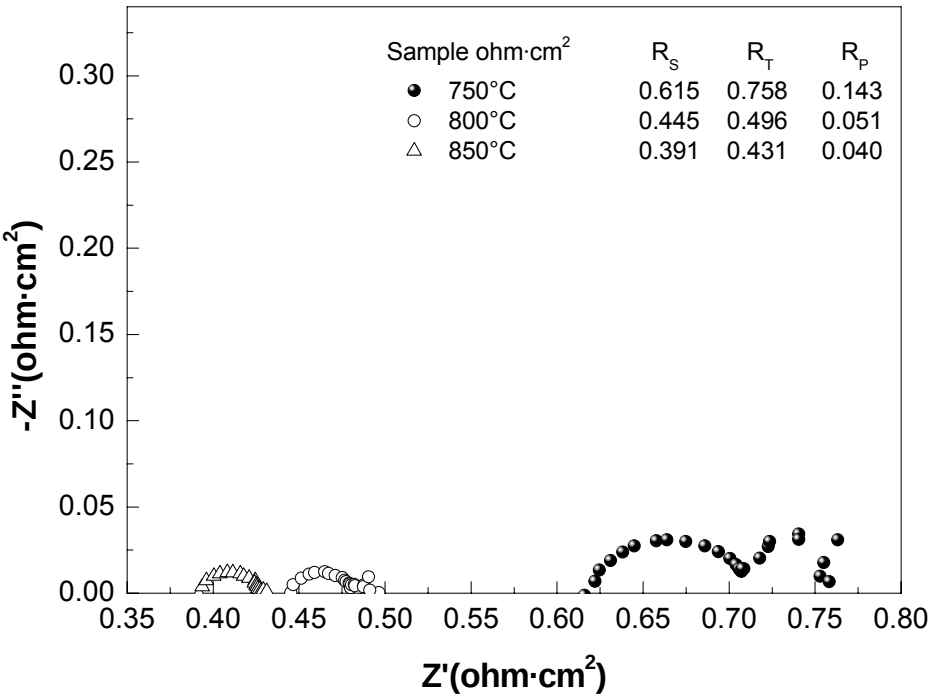

Figure 5: AC impedance spectra for the SOFC cell operating in presence of H_2 at different temperatures and open circuit voltage.

The observed ohmic resistance is only in part due to the supporting membrane electrolyte (about 0.3 $\Omega \cdot cm^2$ at 800°C) [241]. A significant contribution to the ohmic drop is also caused by poor electrode-electrolyte interface, adhesion properties and by a high level of porosity especially present in the anode [242]. However to avoid significant loss of Ru, a low firing temperature was necessary. On the after hand, the polarization resistances (low frequency intercept) are optimal at all temperature (e.g. 0.14 $\Omega \cdot cm^2$ at 750°C and 0.05 $\Omega \cdot cm^2$ at 800°C).

Polarization curves carried out in H_2 (Fig. 6) show that the maximum power density increases with the temperature whereas the OCV decreases due to the electronic conduction of CGO [243, 244, 245].

---

241 V.V. Kharton, A.V. Kovalevsky, A.P. Viskup, A.L. Shaula, F.M. Figueiredo,E.N. Naumovich, F.M.B. Marques, Solid State Ionics 160 (2003) 247– 258

242 Alexandre Closset, Stefan Diethelm, Kemal Nisancioglu, Jan van Herle and A. J. McEvoy, Journal of the European Ceramic Society 19 (1999) 843±846

243 R. Burch, M.J. Hayes, Journal of Molecular Catalysis A: Chemical 100 (1995) 13-33

244 C.W. Sun, J. Sun, G.L. Xiao, H.R. Zhang, X.P. Qiu, H. Li, L.Q. Chen, J. Phys. Chem. B 110 (2006) 13445–13452.

245 N.V. Skorodumova, S.I. Simak, B.I. Lundqvist, I.A. Abrikosov, B. Johansson, Phys. Rev. Lett. 89 (2002) 166601.

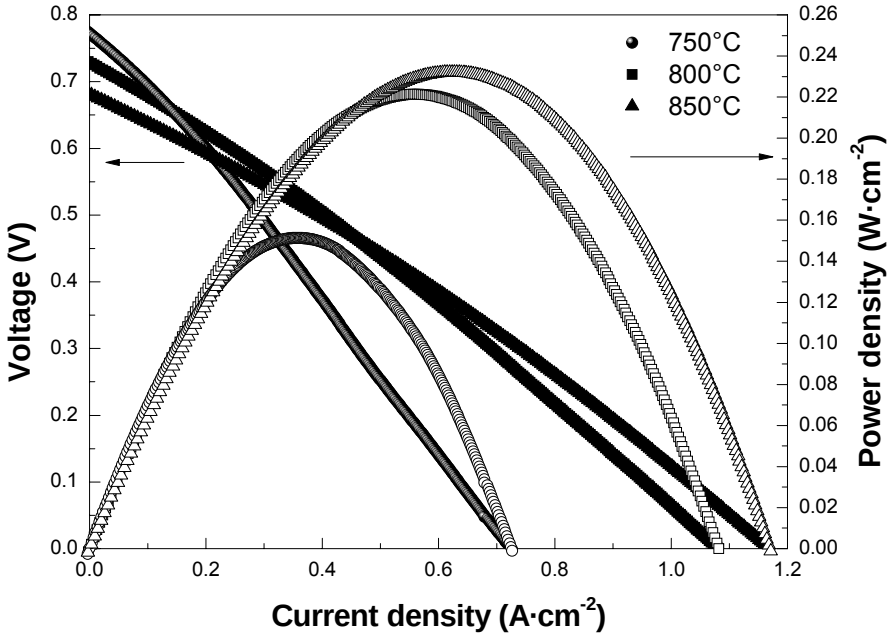

Figure 6: Polarization curves at different temperatures in the presence H_2 feed at the anode.

Impedance spectra were carried out in the presence of dry propane at open circuit voltage conditions. Fig. 7, shows an ohmic resistance slightly larger than was registered in H_2 at all temperatures.

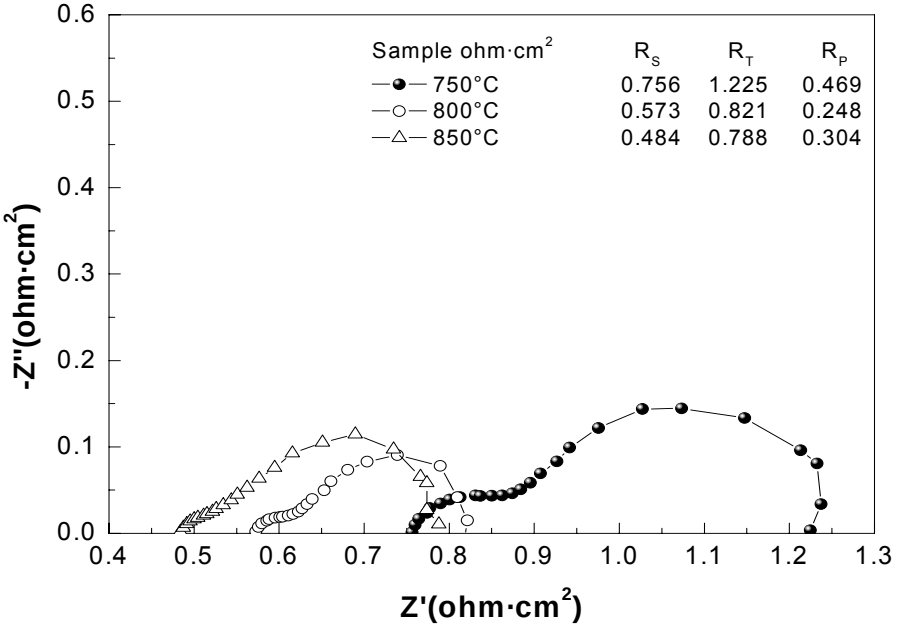

Figure 7: AC impedance spectra for the SOFC cell operating in the presence of C_3H_8 at different temperatures and open circuit voltage.

Whereas, an increase in the polarization resistance was observed as expected due to the slower reaction rate of propane oxidation compared to H_2. However, the observed R_p value in propane at 750°C and 800°C i.e. 0.469 $\Omega \cdot cm^2$ and 0.248 $\Omega \cdot cm^2$ respectively, indicate suitable reaction rates. An inversion of tendency regarding of the polarization resistance is observed at 850°C. Presently where Rp increases again we can not easily identify if any cracking process or gas phase reaction is hindering the anodic process under dry propane operation at 850°C. No carbon deposits or tar formation were observed after cell shut down. Fig. 8 shows polarization curves in dry propane feed at different temperatures.

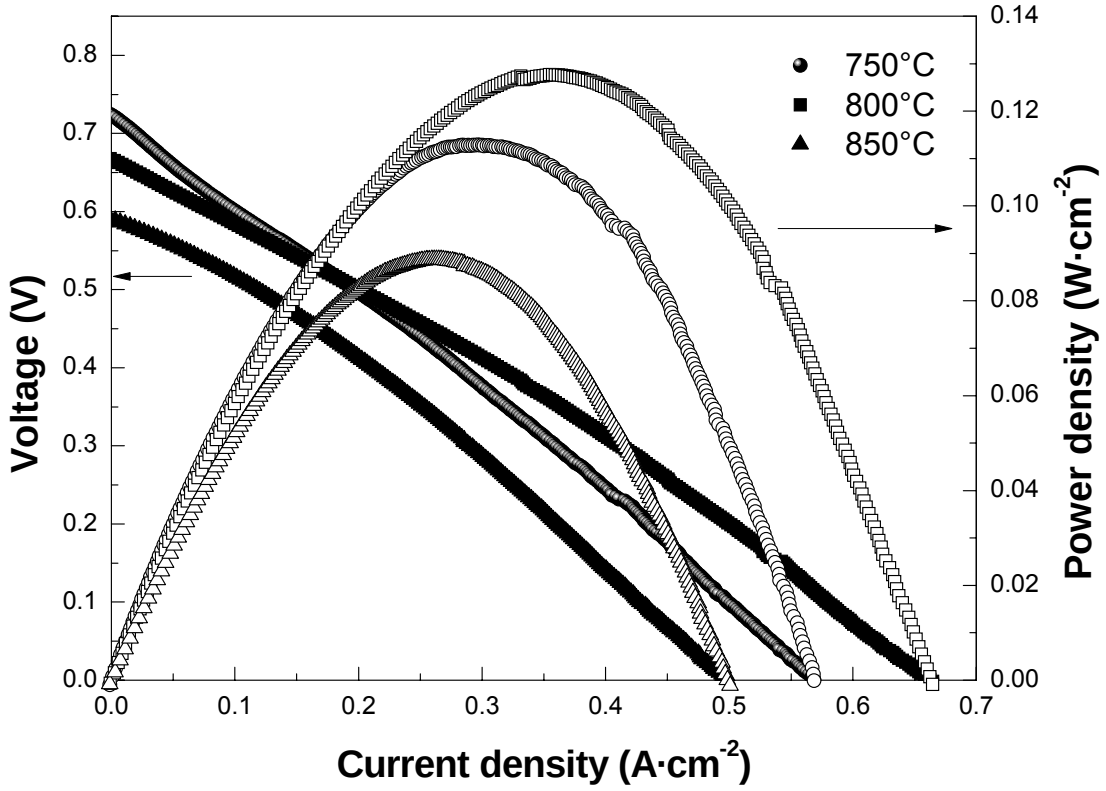

Figure 8: Polarization curves at different temperatures in C_3H_8 fed.

A maximum power density of about 130 mW/cm^2 was obtained at 800°C. Both polarization and impedance spectra indicate that the direct electro-oxidation of propane can be suitable performed in the temperature range of 750°-800°C. The moderate output

power density (130mW·cm^{-2} at 800°C) are mainly affected by ohmic drop and low OCV (essetially related to the electrolyte membrane) than from the catalyst properties.

In order to better evaluate the behaviour of the catalyst under SOFC operation, in the internal reforming process was also investigated.

Fig. 9 shows a comparison of the measured fuel cell performances for the internal reforming of propane and for the dry process at 750°C.

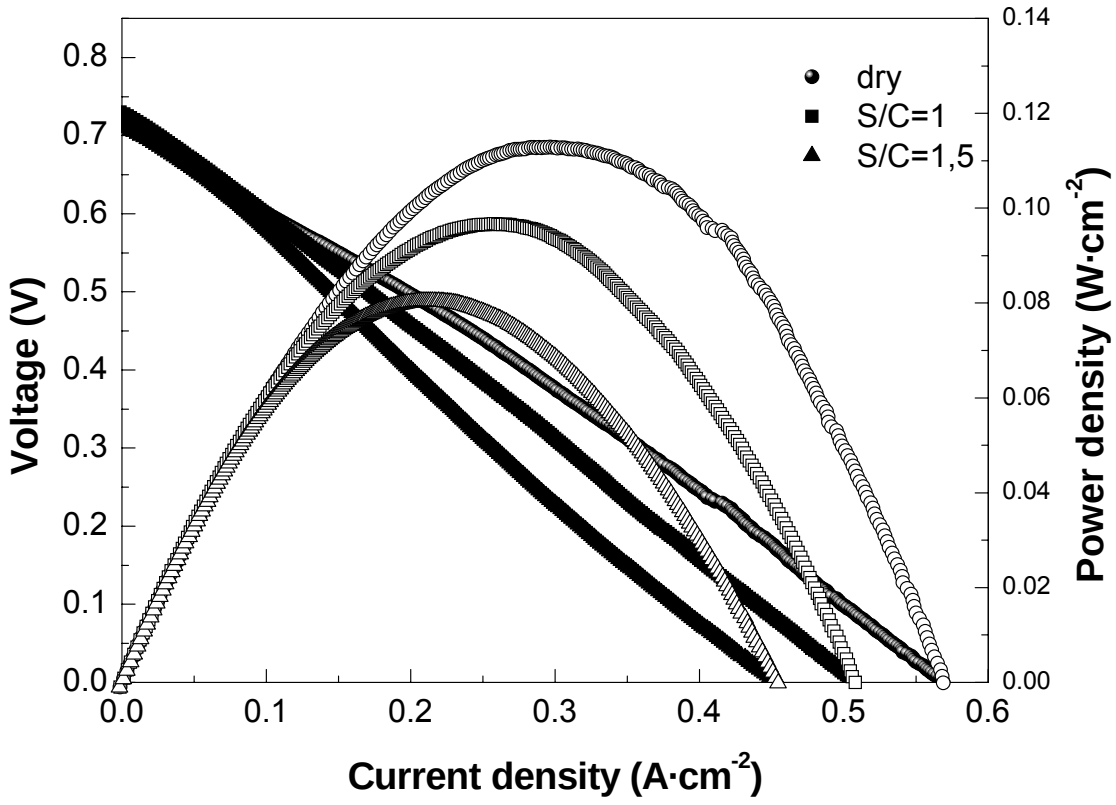

Figure 9: Comparison of dry operation and internal reforming polarization curves at different S/C ratios at 750 °C.

It is observed that the maximum power density measured at 750°C decreases passing from dry propane to wet propane probably due to a more efficient direct electro-oxidation process at 750°C rather than the steam reforming.

The measured maximum power density is in the case of the internal steam reforming S/C=1 (97 mW · cm^{-2}) lower than that observed with dry propane (113 mW·cm^{-2} at 750°C . An increase of the S/C ratio further decreases the performance thus; we avoided to investigate higher S/C ratios. Although we have used in the case of the dry propane a

C_3H_8 flux significantly larger than that required by the faradic process, a promotion of the reforming reaction on the catalyst surfaces by the electrochemically produced water should not be discarded. Yet, it appears that the rate of C_3H_8 oxidation in the of dry processes is better than the internal reforming at least below 750°C.
No carbon deposits were observed from electron microscopy and CHNS-O analyses after shut-down in propane for the anodes which have operated in both direct oxidation and internal reforming modes.

Direct oxidation versus reforming

The catalyst investigated in the present study is a combination of an oxidation (ceria) and reforming (Ru) process promoters. Since water is formed as reaction product on the catalyst surface during the oxidation process of dry hydrocarbons a synergistic effect between direct oxidation and reforming would be expected in the presence of two catalytic functions accelerating both process.
Effectively, the superior performances obtained in the presence of dry propane seems to indicate that the catalyst operates according to what is expected. Clearly, the performance of the present SOFC may be greatly enhanced if a thin electrolyte is adopted (reduced ohmic drop) and if the CGO electrolyte membrane is replaced by another electrolyte characterized by a higher ionic transport number under such conditions. In fact, high ohmic drop and low OCV affect the performance of the present SOFC device. Whereas, the polarization resistances in dry propane were quite promising and indicate that this catalyst can properly operate in absence of Ni. As well know Ni promotes the C-H bond scission and thus, the direct oxidation but it also significantly increases the probability of irreversible deposition of carbon species at the surface blocking the catalytic sites with time.
Breaking of the carbon-hydrogen bond is considered to be the activation step in the direct oxidation process [246] followed by removal of the adsorbed species by O^{2-} ions. Thus, higher performances are initially achieved with Ni based catalysts; yet, long term operation of Ni dry operation is questioned, as above discussed, due to the growth of carbon deposits. On the other hand, CGO has been identified as a suitable oxidation catalyst for both H_2 and methane oxidation [247, 248]. The rate determining step on this

[246] R. Burch, M.J. Hayes, Journal of Molecular Catalysis A: Chemical 100 (1995) 13-33
[247] Olga A. Marina, Carsten Bagger, Soren Primdahl, Mogens Mogensen, Solid State Ionics 123 (1999) 199-208

oxide catalyst presently appears to be related with the scission of C-H bond. On such aspect and the improvement of electrode microstructure our efforts are presently focused to achieve suitable oxidation rates during SOFC operation [249].

Conclusions

Direct oxidation and internal reforming processes of propane at a Cu-Ru/CGO electro-catalyst have been investigated at intermediate temperatures (750°-800°C) in a CGO electrolyte supported cell. The measured electrochemical performances were affected by significant ohmic resistance and low OCV; whereas, interesting polarization resistances were recorded especially high temperatures. Although, out-of-cell catalytic steam reforming tests indicate that the propane conversion to syngas reached 80-90% under these conditions, the measured power densities in hydrogen were more than twice those recorded in the internal reforming of C_3H_8. Interestingly, the SOFC performance recorded for the dry operation was larger than the internal reforming at 750°C. It appears that further optimization of the anode structure is necessary for a better utilization of the Ru/CGO catalyst.

These results have been published on the Journal Applied Electrochemistry, 37 (2007) 203-208 DOI: 10.1007/s10800-006-9245-5

[248] O.A. Marina, M. Mogensen, Appl. Catal. A 189 (1999) 117–126.
[249] C.W. Sun, Z. Xie, C.R. Xia, H. Li, L.Q. Chen, Electrochem. Commun. 8 (2006) 833–838.

INVESTIGATION of COMPOSITE Ni-DOPED PEROVSKITE ANODE CATALYST for ELECTROOXIDATION of HYDROGEN and LIGHT HYDROCARBONS in SOLID OXIDE FUEL CELLs

Introduction

Propane is the main component of liquefied petroleum gases (LPG). This is an interesting fuel for SOFCs. It is cheap, widely available and it can be liquefied to facilitate its storage for specific applications. Due to these properties, desulphurised propane and LPG have good properties to be used as fuel in portable power sources. For such applications, the direct oxidation process is favoured since it does not require any special fuel and water management, thus, reducing the complexity of the system [250]. For portable applications, the main requirements concern with the obtainment of suitable power densities and simplicity of design as well as operation at intermediate temperatures. Thus, ceria based electrolytes have good perspectives since the lower electrical efficiency usually associated to this electrolyte as compared to the conventional yttria-stabilised zirconia is compensated by the higher conductivity at lower temperatures [251].

Recently, several investigations have been addressed to the use of Ru as promoter of propane oxidation in IT-SOFCs [252, 253, 254]. Yet, the high cost of Ru suggests searching for an alternative catalyst formulation with similar activity at intermediate temperatures. In this chapter, the effect of low content of Ni in combination with $La_{0.6}Sr_{0.4}Fe_{0.8}Co_{0.2}O_3$ and ceria as oxidation catalyst for hydrogen and propane in intermediate temperature SOFCs, i.e. Ni-LSFCO/$Ce_{0.8}Gd_{0.2}O_{1.9}$ has been investigated. In addition, to reduce Ni amount could be a good way to achieve fuel cells with improved recyclability, durability, thermal and redox stability. The reaction environment at the

[250] A. Sauvet and J.T.S. Irvine, *Fuel Cells - From Fundamentals to Systems*, 2001, **1**, 205-210.
[251] N. Maffei, A.K. Kuriakose, Solid State Ionics 107 (1998) 67-71
[252] T. Hibino, A. Hashimoto, M. Yano, M. Suzuki, M. Sano, Electrochimica Acta 48 (2003) 2531-2537.
[253] M. Lo Faro, R. Bonfiglio, D. La Rosa, L. R. Gullo, V. Antonucci, A. S. Aricò, in Proceedings of the Sixth European Solid Oxide Fuel Cell Forum, M. Mogensen Editor, European Fuel Cell Forum, Lucerne, Switzerland (2004) 105-113.
[254] M. Lo Faro, D. La Rosa, G. Monforte, V. Antonucci, A. S. Arico and P. Antonucci, Journal of Applied Electrochemistry 37 (2007) 203-208.

anode during the direct oxidation of dry-propane for CGO-electrolyte based SOFCs is not strongly reducing due to the occurrence of several processes. O^{2-} ions flow from the cathode due to the fuel cell electrical process; O_2 molecules are pumped into the anode compartment even under open circuit voltage conditions (oxygen pump effect) due to the different oxygen partial pressure between the cathode and anode separated by the anionic ceramic membrane [255]. A further oxygen flow is promoted by reduction of ceria-based electrolytes at the anode and reoxidation at the cathode. This process is exemplified below in the case of hydrogen as reducing agent:

$$2Ce^{4+} + H_2 + O^{2-} \rightarrow 2Ce^{3+} + H_2O \quad (1)$$

$$2Ce^{3+} + \frac{1}{2}O_2 \rightarrow O^{2-} + 2Ce^{4+} \quad (2)$$

All these effects mitigate the reducing atmosphere at the anode thus limiting the reduction of the transition metals in the perovskite structure. Perovskite materials are characterized by mixed electronic-ionic conductivity and the interaction between the dispersed Ni- phase and LSFCO oxide at high temperature modify the electronic properties and the propensity of Nickel to form carbon deposits. In this catalytic layer, Ni is not present in the bulk form as in a classical cermet but, it is well dispersed on the perovskite support. Accordingly, the electronic conducting properties are exerted by LSFCO whereas Ni acts as promoter for the catalytic activity. Furthermore, this strong interaction between Ni and perovskite may favour the formation of an oxidised Ni-phase that is stable under mild reducing conditions. The overall electrochemical process is:

$$C_3H_8 + 10O^{2-} \rightarrow 3CO_2 + 4H_2O + 20e^- \quad (3)$$

$$5O_2 + 20e^- \rightarrow 10O^{2-} \quad (4)$$

The free energy change for the overall electrochemical process is :

$$\Delta G = -515{,}453 \text{Kcal/mol}$$

[255] Pietro Palmisano, Nunzio Russo, Paolo Fino, Debora Fino, Claudio Badini, Applied Catalysis B: Environmental 69 (2006) 85–92

Besides the main electrochemical process, several other processes may occur at the anode compartment during the fuel cell operation. Some of these are reported below together with their Gibbs free energy change [256]:

$$C_3H_8 + 2O_2 \rightarrow 2CO + CO_2 + 4H_2 \qquad \Delta G = -244{,}825 Kcal/mol \text{ at } 800°C, 1atm \quad (5)$$

$$C_3H_8 + 5O_2 \rightarrow 3CO_2 + 4H_2O \qquad \Delta G = -515{,}457 Kcal/mol \text{ at } 800°C, 1atm \quad (6)$$

$$C_3H_8 + 3H_2O \rightarrow 3CO + 7H_2 \qquad \Delta G = -64{,}433 Kcal/mol \text{ at } 800°C, 1atm \quad (7)$$

$$C_3H_8 \rightarrow 4H_2 + 3C \qquad \Delta G = -51{,}577 Kcal/mol \text{ at } 800°C, 1atm \quad (8)$$

From a thermodynamic point of view the direct oxidation process should be favoured since the Gibbs free energy change compares favourably to the reforming and carbon deposition process. Yet, due to kinetic and electrochemical constraints including C-C bond cleavage for C_3H_8, unefficient transport of O^{2-} ions through the electrolyte and availability at the interface, the side-reactions may readily occur.

Formation of H_2 and CO is not deleterious for the process since both molecules electrochemically react with O^{2-} ions to form H_2O and CO_2; whereas, carbon deposition usually deactivate the catalyst. It has been shown in the literature that some Ni catalysts, such as metallic Ni-Cu, Ni-Co, tolerate small amounts of carbon deposition or carbon fibers formation [257]. These fibers usually improve the electronic conductivity inside the catalytic layer.

In order to evaluate the characteristics of this catalytic system, temperature programmed analyses have been carried out as well as hydrogen and propane direct electro-oxidation process has been evaluated in a ceria-electrolyte supported single cell. The aim of this work is to demonstrate that the direct oxidation of hydrogen and propane can be effectively carried out in a IT-SOFCs using more reversible anodic catalysts rather than Ni, in presence of ceria based electrolytes.

[256] SUPCRT92

[257] S. Lee, J.M. Vohs, R.J. Gorte, J. Electrochem. Soc. 151 (2004) A1319–A1323

Experimental

The Ni-LSFCO/CGO catalyst was prepared by the incipient wetness method [258]. The LSFCO powder (Praxair) was impregnated at 50°C with a solution of Ni nitrate in water. The powder was first dried and then calcined in oven at 500°C for 5 hours (heating rate, 2°C/min; cooling rate: 2°C/min). Reduction was carried out in 5:95 H_2/Ar flow at 400°C (30min) preventing the LSFCO reduction in this phase of catalyst preparation. Reduction at 800°C (30min) was also carried out to study structural modifications. The resulting Ni content was about 10% in LSFCO (wt/wt). XRD analysis was carried out with a X'PERT Philips diffractometer equipped with Cu Kα source. Bragg-Brentano set-up was used.

Temperature programmed measurements for hydrogen and propane stream were carried out at atmospheric pressure in a quartz microreactor placed in a ceramic tube furnace in the temperature range 400-800°C. The temperature of the catalyst bed was monitored with a thermocouple inserted into the reactor cuvette. Gases were fed with properly calibrated mass flow controllers. The total inlet flow was fixed at 20 cc/min, using Argon as balance.

In order to evaluate the behaviour of the Ni-LSFCO/CGO catalyst for the direct oxidation reaction, it has been tested as anode in a SOFC fed with hydrogen and propane stream. The SOFC device used in this study consisted of a button cell (1 cm^2 active area) containing three layers:

Anode: Composite of Ni-LSFCO catalyst (70 wt%) and CGO (30 wt%) (thickness: 15 μm)

Electrolyte membrane: CGO (thickness: 250 μm)

Cathode: Composite of LSFCO ($La_{0.6}Sr_{0.4}Fe_{0.8}Co_{0.2}O_3$) and CGO (thickness: 15 μm).

The synthesis of the CGO powder was made by a co-precipitation method described elsewhere [259]. The CGO powder was compacted by uniaxial pressing (300 MPa). The green pellet was treated at 1450°C for 6 hrs in air to obtain a supporting electrolyte membrane (ρ_{rel} > 95%).

---

[258] M. Lo Faro, R. Bonfiglio, D. La Rosa, L. R. Gullo, V. Antonucci, A. S. Aricò, in Proceedings of the Sixth European Solid Oxide Fuel Cell Forum, M. Mogensen Editor, European Fuel Cell Forum, Lucerne, Switzerland (2004) 105-113.

[259] J. V. Herle, T. Horita, T. Kawada, N. Sakai, H. Yokokawa, M. Dokiya, Ceramic International 24 (1998) 229-241.

The LSFCO cathode was deposited by spraying using isopropanol as dispersant. The raw powder was purchased from Praxair. The cathode layer deposit was fired at 1100°C for 2 hrs in air to ensure good adhesion to the membrane. The anode containing a mixture of calcined Ni-LSFCO catalyst (70 wt%) and 30% of CGO was also deposited by spraying using the same organic vehicle as for the cathode and thermally treated at 1100°C for 2 hrs in air. Finally, the cell was mounted on an alumina tube and sealed with quartz adhesive (AREMCO) and heated to reach 800°C in He stream. At 800°C, the gas was switched to H_2 and suddenly as the potential reached the OCV it was switched to 500 mV allowing electrochemical current flow (O^{2-} ions) preventing an extensive reduction of perovskite. Subsequently, the anode was fed with an excess of dry propane (respect to the stoichiometry requirements) under working condition at 500 mV cell voltage. It is inferred that during its operation in the SOFC, the Ni/LSFCO anode is not subjected to strong reducing conditions for prolonged times. The reducing environment at the anode is mitigated by both flow of O^{2-} ions due to the electrochemical process and the mixed electronic/ionic conduction of CGO electrolyte that does not allow it to reach high OCV associated with a very low oxygen partial pressure at the anode. After the short period of SOFC operation in Hydrogen (60hrs), the structural and chemical properties of the catalyst were not significantly different than those of the catalyst reduced ex-situ at 400°C as a consequence of mild reducing environment. Electrochemical polarizations and ac-impedance measurements were performed on electrolyte supported single cells at 800°C by using an AUTOLAB PGSTAT30 Metrohm potentiostatic frequency-response analyzer equipped with 20A booster. Gold wires were used as current collectors for the cell. A thermocouple was positioned close to the cell. Impedance spectra were obtained in the frequency range from 10 mHz to 1 MHz with applied ac-voltage amplitude of 10 mV rms. The ohmic (series) resistance was obtained from high frequency intercept on the real axis of the Nyquist plot. The polarization (charge transfer) resistance was derived as from difference between low frequency and high frequency intercepts on the real axis. All impedance measurements were taken under open circuit conditions and 500 mV.

Results and discussion

The XRD patterns of the fresh catalyst calcined at 500°C and after reduction at 400°C and at 800°C are shown in Fig.1. The reduction at 800°C represents an accelerated degradation test for the perovskite structure. The reflections due to the perovskite and

NiO are clearly visible in the diffraction pattern of the calcined sample. After reduction in hydrogen at 400°C, Ni peaks become evident without any significant variation of the typical perovskite patterns. After reduction at 800°C, a Ni pattern is evident as well as a change in the perovskite structure. It is pointed out that before electrode preparation, the maximum temperature at which the catalyst is reduced is 400°C. The X-ray reflection at about 28° appearing on both calcined and reduced samples is probably owing to the discharge of La from the original perovskite. This pattern identifies the resulting residual structure. The double peak between 31.3° and 32.7° appearing in the reduced sample at 800°C are assigned to La_2NiO_4 [260].

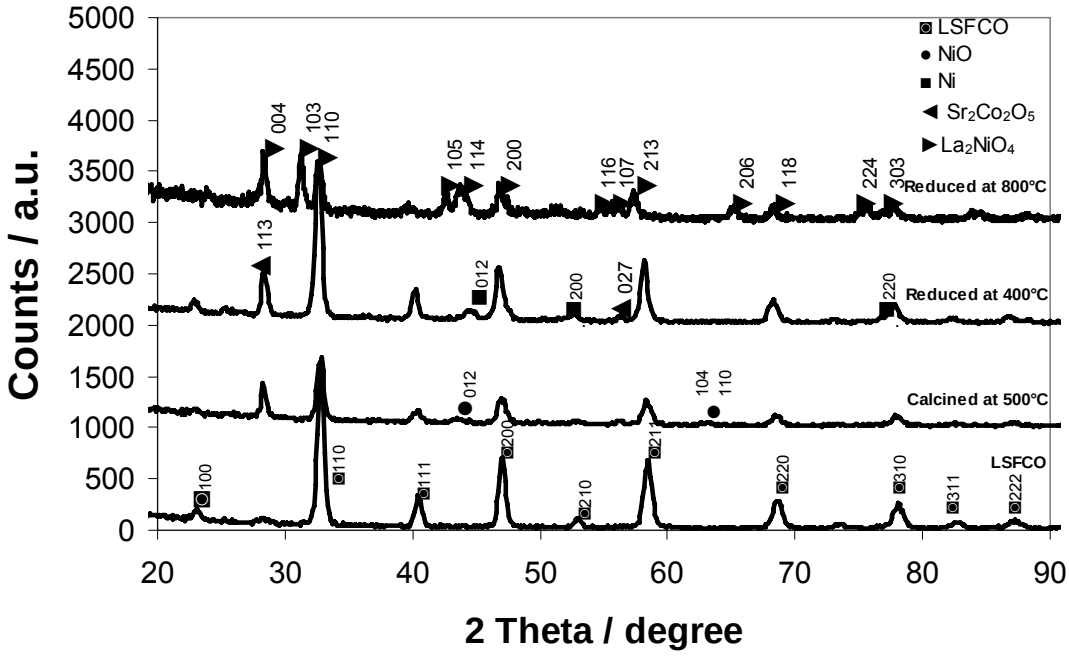

Fig.1. XRD patterns of the Ni-LSFCO catalyst calcined at 500°C and reduced at 400°C and at 800°C

The effect of temperature on the reduction in dry propane in an out-of-cell process of 10 wt% Ni/LSFCO catalyst previously reduced in hydrogen at 400 °C was investigated. XRD spectra of the catalyst discharged from the reactor are presented in Fig. 2. The perovskite structure is practically not affected after reduction at 400°C (untreated); it shows no modification at 600 °C; carbon deposition and perovskite structure modifications are observed above 700 °C.

[260] JCPDS

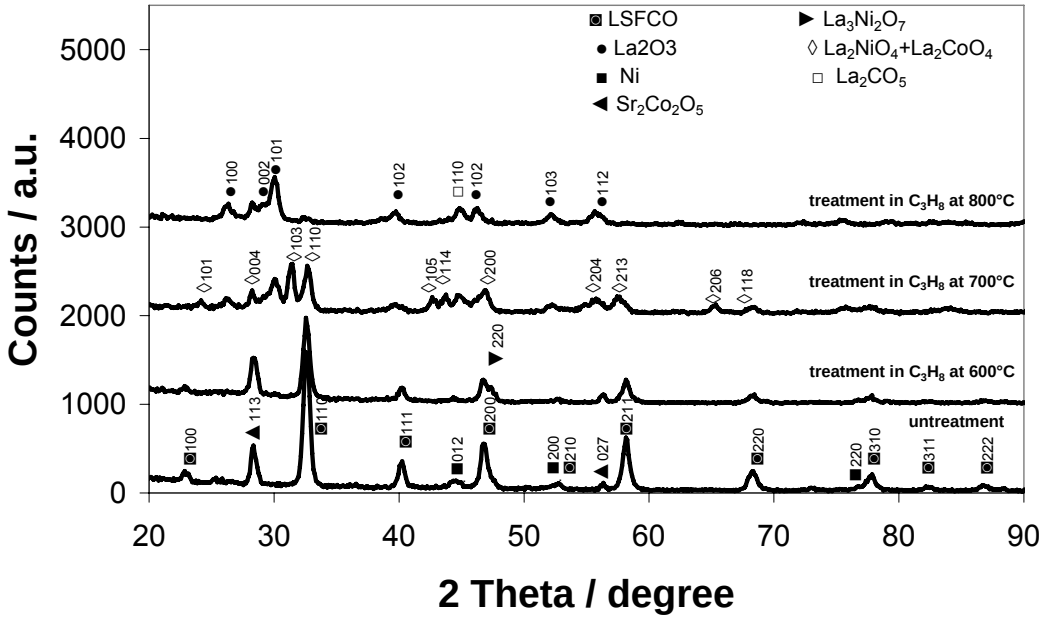

Fig. 2. XRD patterns of the Ni/LSFCO-CGO catalyst as reduced and after treatment in C_3H_8 at different temperatures.

It has been observed in a previous work [261], that although LSFCO perovskite is not stable at 800°C in the presence of dry methane in out-of-cell experiments, it improves its stability during SOFC operation in a CGO based cell due to the mild anodic reducing conditions. It is pointed out that the strong reducing conditions in the presence of hydrogen and hydrocarbons in the out of cell experiment are significantly alleviated during SOFC operation thanks to oxygen pumping effect from the cathode to the anode. AC impedance analysis of the SOFC cell operating in the presence of H_2 in the range 700-800°C (Fig. 3) under working conditions (500 mV) shows appropriate polarization resistances essentially above 700°C. The series resistance (Rs) derived from both frequency intercept on the real axis of the Nyquist plot decreases from 0.43 $\Omega \cdot cm^2$ at 700°C to 0.25 $\Omega \cdot cm^2$ at 800°C. These ohmic losses are due to the supporting 250 μm membrane electrolyte. Polarization resistance is lower than 0.3 $\Omega \cdot cm^2$ at 750°C.

[261] A. Sin, E. Kopnin, Y. Dubitsky, A. Zaopo, A. S. Aricò, L. R. Gullo, D. La Rosa, V. Antonucci, Journal of power Sources 145 (2005) 68-73.

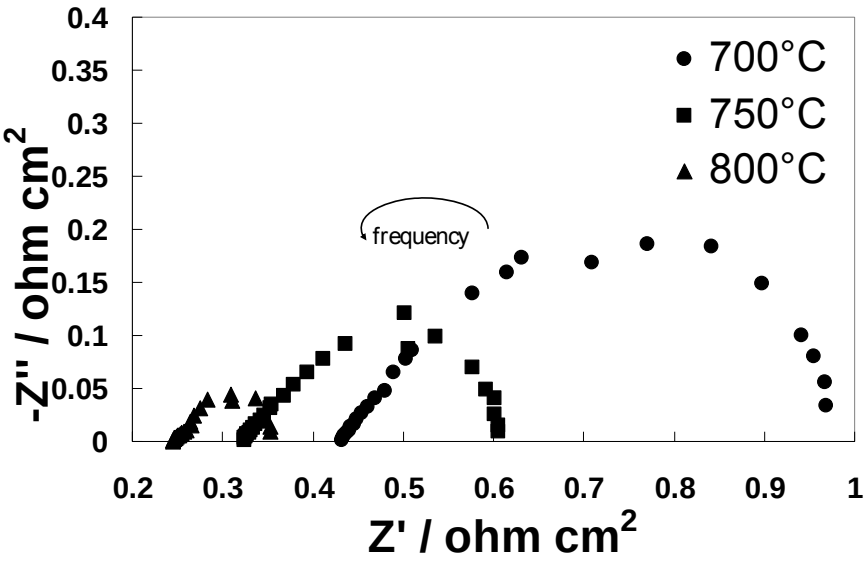

Fig. 3. AC impedance spectra for the SOFC cell operating at 500 mV in the presence of H_2 at different temperatures.

Polarization curves carried out in H_2 (Fig. 4) show that the maximum power density increases with temperature (421 mW/cm^2 at 800°C) whereas the OCV decreases due to the electronic conduction of CGO [262].

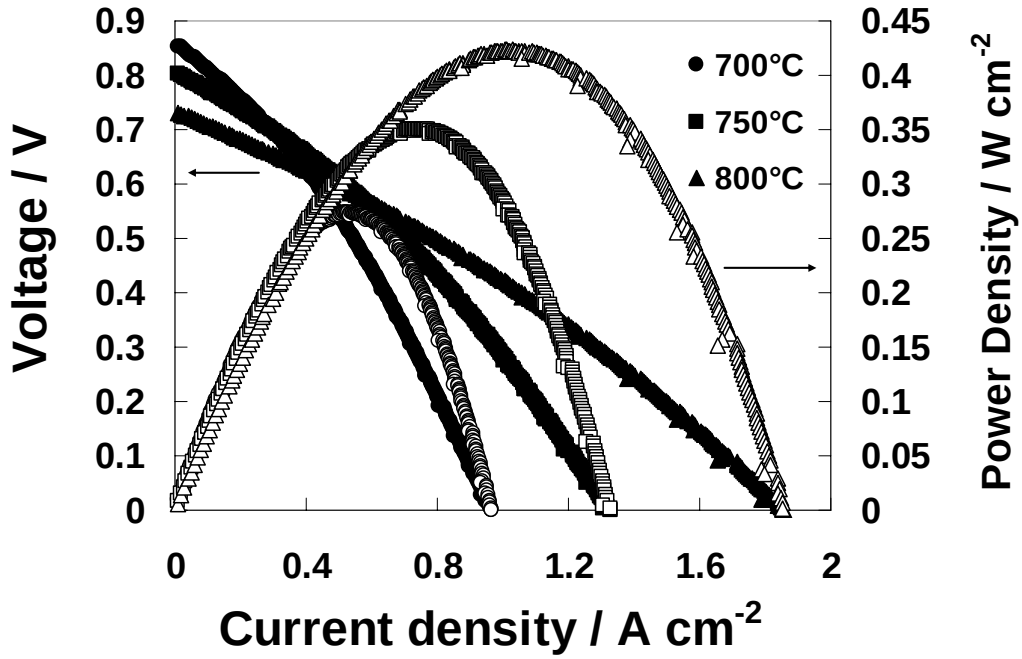

Fig. 4 Polarization curves at different temperatures in the presence H_2 feed at the anode.

[262] Y. Ji, J. A. Kilner, M. F. Carolan, Journal of the European Ceramic Society 24 (2004) 3613-3616.

The performance of perovskite anodes in the presence of methane feed has been previously investigated [263]. In the present work, the attention is addressed to operation of the Ni-doped perovskite anode with propane. Impedance spectra were carried out at 800°C after different operating times of the cell in the presence of dry propane at open circuit voltage conditions. Fig. 5 shows that the initial resistance in propane is larger than in H_2 (0.32 vs. 0.25 Ω cm^2). Possibly, after the switch to C_3H_8, the electrode is partially reoxidized due to a decrease in reducing conditions with respect to pure hydrogen. During operation, the increasing depth of the reduction process and possibly a small amount of carbon deposition on the catalyst causes decrease of both ohmic and polarization resistances practically achieving the same results obtained in hydrogen, i.e. Rs= 0.25 Ω cm^2 and Rp=0.07 Ω cm^2 at 800 °C. The observed R_p value in propane at 800 °C (0.10 Ω cm^2 at 0 hrs and 0.07 Ω cm^2 after 101 hrs), indicate suitable reaction rates.

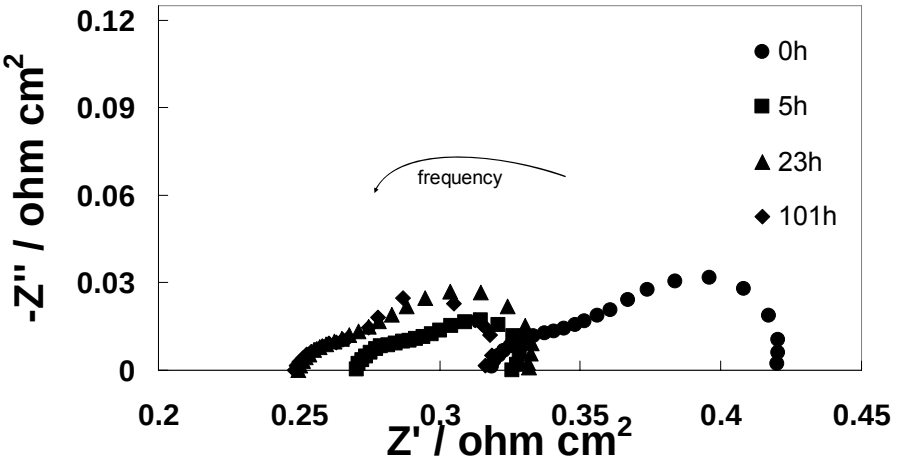

Fig. 5. AC impedance spectra at 800 °C for the SOFC cell operating in the presence of C_3H_8 at different times and open circuit voltage.

Fig. 6 shows polarization curves in dry propane feed at 800 °C after different operating times of the cell. A maximum power density of about 300 mW cm^{-2} was obtained after 101 h of lifetime. Both polarization and impedance spectra indicate that the direct electro-oxidation of propane can be suitably performed in the temperature range of 800 °C. The output power densities of the present device (421 mW cm^{-2} at 800 °C in hydrogen and 300 mW cm^{-2} at 800 °C in propane) are quite promising if one considers that they are mainly affected by ohmic drop and low OCV, essentially related to the

[263] A. Sin, E. Kopnin, Y. Dubitsky, A. Zaopo, A. S. Aricò, L. R. Gullo, D. La Rosa, V. Antonucci, Journal of power Sources 145 (2005) 68-73.

electrolyte membrane thickness and electronic conduction, respectively, than to the catalyst properties.

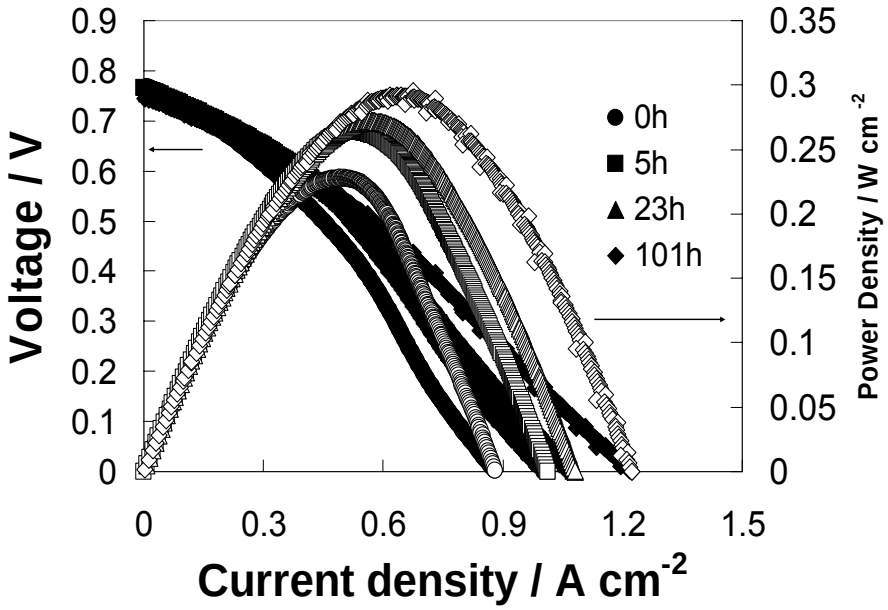

Fig. 6. Polarization curves at different times in C_3H_8 at 800 °C.

IR-free polarization curves are shown in Fig.7 for propane (101hrs). It is observed that a power density approach 400 mW cm^{-2} may be possible if a thin electrolyte based cell is manufactured with the present catalysts. Such results show that there are good perspectives to use the direct propane oxidation process in SOFC devices.

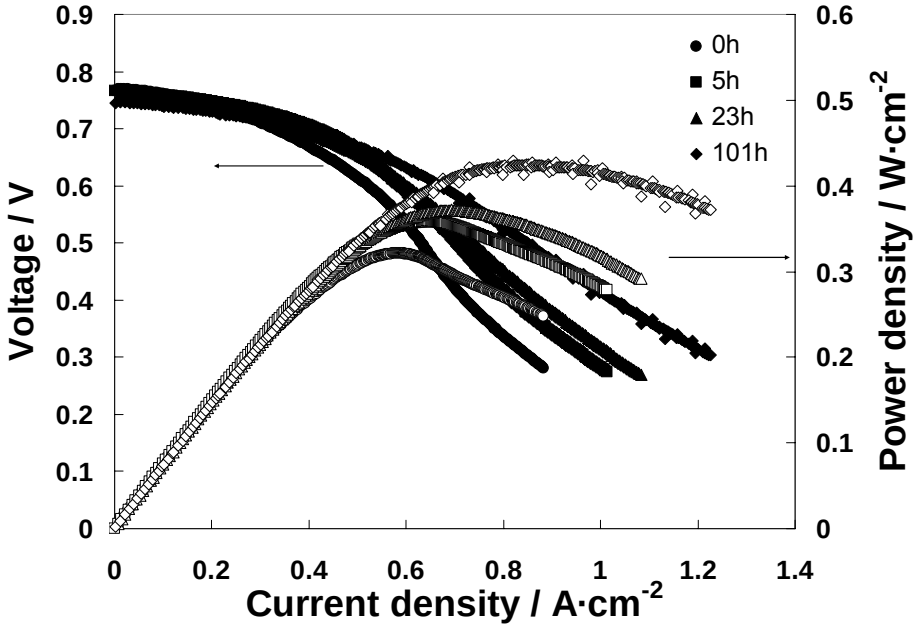

Fig.7 IR-Free polarization curves at different operation times in C_3H_8 at 800°C

The time study shows that the cell performances in the initial conditioning process; after a maximum performance is achieved, the cell potential decreases progressively. Such behaviour is typically owing to an initial improvement of conductivity within the anode layer due to carbon deposition; whereas, when the excess of deposited carbon blocks the reactant to get on the catalytic sites, the performance decreases. Several redox cycles were carried out during this period but these produced only temporarily an increase of cell voltages, possibly due to the burn-off (Fig. 8). It is expected that feeding opportunely propane in stoichiometric flux, this decay can be hampered [264].

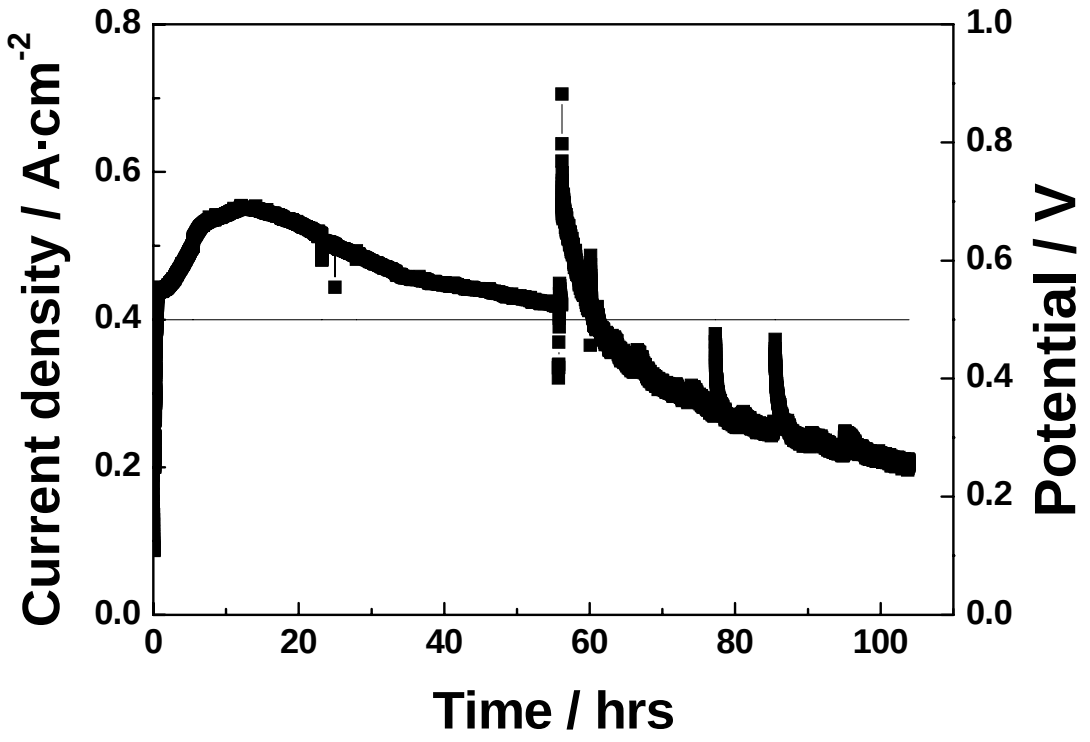

Fig.8 Time stability test in presence of C_3H_8 at 800°C

After the electrochemical tests, the cell was shut-down up to room temperature by feeding hydrogen at the anode and the cell was subsequently dismantled from the alumina tube-support.

The XRD analysis (Fig. 9) of the cell after operation shows that the catalyst structure is modified. A small peak at 24° associated to graphitic C (001) reflection is present. It

[264] Zongping Shao, Sossina M. Haile, Nature, 2004, 431(7005), 170

appears from XRD that only small amounts of carbon deposits are present on the anode surface after cell shut down. A small amount of carbon was also present in the wall of the alumina tube.

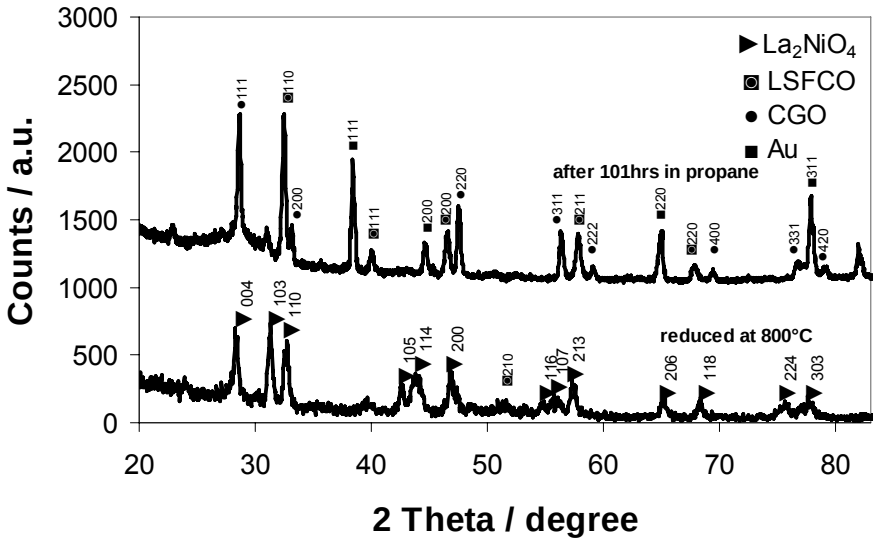

Fig.7 Comparison between the Perovskite before and after 101hrs operation at 800°C.

The formation of small amounts of carbon deposits did not negatively affect the performance, in the operation time period of the present investigation. It is pointed out that the oxide anode catalyst support is more tolerant than Ni cermets to redox cycles, thus, the excess of carbon deposits may be burned off by transient exposure to small amounts at oxygen. This can be pumped from the cathode through the electrolyte by using the oxygen pump effect.

Clearly, the performance of the present SOFC may be greatly enhanced if a thin electrolyte is used (reducing ohmic drop) and if the CGO electrolyte membrane is replaced by another electrolyte characterized by a higher ionic transport number under such conditions. Furthermore, a higher electrical efficiency may be achieved but a lower amount of oxygen species at the anode compartment may be expected especially under OCV. A high ohmic drop and low OCV affect the performance of the present SOFC device. Whereas, the polarization resistances in dry propane were quite promising and indicate that this catalyst can properly operate without the need to use noble metals like Ru, Rh, etc. to promote the oxidation process. As well known Ni promotes the C-H bond scission and thus, the direct oxidation but it also significantly increases the

probability of irreversible deposition of carbon species at the surface blocking the catalytic sites with time [265,266, 267].

Breaking of the carbon-hydrogen bond is considered to be the activation step in the direct oxidation process [268] followed by removal of the adsorbed species by O^{2-} ions. Long term operation of Ni under dry operation is questioned, as discussed above, due to the growth of carbon deposits. On the other hand, CGO has been identified as a suitable oxidation catalyst for both H_2 and methane [269]. The rate determining step on this oxide catalyst presently appears to be related with the scission of C-H bond. Thus, the combination of highly dispersed Ni in a stable oxide form i.e. La_2NiO_4 with a highly electronic/ionic conductor such as LSFCO perovskite, significantly reduces the carbon deposition under mild anode reducing condition in the presence of CGO. These Ni sites are still capable of C-H bond cleavage as shown by TPR experiments but less prompt to form carbon deposits as opposite of metallic Ni. Moreover, it opens new way to avoid the use of NiO as well which is well known to be carcinogenic agent. On such aspect and the improvement of electrode microstructure, our efforts are presently focused to achieve suitable performance and stability during SOFC operation.

Conclusions

Direct oxidation of hydrogen and propane on a Ni-LSFCO/CGO electro-catalyst has been investigated at intermediate temperatures (800°C) in a CGO electrolyte supported cell. The measured electrochemical performances were affected by low OCV, whereas interesting polarization resistances were recorded. Although, out-of-cell tests indicate that the reaction with propane at high temperature may cause a degradation of the perovskite structure. Yet, less degradation than that expected was observed after fuel cell experiments due to the presence of mild reducing conditions in the anode compartment during operation. Low carbon deposit than expected were also observed in the catalyst discharged after SOFC operation with an excess of propane stoichiometry (respect to the

[265] S.C. Singhal, K. Kendall, High Temperature Solid Oxide Fuel Cells: Fundamentals, Design, and Applications, Elsevier, 2003.
[266] S. Mclntosh, R.J. Gorte, Chem. Rev. 104 (2004) 4845–4865.
[267] W.Z. Zhu, S.C. Deevi, Mater. Sci. Eng., A 362 (2003) 228–239.
[268] R. Burch, M. J. Hayes, Journal of Molecular Catalysis A: Chemical 100 (1995) 13-33.
[269] O. A. Marina, M. Mogensen, Appl. Catalysis A: General 189 (1999) 117-126.

stoichiometry requirements). The achieved performances for hydrogen and propane oxidation are acceptable even in the presence of a thick electrolyte membrane. However, the electric efficiency is still not appropriate (the maximum power density is achieved at about 500 mV). To further ameliorate this process, it is envisaged that an increase of electric efficiency may be achieved by improving the reversibility of the process (i.e. decreasing the polarization resistance) and reducing the ohmic resistance while maintaining mild reducing conditions at the anode that are essential to preserve the perovskite structure.

Future planning

Next tasks will be demonstrate the stability along the time up to 1000hrs including accelerated test as well as redox/thermal-load cycles. These procedures save time providing important information on durability issues under practical condition. Furthermore, will be investigated the anodic catalyst by ex-situ testing associated to physical-chemical analyses (XPS and TEM) and electrochemical studies in order to better interpret the behaviour of this catalyst. The aim is to achieve a better understanding of the relationship among performance issues and structural, chemical and morphological characteristics.

At the same time, will be provided the use of alternative highly conductive electrolytes allowing to further decrease the operating temperature will be investigate.

The results obtained in this work have been accepted to be published on the International Journal of Hydrogen Energy

SCIENTIFIC PRODUCTION

Publications on International Refereed Journals

- Giovanni Brunaccini, **Massimiliano Lo Faro**, Daniela La Rosa, Vincenzo Antonucci, Antonino Salvatore Aricò
  CNR-ITAE Institute,Via Salita S. Lucia sopra Contesse 5 IT-98126 Messina, Italy
  "Investigation of Composite Ni-Doped Perovskite Anode Catalyst for Electrooxidation of Hydrogen In Solid Oxide Fuel Cell" International Journal of Hydrogen Energy **"in press"** DOI: 10.1016/j.ijhydene.2008.01.021

- **M. Lo Faro**, D. La Rosa , G. Monforte, , V. Antonucci, A.S. Aricò, CNR-ITAE; P. Antonucci, University of Reggio Calabria.
  "Propane conversion over a Ru/CGO catalyst and its application in Intermediate temperature solid oxide fuel cells" Journal of Applied Electrochemistry 37 (2007) 203-208 DOI: 10.1007/s10800-006-9245-5

- D. Montinaro, V.M. Sglavo, DIMTI, Università degli Studi di Trento, M. Bertoldi, T. Zandonella, EUROCOATING SpA, A. Aricò, **M. Lo Faro**, V. Antonucci CNR-ITAE
  "*Tape Casting Fabrication and Co-Sintering of Solid Oxide "Half-Cells" with a Cathode-Electrolyte Porous Interface*" Solid State Ionics, 177 (2006) 2093-2097 DOI: 10.1016/j.ssi.2006.01.016

National Conferences Proceedings

- **M. Lo Faro**, D. La Rosa, V. Antonucci, A. S. Aricò, G. Monforte, G. Brunaccini, M. Minutoli**,** CNR-ITAE
  "*Investigation of Composite Ni-Doped Perovskite Anode Catalyst for Electrooxidation of Hydrogen and Hydrocarbons in Intermediate Temperature Solid Oxide Fuel Cells"* GEI-ERA 2007 ***D-4***

- G. Brunaccini, **M. Lo Faro**, D. La Rosa, V. Antonucci, A. S. Aricò, G. Manforte, M. Minutoli**,** CNR-ITAE
  "*Investigation of Composite Ni-Doped Perovskite Anode Catalyst for Electrooxidation of Hydrogen and Hydrocarbons in Intermediate Temperature Solid Oxide Fuel Cell"* HYSYDAYS 2007 ***CD***

- Antonino S. Aricò, Daniela La Rosa, **M. Lo Faro**, Vincenzo Antonucci (CNR-ITAE)
  "*Materiali nanostrutturati per celle a combustibile ad ossidi solidi operanti a temperature intermedie****"*** AIM, Materiali per l'impiego dell'idrogeno nella produzione di energia Milano, 2006 ***CD***

- **M. Lo Faro**, Vincenzo Antonucci, Antonino Salvatore Aricò, Massimo Bertoldi, Thomas Zandonella, Dario Montinaro, Vincenzo M. Sglavo
  "Caratterizzazione di celle SOFC di produzione Eurocoating" XXII Congresso Nazionale della Società Chimica Italiana ***ELE-O-6***

- **Massimiliano Lo Faro**, Daniela La Rosa, Giuseppe Monforte, Vincenzo Antonucci, Pierluigi Antonucci, Antonino S. Aricò
  "Ru/CGO per l'ossidazione diretta di propano per applicazioni IT-SOFCs" GEI 2005-Giornate dell'Elettrochimica Italiana ***C5***

International Conferences Proceedings

- D. La Rosa, **M. Lo Faro**, G. Monforte, M. Minutoli, G. Brunaccini, V. Antonucci, A. S. Aricò, CNR-ITAE
  "*Electrode effects on cell performance***"** ESF Exploratory Workshop on Proton Conducting Materials for Next-Generation Solid Oxide Fuel Cells 22-24 October 2007

- **M. Lo Faro**, D. La Rosa, V. Antonucci, A. S. Aricò, G. Monforte, G. Brunaccini, M. Minutoli, CNR-ITAE
  "Investigation of composite Ni-doped perovskite anode for direct oxidation of hydrocarbon" Nara, Japan 10th Symposium on Solid Oxide Fuel Cells, 2007 ***S1124-S1127***

- D. La Rosa, **M. Lo Faro**, V. Antonucci, A. S. Aricò, G. Monforte, CNR-ITAE
  Sin Agusti, Pirelli Labs S.p.A
  "Recent advances on the development of NiCu alloy catalyst for IT-SOFCs" **Nara, Japan 10th Symposium on Solid Oxide Fuel Cells, 2007** *S1328-S1332* doi:10.1149/1.2729278

- D. La Rosa, **M. Lo Faro**, V. Antonucci, A. S. Aricò, G. Monforte, G. Brunaccini, CNR-ITAE
  "*Direct electrochemical oxidation of propane in solid oxide fuel cells***"** Edinburgh, 5 7th Meeting ISE, 2006 ***S10-O-39***

- **M. Lo Faro**, D. La Rosa, G. Monforte, A. S. Aricò, V. Antonucci, CNR-ITAE
  Pierluigi Antonucci, Università di Reggio Calabria
  "*Propane conversion on Ru/CGO catalyst for application in Intermediate Temperature Solid Oxide Fuel Cells"* 7th European Fuel Cell Forum, 2006 ***233-237***

- **Massimiliano Lo Faro**, Daniela La Rosa, Giuseppe Monforte, Antonino S. Aricò, Vincenzo Antonucci (CNR-ITAE), PierLuigi Antonucci (Department of Mechanics and Materials, University of Reggio Calabria, Italy).
  "Propane conversion on Ru/CGO catalysts for application in Intermidiate Temperature Solid Oxide Fuel Cells" - *Ninth International Symposium on Solid Oxide Fuel Cells (SOFC-IX), Quebec City; 15-20 May 2005* ***1131***

- M. Bertoldi, T. Zandonella (EUROCOATING SpA, via Al Dos de la Roda 60, I-38057 Pergine, Italy), V. Sglavo, D. Montinaro (DIMTI, Universi di Trento, via Mesiano 77, I-38050 Trento, Italy), A. Aricò, **M. Lo Faro**, V. Antonucci (CNR-ITAE, Via Salita Santa Lucia Sopra Contesse 5, I-98125 Messina, Italy)
  "Improved Cathode-Electrolyte Interface for Planar Solid Oxide Fuel Cells" - *Ninth International Symposium on Solid Oxide Fuel Cells (SOFC-IX), Quebec City; 15-20 May 2005* ***1193***

- Vincenzo Antonucci, **Massimiliano Lo Faro**, Daniela La Rosa, Giuseppe Monforte, Antonino S. Aricò (CNR-ITAE), PierLuigi Antonucci (Department of Mechanics and Materials, University of Reggio Calabria, Italy).
  "Propane conversion on Ru/CGO catalysts for application in Intermidiate Temperature Solid Oxide Fuel Cells" - *International Hydrogen Energy Congress & Exhbition IHEC2005*

- M. Bertoldi, T. Zandonella (EUROCOATING SpA, via Al Dos de la Roda 60, I-38057 Pergine, Italy), V. Sglavo, D. Montinaro (DIMTI, Universi di Trento, via Mesiano 77, I-38050 Trento, Italy), A. Aricò, **M. Lo Faro**, V. Antonucci (CNR-ITAE, Via Salita Santa Lucia Sopra Contesse 5, I-98125 Messina, Italy)
  "Functionalization of the cathode-electrolyte interface in Solid Oxide Fuel Cells" - *15th International Conference on Solid State Ionics* ***537***

- **Massimiliano Lo Faro,** Roberto Bonfiglio, Daniela La Rosa, Laura R. Gullo, Vincenzo Antonucci, Antonino S. Aricò CNR-ITAE.
  "Analysis of hydrogen and methane-fed SOFC devices based on Ru doped Ni/CGO cermets" - *Scientific Advances in Fuel Cell System, Munich; 6-7 October 2004*